Nanoreactors in Catalysis

Nanoreactoren voor katalyse

(met een samenvatting in het Nederlands)

Proefschrift

ter verkrijging van de graad van doctor aan de Universiteit Utrecht op gezag van de rector magnificus, prof.dr. G.J. van der Zwaan, ingevolge het besluit van het college voor promoties in het openbaar te verdedigen op woensdag 3 juni 2015 des ochtends te 10.30 uur

door

Rafael de Lima Oliveira

geboren op 20 november 1984 te Fortaleza, Brazilië

Promotoren: Prof. dr. K. P. de Jong

Prof. dr. P. E. de Jongh

This thesis is accomplished with financial support from the National Research School Combination- Catalysis (NRSC-C)

Table of Contents

de Lima Oliveira, Rafael
Title: Nanoreactors in Catalysis
ISBN: 978-90-393-6341-6
Printed by: Gildeprint

Chapter 1

General Introduction

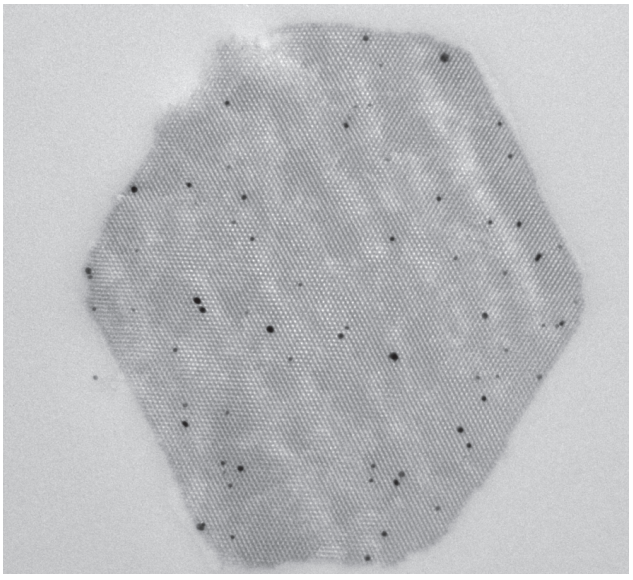

Supported Catalysts

Supported catalysts are composed of an active phase, in general transition metal particles or complexes, supported on a solid matrix such as oxides, carbon structures or polymers. Before 1930, the majority of solid catalysts were obtained from nature without man-made synthesis steps.[1] After 1930, more controlled synthesis methodologies were introduced into the catalysis field giving a tremendous improvement of catalytic performances. Nowadays, supported catalysts are integral components of chemical processes. Thus, the design of catalysts with desired properties such as particle size, porosity and stability is extremely important for academia and industry. From the industrial point of view, catalysts with a long lifetime and high activity and selectivity are desirable. Moreover, well-designed solids allow a deeper understanding of the performance in relation to structure.[2]

The purpose of a catalyst is to lower the energy barrier between reactants and products by providing an alternative reaction path. A catalyst decreases the activation energy of a specific reaction and as a consequence increases the rate of the reaction, but it does not affect the chemical equilibrium of the reaction. A catalyst can be very specific under ideal conditions, resulting in selective formation of the desired products and suppression of side reactions. One important aspect of catalyzed reactions is the reduction of the use of raw materials and enhancement of energy efficiency when compared to a non-catalyzed systems.[3]

In general, heterogeneous catalysts are less selective than their homogeneous counterparts.[4] Thus, the development of innovative approaches to create recoverable and reusable catalysts which combine the advantages of heterogeneous and homogeneous catalysis is very desirable. In the last three decades, many new methodologies have been developed to produce more efficient supports, for example; well-ordered mesoporous materials,[5–14] magnetic supports,[15–23] metal organic frameworks,[24–29] zeolites,[30–34]nanotubes and others.[35–45]All these new materials have an impact on activity, recyclability and improvement of lifetime of the catalysts.

Despite these developments in the last decades, the majority of catalytic processes involving solid catalysts is not well understood. Gas phase reactions on solid surfaces were

partially rationalized for simple molecules on defined model catalysts[46,47] (Nobel Prize-2007), but reactions with more complex molecules are still less well understood. In liquid phase reactions, such as hydrogenation, oxidation and C-C coupling, several controversial results have been published in literature about the true nature of the catalysts, e.g. on the role of homogeneous species leached from the supported metal.[17,48–57]

Many efforts have been made to develop new techniques which permit the study of catalytic performance in-situ, giving a deeper understanding about active phases and how the catalytic process takes place. For example, Reimann et al. used EXAFS techniques to identify active species in the Heck reaction using Pd/Al_2O_3 as catalysts. They concluded that homogeneous species leached from the support to the liquid phase were the true catalysts.[58] In another example, Yoshida et al. showed the adsorption of CO molecules on gold nanoparticles using environmental TEM, and observed changes on nanoparticle structure during adsorption.[59]

Ordered mesoporous silica in catalysis

Porous materials such as silica, alumina and carbon have been used for a long time as supports in catalysis. In the 1990's a new class of porous materials was discovered, the ordered mesoporous silica MCM materials (1992) and SBA-15(1998).[13,60–62] SBA-15 family materials were synthesized in the groups of Stucky and Chmelka for the first time, they used non-ionic triblock co-polymers (P123 ($EO_{20}PO_{70}EO_{20}$)) as templates. The poly(ethylene oxide) (PEO) blocks are considered hydrophilic and the poly(propylene oxide) (PPO) blocks are hydrophobic which leads to amphiphilic behavior in water, causing the block co-polymer to self-assemble just like surfactant solutions. Surfactant concentrations above the critical micelle concentration are employed during the synthesis, this leads to the formation of micelles which pack into rods, and the rods pack into hexagonal arrays (Figure 1). Subsequently or co-operatively, silica condensation takes place around the hexagonal arrays. The last step involves removal of the template by calcination or extraction leading to the formation of an ordered mesoporous silica network.

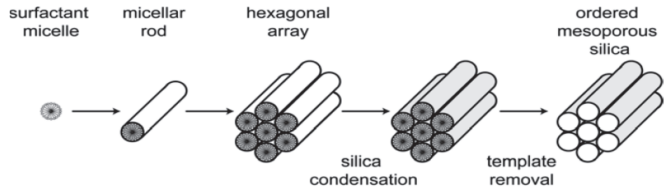

Figure 1- Sechematic overview of the synthesis of ordered mesoporous materials.

Ordered mesoporous silica materials have large specific surface areas as other porous materials but a very uniform pore size distribution, tunable periodic pore arrangement and concavity of the pore walls. All these properties make them unique materials. However, in the catalysis field siliceous mesoporous materials do not have sufficient intrinsic activity as a catalyst in most cases. Thus, a lot of effort has been invested to introduce actives species in their structure such as metal particles, metal complexes and molecules with alkaline or acidic properties.

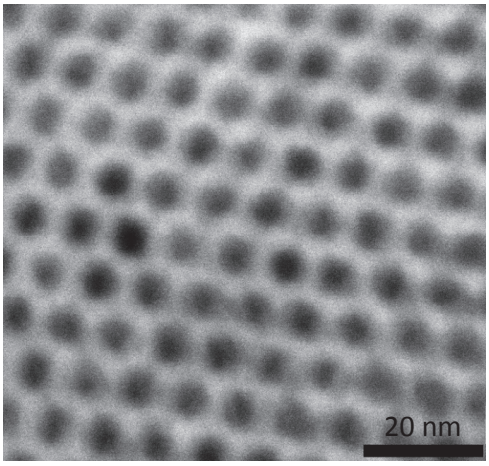

Figure 2 STEM image showing the pore structure of SBA-15

SBA-15 is the most studied mesoporous silica, because its stability is higher than for the MCM materials family. In general, SBA-15 pore walls are typically around 2-4 nm thick which is more than MCM type materials. Figure 2 shows a STEM image of an SBA-15 material. Another advantage of SBA-15 is the connection between its pores via intra-wall

porosity which provides a better mass transfer. After the synthesis of SBA-15, the use of different co-polymers and a combination of them as templates allowed the possibility to create several types of silica with various morphologies and symmetries such as SBA-16, FDU and KIT. [63–66]

Zeolites were initially perceived as the closest relatives of ordered mesoporous silica. Now, it is clear that OMMs (Ordered Mesoporous Materials) have at least as much in common with xerogels as with zeolites. The critical comparison of OMMs with disordered silica showed advantages of the former in a lot of fields.[67–71] For example, Mercier et al. showed that the thiol groups grafted on ordered mesoporous materials are more accessible than those grafted on disordered silica, resulting in a material with a higher capacity to scavenge mercury in contaminated water.[72] Pietro et al. compared different solids based on CuZnO-SBA-16 and CuZnO-silica-gel using them as catalysts for methanol synthesis. They observed that SBA-16 based material did not deactivate as fast as the catalysts based on silica-gel, concluding that the confinement of metal particles in the cages of SBA-16 decreased the metal particle growth, producing more stable catalysts.[73]

Plugged SBA-15 and cage like mesoporous silica (SBA-16, FDU-12 and m-MCF)

In 2002, a new type of SBA-15 was produced, i.e., "plugged hexagonal templated silica" (PHTS) also called Plugged SBA-15 (P.SBA-15).[74,75] The synthesis of these materials is similar to SBA-15 but an excess of the silica precursor tetraethyl orthosilicate (TEOS) is used leading to an ordered mesoporous silica with constricted pores. By varying the synthesis parameters, the extent of the plugging can be influenced. Moreover, these solids exhibited a remarkable mechanical stability when compared to normal SBA-15 due to the pillars inside their structure and the increase of wall thickness (3-7 nm). Thus, PHTS is put forward as a good candidate for industrial applications of ordered mesoporous materials because the stability is one of the factors that may impede catalytic applications.

Typical nitrogen sorption isotherms at 77K for both SBA-15 and Plugged SBA-15 are shown in Figure 3. In the case of Plugged SBA-15, ink-bottle hysteresis is observed,

showing that liquid N_2 remained condensed by the narrow entrances of the pores, resulting in a delayed desorption at relative pressure around 0.45 (Figure 3-B), confirming the presence of pores with a smaller entrance size (cavities). In the case of SBA-15, a typical parallel hysteresis of the open mesopores is observed in Figure 3 A.

Recently, different methodologies have been used to study the nature of the constrictions, their distribution inside the pores and their entrance sizes. Shakeri et al. and Celer et al. proposed a study based on modification of the silica surface with organosilanes with different carbon lengthes to estimate the entrance size of the pores.[76,77] Kjellman et al. used low voltage high resolution scanning microscopy to observe plugs and intrawall pores in a partially plugged SBA-15[78] and Mandal et al. used transmission electron microscope to observe the plugs inside the pores and "hemispherical ends" of the pores.[79]

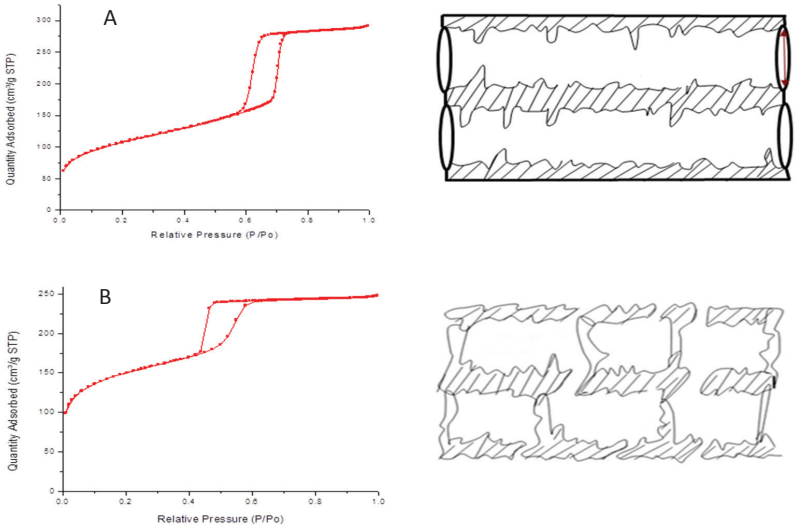

Figure 3 Typical N_2 physisorption isotherms of ordered mesoporous materials (A) SBA-15 with open cylindrical pores (B) ink-bottle hysteresis typical of cage-like materials and plugged SBA-15

Zhao et al. used larger EO chains ($EO_{106}PO_{70}EO_{106}$=F127) which promoted the formation of globular aggregated structures of the template. After the silica growth and removal of the template, a material with a cage structure was obtained.[13] This new material

was called SBA-16. In general, SBA-16 has cages around 6 nm and wall thickness around 4-6 nm.[80,81] SBA-16 has higher chemical, thermal and hydrothermal stability when compared to SBA-15. The nitrogen sorption isotherms of cage like materials have similar hysteresis (ink-bottle) as observed for plugged SBA-15.

FDU-12 is another cage-like material synthesized using a mixture of copolymers F-127 or F108 assisted by a swelling agent (mesitylene) and inorganic salts. This solid presents a cubic mesostructure with larger cage sizes when compared to SBA-16 (10-22 nm) and the entrance sizes from 4 to 8.9 nm respectively.[66,82] FDU-12 prepared at a low temperature can be regarded as a face-centered cubic (fcc) close-packing with spherical cages, moreover, Yu et al. showed that the cages are connected to 12 nearest neighbor cages.[83]

Recently, our group reported a synthesis of a new material called modified mesocellular silica foam (m-MCF). The procedure is based on P.SBA-15 synthesis, but in this case a swelling agent (mesitylene) was introduced during the synthesis. A very interesting characteristic of this material is its narrow entrance sizes (1.8-5.0 nm) and large cages (16-22 nm). Moreover, as was shown using electron tomography the cages are connected to 9-12 neighboring cavities resulting in a highly interconnected network (Figure 4).[84]

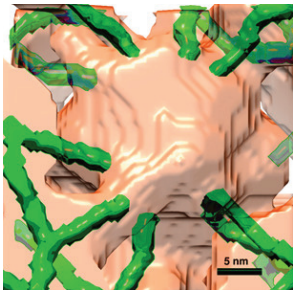

Figure 4 Electron tomography model of single cavity of m-MCF, the cage is colored with orange and nine neighboring pores are colored with green[84]

Synthesis of supported metal nanoparticles in porous materials

Metal nanoparticles are receiving much attention due to their relatively high chemical activity and specific interactions. Thus, deposited nanoparticles on a solid matrix, such as porous materials, with control of size, shape and distribution has been a hot topic explored in the last years.[71,85–90] These metal nanoparticles deposited on porous materials are not only important in the catalysis field, but also in other fields such as drug delivery systems, sensors and others.[91–93]

There are many preparation routes to deposit metal nanoparticles on porous materials that can be divided into physical approaches (such as sonication, microwaves) and chemical approaches (such as impregnation, electrochemical, ligand assisted). Herein, some of the chemical methods are described.

Incipient wetness impregnation is one of the most applied chemical methodologies. In this method, the support is put in contact with a solution of a metal precursor, typically a salt (metal nitrate or metal chloride). In general, this salt is dissolved in an amount of solvent that matches the pore volume of the support. After impregnation, drying and calcination, a reduction treatment is carried out to obtain metal nanoparticles. This is a very simple method, however, a lack control of the nucleation and growth of metal nanoparticles might result in e.g. a bimodal distribution of particle size or a mixture of particles with different shapes, for example nanoparticles and nanowires.[94–96]

Another method to deposited nanoparticles on a solid matrix is ion adsorption. In this methodology, a strong interaction between the support and the metal precursor is created (Figure 5). An oxide surface, such as silica and alumina, contains terminal hydroxyl groups, these groups can be protonated or deprotonated depending on the pH of the impregnating solution. The pH at which the hydroxyl groups are neutral is called point of zero charge (PZC). If the pH is below the PZC, these hydroxyl groups are protonated, becoming positively charged, thus, the surface is able to adsorb anionic metal complex. At a pH above the PZC, the hydroxyl groups are deprotonated and become negatively charged, then, the

surface can adsorb cationic species.[97–99] Normally, this methodology gives a better dispersion of metal nanoparticles over the solid matrix than incipient impregnation.[100,101]

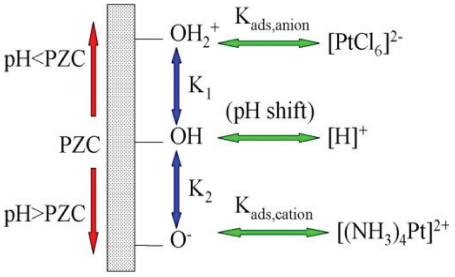

Figure 5 Components of an electrostatic adsorption mechanism; surface charging, metal adsorption and proton transfer.[101]

Another method that has been explored recently is based on ligand assistance. In this method the hydroxyl groups of an oxide are substituted by organic modifiers (Scheme 1).[102] The surface of an oxide can be modified with commercially available organosilanes and many other derived groups can be prepared by a simple synthesis procedure.[103–109] Various procedures and ligands have been reported for functionalization of metal oxides surfaces, carbon structures and polymers, for example bisphosphinoamino moiety, dendrimers, alkyllimidazolium, ionic liquids and others. These groups can be used to control the metal adsorption, creating a strong metal-support interaction and improving the catalytic performance in some cases. For example, Rossi et al. showed that amino groups grafted on silica were able to reduce metal leaching for hydrogenation of alkenes when compared with non-functionalized catalyst, producing a more efficient material.[110] A disadvantage of the ligand assisted method is that the presence of these ligands limits the temperature operation of the catalysts because at high temperatures the organic linkers may decompose.

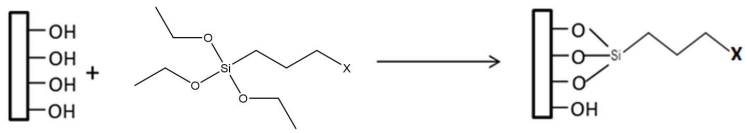

Scheme 1 Functionalization of silica surface, where X can be amine, thiol or other functional groups.

Nano-reactors in catalysis

Confined active species in porous materials have been reported for a long time.[111] Zeolites were an early form of 'nanoreactors' due to their small cage structure and narrow pore entrance sizes. Mobil in 1977 developed the first method to customize the structure of zeolites (HZSM-5).[112] They use the hole in the structure to select the molecules with desired size to diffuse and react inside the HZSM-5 structure. In another example, Ogunwumi et al. immobilized a metal complex inside zeolite EMT and applied this material as a catalyst for epoxidation of alkenes. Due to small pores and entrance sizes of zeolites, lower activity when compared with the homogeneous counterparts was reported.[113]

In recent years, many new materials and strategies have been developed to produce structures with nanoreactors. These are based on many different approaches and materials such as porous oxides, dendrimes, microgels, polymers (core-shell structure) and carbon nanotubes.[5,7,113–129] Some examples are given below.

Chen et al. designed a material based on a three step procedure for producing hollow nanocomposites (Scheme 2). In this strategy, palladium nanoparticles were deposited on the surface of carbon spheres, after this procedure, a porous silica layer was synthesized on top of Pd/C by a sol-gel methodology. A calcination in air was used to remove the carbon structure, resulting in silica hollow spheres with mesoporous walls. This nanocomposite was used as a catalyst for the Suzuki reaction giving high conversion and low Pd leaching.[130]

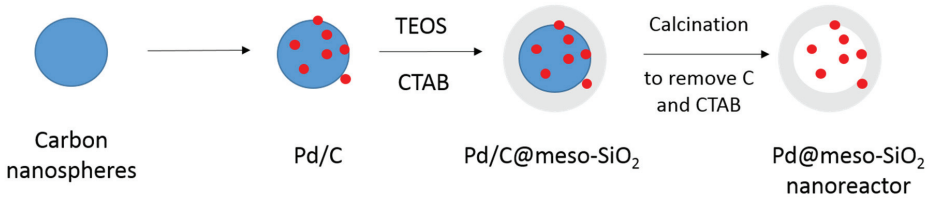

Scheme 2 Synthesis route of the composite nanoreactors

In another elegant strategy, Rossbach et al. immobilized a Co^{III} (salen) complex on amphiphilic block copolymers, which self-assemble in water, giving micellar aggregates with hydrophobic Co(salen) core and a water-soluble shell. The aggregates were used as a catalyst for hydrolytic kinetic resolution (HKR) of racemic epoxides, showing very high enantioselectivity (up to 99%) and no lost of activity after four cycles.[131]

Lu et al. developed a system based on microgels in which the core consists of poly(styrene) whereas the network consists of poly(N-isopropylacrylamide). At low temperature (T < 32ºC) the microgel network is hydrophilic and swollen in water, while at higher temperatures, the network shrinks and becomes hydrophobic. The microgel particles in which gold nanoparticles were immobilized were able to take up the hydrophobic substrates, producing a very active catalyst for oxidation of alcohols.[132]

Recently, a lot of reports have been based on the use of ordered mesoporous silicas and their ability to confine metal particles, complexes and molecules. Hao et al. functionalized SBA-16 and silica gel structures with amino groups and immobilized gold nanoparticles on their surface and they compared the catalytic activity of gold nanoparticles on the oxidative esterification of alcohols. They concluded that gold nanoparticles encapsulated in the cages of SBA-16 did not grow as severely as particles immobilized on silica gel based material and as a consequence Au/SBA-16 showed a longer life time than the catalyst based disordered silica.[133]

Li et al. encapsulated a chiral vanadium salen complex in the cage of SBA-16 and applied this material as catalyst for cyanosilylation of benzaldehyde, obtaining enantioselectivities as high as 90%. It is interesting to point out that using hexane and heptane as solvents the heterogeneous catalyst exhibits higher enantioselectivity than its homogeneous counterpart. The authors suggested that an altered microenvironment could be the explanation of this observation. [134]

C-C coupling reaction

Coupling reactions to form carbon-carbon bond are one of the most important transformations in organic chemistry.[135] Traditionally, these reactions are done using strong basic reagents such as Grignards and lithiated carbon nucleophiles, however these reagents drive the formation of a lot of waste and low selectivity.[136] New routes using palladium complexes and palladium salts were discovered by Heck (1968-1972),[137–143] Suzuki (1977)[144,145] and Negishi (1976).[146–148] Their discoveries revolutionized the way that chemists construct molecules, providing methods more efficient than previous procedures. Heck, Suzuki and Negishi received the Nobel Prize in 2010 for their contribution in chemistry. Despite the discovery of Heck, Suzuki and Negishi taking place in the 1970s, a limited number of publications and patents were reported before the 1990s (Figure 6), that has increased drastically since 2000.[149] As can be seen from Figure 6, the Suzuki and the Heck reactions are by far the most explored reactions.

Many applications of these reactions have been reported in the last decades, such as synthesis of conducting polymers, light-emitting electrodes and organic synthesis, especially in the synthesis of natural products and biologically active compounds.[149–157] More than 100 different biologically active compounds have been synthesized using the Heck reaction in the last two decades. For example, Hong et al. proposed a new route to produce morphine based on an intramolecular Heck type coupling reaction which provides the morphine skeleton and the final product in few steps.[158]

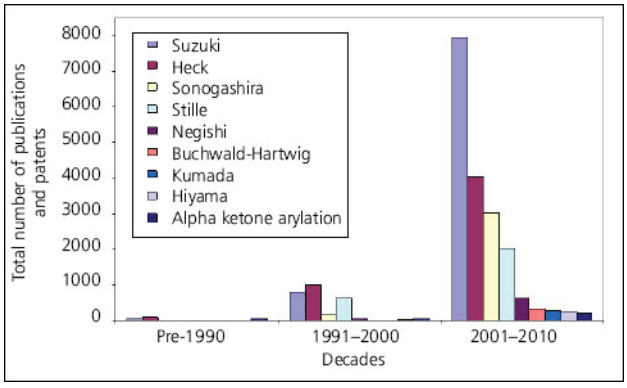

Figure 6 Growth in number of publications and patents on coupling reactions in the last decades[149]

The principle of palladium-catalyzed cross coupling is that two molecules react via the formation of a bond between carbon and palladium. Thus, palladium is responsible for bringing the carbon atoms very close to each other, leading to the formation a new carbon-carbon single bond. In general, there are two types of cross-coupling reactions based in this principle (equation 1 and 2).

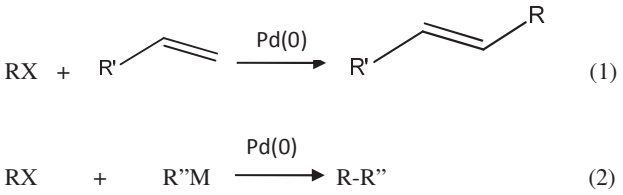

Equation 1 shows a cross-coupling reaction between an organohalide and an alkene in the presence of a palladium catalyst generating a substituted alkene. This reaction is known as the Heck reaction. The second equation applies an organometallic compound as a nucleophilic part, depending on the organometallic used, this reaction can have different names, for example, if a boronic acid is employed this reaction is known as the Suzuki reaction.

Figure 7 shows the mechanism of the Heck and the Suzuki reactions. The first step of these reactions involves the organohalide RX to react with palladium (oxidative addition) forming an organopalladium compound.[135] In the heterogeneous catalysis field, many researchers believe that this step is related with the extraction of Pd species from Pd nanoparticles, producing soluble species that are the true catalysts. Niu et al. concluded using two different Pd nanocatalysts, one based on amorphous Pd NPs and the second based on bimetallic Pd-Au NPS, that oxidative addition was responsible for Pd leaching. When they mixed iodoanisole or bromoanisole and the metal particles, they observed an enhancement in the crystallinity (particle growth) and the bimetallic system underwent phase segregation and

formation of distinct monometallic Pd particles.[159] In another example, Jones et al. used different tests such as hot filtration, PVPy poisoning and three phase test to identify the active species in the Heck and the Suzuki reactions. They studied Pd immobilized on modified SBA-15, and concluded that the Pd served as a reservoir for homogeneous species that were formed during the reaction.[56]

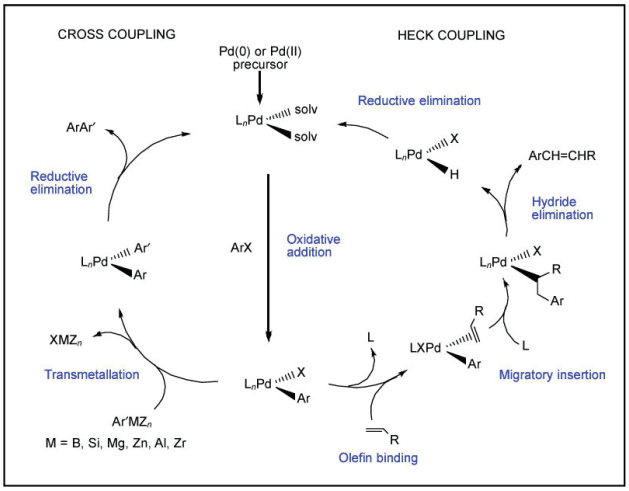

Figure 7-Mechanism of the Heck coupling and other cross coupling reactions[149]

As mentioned before, the invention of Heck, Suzuki and Negishi was based on homogeneous catalysis. Despite having high activity and selectivity, homogeneous catalysts have a number of drawbacks. The lack of reuse of the catalysts or at least the problems of recycling them leads to a loss of expensive metal and in some cases ligands, causing the contamination of products and as a consequence the necessity of metal removal.[160,161] These problems have to be overcome in the application of Pd-catalyzed coupling reactions in industry. Heterogeneous catalysts surge as a promising option to solve these problems. In the last decades, Pd nanoparticles and complexes have been immobilized on many solids such as activated carbon, metal oxides (mainly silica and alumina, but also MgO, ZnO, TiO_2), organic polymers, zeolites, alkaline earth salts and others. [8,149–157,162–186]

Heterogeneous catalysts applied to C-C cross coupling suffer from deactivation, which limits their life time and recyclability. This deactivation can be caused by different phenomena such as (i) aggregation of nanoparticles, resulting in a decrease of available metal species; (ii) leaching of Pd; (iii) poisoning of the active surface sites and (iv) salt accumulation. Thus, producing a catalyst with a long life time, keeping high activity and selectivity is still a challenge.

Salen complexes

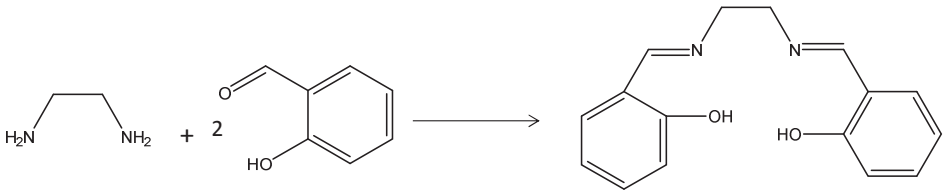

Scheme 3- Salen ligand synthesis

The first synthesis of a salen-metal complex was reported by Pfeiffer et al. in 1933.[187] As indicated in Scheme 3, salen ligands are normally synthesized by an uncatalyzed reaction between a salicyaldehyde with a 1,2-diamine. The salicylidene imine group is prone to undergo an acid-catalyzed hydrolysis, reverting to the corresponding salicyaldehyde and diamine in the presence of water. However, the stability of a Schiff base increases tremendously upon coordination with a metal ion and formation of a salen-metal complex. Due to this fact, salen-metal complexes can be used in wet solvents or even in aqueous media without undergoing hydrolysis. [188]

For most of the transition metals, the corresponding metal salen complexes syntheses have already been reported and the catalytic performance of these complexes have been extensively studied for a lot of reactions such as epoxidation,[189–192] sulfoxidation,[193–197] aziridination,[198,199] coupling reaction,[200–202] cyanosilylation of aldehydes[203–205] and others.[206–209] Despite good catalytic performance and good selectivity reported for these complexes, the

separation of expensive homogeneous catalysts from the reaction mixture is necessary. In some cases, multiple steps are required which can cause the degradation of the complexes limiting their recovery.

Several new methodologies have been developed for immobilizing metal complexes on solid matrices such as grafting, anchoring, encapsulation and others. In the case of grafting the complex is immobilized via direct coordination of the metal with the support (Figure 8A). In general this approach leads to distortion of the stereogenic center, producing catalysts with a lower activity than the homogeneous counterpart. Alternatively, complexes can be immobilized by anchoring them to the support surface by a periphery of the ligand, avoiding modifications on the active metal site (Figure 8B).

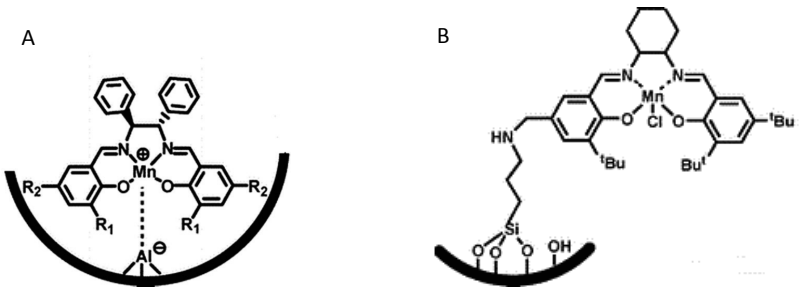

Figure 8 Examples of different approaches to graft metal complexes on metal oxide surface (adapted from reference 7)

Another method to immobilize complexes on porous materials is encapsulation, often referred to as "ship in the bottle" approach. In this approach a metal complex is assembled from smaller building blocks inside the cage of porous materials and after the synthesis the relatively large metal complex is trapped inside the structure. The advantage of this approach is that the complex does not suffer much modification, having the possibility to keep the same catalytic activity as the homogeneous counterpart. If the synthesis of the complex is carried out directly inside the pores, it can result in the incomplete formation of complex. For example, Garcia et al. showed using thermogravimetry–differential scanning calorimetry (TG–DSC) that the ratio between salen ligand/Mn(III) was 1.3, indicating a slight excess of the uncomplexed ligand inside zeolite cages.

Thesis Outline and Scope

The research in this PhD thesis is focused on confinement of metal species (particles and complexes) inside mesoporous silica. The resulting materials were used as catalysts for the Heck, the Suzuki and sulfoxidation reactions. For this purpose, a number of methodologies were used to produce active phases inside mesoporous silica such as incipient wetness impregnation, ion adsorption, ligand assisted methods and the ship in the bottle approach.

In the first part of this thesis **(Chapter 2)**, we report the synthesis and characterization of plugged hexagonal templated silica or plugged SBA-15. Plugged SBA-15 materials were prepared with a variation in the degree of constriction of the pores by changing the hydrothermal treatment temperature and the silica precursor addition step. We showed the presence of nanocavities in plugged SBA-15, provided quantitative information about the nanocavities dimensions and the plugs distribution of these materials using gas physisorption (argon and nitrogen) and imaging silver nanostructures inside SBA-15 and plugged SBA-15.

In the second part of this thesis **(Chapter 3)**, Pd nanoparticles were synthesized on non-functionalized and functionalized SBA-15 grafted with thiol or amine groups. The resulting materials were used as catalysts to study the influence of these functional groups for Pd particles of similar size (~2 nm) on the Heck reaction using iodide substrates. The non-functionalized catalysts lost their activity quickly because of Pd leaching and particle growth. However, if a mixed solvent that consisted of toluene and DMF was used and thiol groups were grafted onto SBA-15, we were able to reduce the Pd leaching and particle growth and thus obtain a more stable catalyst in which an important role of the ligands was to recapture Pd. However, heterogeneity tests, such as a hot filtration test and poisoning experiments, gave a strong indication that Pd leached from the support and that homogeneous Pd species were mainly responsible for the activity. Pd on S-functionalized SBA-15 was able to catalyze the Heck reaction using different substrates to achieve good activity and selectivity in most cases.

In **Chapter 4**, palladium nanoparticles of similar size of ~2 nm were synthesized on different silica-based materials all functionalized with thiol groups i.e., Aerosil-380, SBA-15, Plugged SBA-15 and m-MCF. The resulting materials were used to study the influence of confinement of Pd nanoparticles in functionalized silica support on the Heck and the Suzuki reaction. In the case of the Heck reaction, for all catalysts it was proven that leached Pd species were responsible for activity. However, the catalysts based on ordered mesoporous silica were still able to restrict Pd particle growth giving rise to an enhanced stability. For the Suzuki reaction, stronger alkaline conditions were required and catalysts based on plugged SBA-15 showed a higher stability than those based on SBA-15 and m-MCF which both collapsed after the first cycle. At almost identical Pd particle size, ordered mesoporous materials enhanced stability and Pd particle growth was slowed down but not fully suppressed.

In **Chapter 5**, solid catalysts which are heterogeneous at macroscopic scale but homogeneous at microscopic level were prepared by the encapsulation of Fe(salen) by a "ship in a bottle" approach. This approach permits to synthesize inside the nanocages of SBA-16 and m-MCF a Fe(salen) complex having conformational freedom and behaving as a complex in solution. These materials were used as catalysts for asymmetric oxidation of sulfides. The entrance sizes of SBA-16 and m-MCF were tuned by changing synthesis parameters and the silylation of silica surface with n-propyl groups. This control of entrance sizes resulted in materials with different Fe(salen) loading. Chiral Fe(salen) trapped in the mesoporous materials showed almost the same activity and enantioselectivity as the homogeneous counterpart albeit that stability was limited as yet.

References

1. K. P. de Jong, *Synthesis of Solid Catalysts*, Wiley-VCH, Weinheim, 2009.
2. W. Schmidt, *ChemCatChem*, 2009, **1**, 53.
3. J. M. Thomas and R. J. P. Williams, *Philos. Trans. A. Math. Phys. Eng. Sci.*, 2005, **363**, 765.

4. R. Ballini, *Eco-Friendly Synthesis of Fine Chemicals*, Royal Society of Chemistry, 2009.

5. R. Kureshy, I. Ahmad, N. Khan, S. Abdi, K. Pathak and R. Jasra, *J. Catal.*, 2006, **238**, 134.

6. R. L. Oliveira, J. B. F. Hooijmans, P. E. de Jongh, R. J. M. Klein Gebbink and K. P. de Jong, *ChemCatChem*, 2014, **6**, 1.

7. C. Li, H. Zhang, D. Jiang and Q. Yang, *Chem. Commun. (Camb).*, 2007, 547.

8. X. Ma, Y. Zhou, J. Zhang, A. Zhu, T. Jiang and B. Han, *Green Chem.*, 2008, **10**, 59.

9. A. Taguchi and F. Schüth, *Microporous Mesoporous Mater.*, 2005, **77**, 1.

10. C. M. Crudden, M. Sateesh, R. Lewis and C. Kl, *J. Am. Chem. Soc.*, 2005, **127**, 10045.

11. M. Shakeri, R. J. M. Klein Gebbink, P. E. de Jongh and K. P. de Jong, *Angew. Chemie*, 2013, **125**, 11054.

12. K. Shimizu, S. Koizumi, T. Hatamachi, H. Yoshida, S. Komai, T. Kodama and Y. Kitayama, *J. Catal.*, 2004, **228**, 141.

13. D. Zhao, Q. Huo, J. Feng, B. F. Chmelka and G. D. Stucky, *J. Am. Chem. Soc.*, 1998, **120**, 6024.

14. F. Hoffmann, M. Cornelius, J. Morell and M. Fröba, *Angew. Chem. Int. Ed. Engl.*, 2006, **45**, 3216.

15. R. L. Oliveira, D. Zanchet, P. K. Kiyohara and L. M. Rossi, *Chemistry*, 2011, **17**, 4626.

16. L. M. Rossi, L. L. R. Vono, F. P. Silva, P. K. Kiyohara, E. L. Duarte and J. R. Matos, *Appl. Catal. A Gen.*, 2007, **330**, 139.

17. N. J. S. Costa, P. K. Kiyohara, A. L. Monteiro, Y. Coppel, K. Philippot and L. M. Rossi, *J. Catal.*, 2010, **276**, 382.

18. M. Guerrero, N. J. S. Costa, L. L. R. Vono, L. M. Rossi, E. V. Gusevskaya and K. Philippot, *J. Mater. Chem. A*, 2013, **1**, 1441.

19. R. L. Oliveira, P. K. Kiyohara and L. M. Rossi, *Green Chem.*, 2010, **12**, 144.

20. S. C. Tsang, V. Caps, I. Paraskevas, D. Chadwick and D. Thompsett, *Angew. Chemie*, 2004, **116**, 5763.

21. A.-H. Lu, E. L. Salabas and F. Schüth, *Angew. Chem. Int. Ed. Engl.*, 2007, **46**, 1222.

22. V. Polshettiwar, R. Luque, A. Fihri, H. Zhu, M. Bouhrara and J.-M. Basset, *Chem. Rev.*, 2011, **111**, 3036.

23. L. M. Rossi, M. A. S. Garcia and L. L. R. Vono, *J. Braz. Chem. Soc.*, 2012, **23**, 1959.

24. L. Shen, W. Wu, R. Liang, R. Lin and L. Wu, *Nanoscale*, 2013, **5**, 9374.

25. L. Ma, C. Abney and W. Lin, *Chem. Soc. Rev.*, 2009, **38**, 1248.

26. J. Lee, O. K. Farha, J. Roberts, K. a Scheidt, S. T. Nguyen and J. T. Hupp, *Chem. Soc. Rev.*, 2009, **38**, 1450.

27. M. Ranocchiari and J. A. van Bokhoven, *Phys. Chem. Chem. Phys.*, 2011, **13**, 6388.

28. F. Llabresixamena, a Abad, a Corma and H. Garcia, *J. Catal.*, 2007, **250**, 294.

29. J. Liu, L. Chen, H. Cui, J. Zhang, L. Zhang and C.-Y. Su, *Chem. Soc. Rev.*, 2014, **43,** 6011.

30. S. van Donk, A. H. Janssen, J. H. Bitter and K. P. de Jong, *Catal. Rev.*, 2003, **45**, 297.

31. A. Corma, V. Fornes, S. B. Pergher, T. L. M. Maesen and J. G. Buglass, *Nature*, 1998, **396**, 353.

32. B. W. Holderich, M. Hesse and F. Naumann, *Angew. Chem. Int. Ed. Engl.*, 1988, **27**, 226.

33. A. Corma, *J. Catal.*, 2003, **216**, 298.

34. J. Weitkamp, *Solid State Ionics*, 2000, **131**, 175.

35. D. Bavykin, a Lapkin, P. Plucinski, J. Friedrich and F. Walsh, *J. Catal.*, 2005, **235**, 10.

36. B. Abida, L. Chirchi, S. Baranton, T. W. Napporn, H. Kochkar, J.-M. Léger and A. Ghorbel, *Appl. Catal. B Environ.*, 2011, **106**, 609.

37. S. van Dommele, K. P. de Jong and J. H. Bitter, *Chem. Commun.*, 2006, 4859.

38. Y. Zhang and S. N. Riduan, *Chem. Soc. Rev.*, 2012, **41**, 2083.

39. M. a. Bizeto, A. L. Shiguihara and V. R. L. Constantino, *J. Mater. Chem.*, 2009, **19**, 2512.

40. T. C. Damato, C. C. S. De Oliveira, R. A. Ando and P. H. C. Camargo, *Langmuir*, 2013, **29**, 1642.

41. T. S. Reger and K. D. Janda, *J. Am. Chem. Soc.*, 2000, **122**, 6929.

42. W. Chen, Z. Fan, X. Pan and X. Bao, *J. Am. Chem. Soc.*, 2008, **130**, 9414.

43. L. Yang, W. Yang and Q. Cai, *J. Phys. Chem. C*, 2007, **111**, 16613.

44. M. Lefèvre, E. Proietti, F. Jaouen and J.-P. Dodelet, *Science*, 2009, **324**, 71.

45. L. Torrentemurciano, a Lapkin, D. Bavykin, F. Walsh and K. Wilson, *J. Catal.*, 2007, **245**, 272.

46. G. Ertl, M. Huber, S. B. Lee, Z. Paal and M. Weiss, *Appl. Surf. Sci.*, 1981, **8**, 373.

47. G. Ertl, S. B. Lee, M. Weiss, *Surf. Sci.*, 1982, **114**, 515.

48. C. C. Cassol, A. P. Umpierre, G. Machado, S. I. Wolke and J. Dupont, *J. Am. Chem. Soc.*, 2005, **127**, 3298.

49. Y. Ji, S. Jain and R. J. Davis, *J. Phys. Chem. B*, 2005, **109**, 17232.

50. N. T. S. Phan, M. Van Der Sluys and C. W. Jones, *Adv. Synth. Catal.*, 2006, **348**, 609.

51. J. a. Widegren and R. G. Finke, *J. Mol. Catal. A Chem.*, 2003, **198**, 317.

52. J. M. Richardson and C. W. Jones, *Adv. Synth. Catal.*, 2006, **348**, 1207.

53. G. Budroni, a Corma, H. Garcia and a Primo, *J. Catal.*, 2007, **251**, 345.

54. G. Park, S. Lee, S. J. Son and S. Shin, *Green Chem.*, 2013, **15**, 3468.

55. J. Webb, S. Macquarrie, K. Mceleney and C. Crudden, *J. Catal.*, 2007, **252**, 97.

56. J. Richardson and C. Jones, *J. Catal.*, 2007, **251**, 80.

57. S. G. Fiddy, J. Evans, T. Neisius, M. a Newton, N. Tsoureas, A. a D. Tulloch and A. A. Danopoulos, *Chemistry*, 2007, **13**, 3652.

58. S. Reimann, J. St, R. Frahm, W. Kleist, J. Grunwaldt and A. Baiker, *J. Am. Chem. Soc.*, 2011, **133**, 3921..

59. H. Yoshida, Y. Kuwauchi, J. R. Jinschek, K. Sun, S. Tanaka, M. Kohyama, S. Shimada, M. Haruta and S. Takeda, *Science*, 2012, **335**, 317.

60. C. T. Kresge, M. E. Leonowicz, W. J. Roth, J. C. Vartuli and J. S. Beck, *Nature*, 1992, **359**, 710.

61. J. S. Beck, K. D. Schmitt, J. B. Higgins and J. L. Schlenkert, *J. Am. Chem. Soc.*, 1992, **114**, 10834.

62. D. Zhao, J. Feng, Q. Huo, N. Melosh, G. H. Fredrickson, B. F. Chmelka and G. D. Stucky, *Science*, 1998, **279**, 548.

63. F. Kleitz, D. Liu, G. M. Anilkumar, I. Park, L. A. Solovyov, A. N. Shmakov and R. Ryoo, *J. Phys. Chem. B*, 2003, **107**, 14296.

64. Y. Wan and D. Zhao, *Chem. Rev.*, 2007, **107**, 2821.

65. V. Meynen, P. Cool and E. F. Vansant, *Microporous Mesoporous Mater.*, 2009, **125**, 170.

66. J. Fan, C. Yu, F. Gao, J. Lei, B. Tian, L. Wang, Q. Luo, B. Tu, W. Zhou and D. Zhao, *Angew. Chem. Int. Ed. Engl.*, 2003, **42**, 3146.

67. R. Métivier, I. Leray, B. Lebeau and B. Valeur, *J. Mater. Chem.*, 2005, **15**, 2965.

68. I. I. Slowing, J. L. Vivero-Escoto, C.-W. Wu and V. S.-Y. Lin, *Adv. Drug Deliv. Rev.*, 2008, **60**, 1278.

69. M. Vallet-Regí, F. Balas and D. Arcos, *Angew. Chem. Int. Ed. Engl.*, 2007, **46**, 7548.

70. A. Walcarius, *Chem. Soc. Rev.*, 2013, **42**, 4098.

71. R. J. White, R. Luque, V. L. Budarin, J. H. Clark and D. J. Macquarrie, *Chem. Soc. Rev.*, 2009, **38**, 481.

72. L. Mercier, *Adv. Mater.*, 1997, **9**, 500.

73. G. Prieto, M. Shakeri, K. P. de Jong and P. E. de Jongh, *ACS Nano*, 2014, 8, 2522.

74. P. Van der Voort, P. I. Ravikovitch, K. P. De Jong, a V Neimark, a H. Janssen, M. Benjelloun, E. Van Bavel, P. Cool, B. M. Weckhuysen and E. F. Vansant, *Chem. Commun. (Camb).*, 2002, 1010.

75. P. Van Der Voort, P. I. Ravikovitch, K. P. De Jong, M. Benjelloun, E. Van Bavel, A. H. Janssen, A. V Neimark, B. M. Weckhuysen and E. F. Vansant, *J. Phys. Chem. B*, 2002, **123**, 5873.

76. E. B. Celer, M. Kruk, Y. Zuzek and M. Jaroniec, *J. Mater. Chem.*, 2006, **16**, 2824.

77. M. Shakeri, R. J. M. Klein Gebbink, P. E. de Jongh and K. P. de Jong, *Microporous Mesoporous Mater.*, 2013, **170**, 340.

78. T. Kjellman, S. Asahina, J. Schmitt, O. Terasaki and V. Alfredsson, *Chem. Mater.*, 2013, **25**, 4105.

79. M. Mandal and M. Kruk, *Chem. Mater.*, 2012, **24**, 149.

80. F. Kleitz, T. Kim and R. Ryoo, *Langmuir*, 2006, **22**, 440.

81. P. I. Ravikovitch and A. V Neimark, *Langmuir*, 2002, **18**, 1550.

82. J. Fan, C. Yu, J. Lei, Q. Zhang, T. Li, B. Tu, W. Zhou and D. Zhao, *J. Am. Chem. Soc.*, 2005, **127**, 10794.

83. T. Yu, H. Zhang, X. Yan, Z. Chen, X. Zou, P. Oleynikov and D. Zhao, *J. Phys. Chem. B*, 2006, **110**, 21467.

84. M. Shakeri, L. Roiban, V. Yazerski, G. Prieto, J. M. K. Gebbink, P. E. de Jongh and K. P. de Jong, *ACS Catal.*, 2014, **4**, 3791.

85. J. E. Mondloch, E. Bayram and R. G. Finke, *J. Mol. Catal. A Chem.*, 2012, **355**, 1.

86. L. S. Ott and R. G. Finke, *Coord. Chem. Rev.*, 2007, **251**, 1075.

87. J. D. A. Iii and R. G. Finke, *J. Mol. Catal. A Chem.*, 1999, **145**, 1.

88. J. M. Campelo, D. Luna, R. Luque, J. M. Marinas and A. a Romero, *ChemSusChem*, 2009, **2**, 18.

89. J. Sun and X. Bao, *Chemistry*, 2008, **14**, 7478.

90. N. Zheng and G. D. Stucky, *J. Am. Chem. Soc.*, 2006, **128**, 14278.

91. D. Cai, J. M. Mataraza, Z.-H. Qin, Z. Huang, J. Huang, T. C. Chiles, D. Carnahan, K. Kempa and Z. Ren, *Nat. Methods*, 2005, **2**, 449.

92. X. Hu and S. Dong, *J. Mater. Chem.*, 2008, **18**, 1279.

93. D. Astruc, F. Lu and J. R. Aranzaes, *Angew. Chem. Int. Ed. Engl.*, 2005, **44**, 7852.

94. U. Junges and B. Krutzschc, *J. Chem. Soc. Chem. Commun.*, 1995, 2283.

95. S. Besson, T. Gacoin, C. Ricolleau and J.-P. Boilot, *Chem. Commun.*, 2003, 360.

96. M. H. Huang, A. Choudrey and P. Yang, *Chem. Commun.*, 2000, 1063.

97. W. A. Spieker and J. R. Regalbuto, *Chem. Eng. Sci.*, 2001, **56**, 3491.

98. M. Schreier, J. R. Regalbuto, *J. Catal.*, 2004, **225**, 190.

99. J. Miller, M. Schreier, A. J. Kropf, J. R. Regalbuto *J. Catal.*, 2004, **225**, 203.

100. L. Jiao and J. R. Regalbuto, *J. Catal.*, 2008, **260**, 329.

101. L. Jiao and J. R. Regalbuto, *J. Catal.*, 2008, **260**, 342.

102. N. J. S. Costa and L. M. Rossi, *Nanoscale*, 2012, **4**, 5826.

103. A. R. Hajipour and G. Azizi, *Green Chem.*, 2013, **15**, 1030.

104. T. Posset, F. Rominger, J. Blumel, , *Chem. Mater.*, 2005, **17**, 586.

105. C. P. Mehnert, *Chemistry*, 2004, **11**, 50.

106. S. Udayakumar, M. Lee, H. Shim, S. Park and D. Park, *Catal. Commun.*, 2009, **10**, 659.

107. J. Huang, M. Wang, S. Zhang, B. Hu and H. Li, *Journal Phys. Chem. C*, 2011, **115**, 22514.

108. S. C. Bourque, F. Maltais, W.-J. Xiao, O. Tardif, H. Alper, P. Arya and L. E. Manzer, *J. Am. Chem. Soc.*, 1999, **121**, 3035.

109. S. Antebi, P. Arya, L. E. Manzer and H. Alper, *J. Org. Chem.*, 2002, **67**,6623.

110. M. J. Jacinto, F. P. Silva, P. K. Kiyohara, R. Landers and L. M. Rossi, *ChemCatChem*, 2012, **4**, 698.

111. J. Weitkamp, *Solid State Ionics*, 2000, **131**, 175.

112. J. C. Kuo, (Mobil Oil Corporation) US Patent 4046830 A, 1977.

113. S. B. Ogunwumi and T. Bein, *Chem. Commun.*, 1997, 901.

114. A. Nisar, Y. Lu, J. Zhuang and X. Wang, *Angew. Chem. Int. Ed. Engl.*, 2011, **50**, 3187.

115. R. M. Anisur, J. Shin, H. H. Choi, K. M. Yeo, E. J. Kang and I. S. Lee, *J. Mater. Chem.*, 2010, **20**, 10615.

116. N. Erathodiyil, S. Ooi, A. M. Seayad, Y. Han, S. S. Lee and J. Y. Ying, *Chemistry*, 2008, **14**, 3118.

117. J. Lee, J. C. Park and H. Song, *Adv. Mater.*, 2008, **20**, 1523.

118. R. W. J. Scott, A. K. Datye and R. M. Crooks, *J. Am. Chem. Soc.*, 2003, **1**, 3708.

119. P. Core, S. Fibers, R. V April, V. Re, M. Recei and V. June, *Macromolecules*, 2007, **40**, 6032.

120. I. Gitsov, J. Hamzik, J. Ryan, A. Simonyan, J. P. Nakas, S. Omori, A. Krastanov, T. Cohen and S. W. Tanenbaum, *Biomacromolecules*, 2008, **9**,804.

121. F. Bedioui, *Coord. Chem. Rev.*, 1995, **144**, 39.

122. M. Shakeri, R. J. M. Klein Gebbink, P. E. de Jongh and K. P. de Jong, *Angew. Chem. Int. Ed. Engl.*, 2013, **52**, 10854.

123. B. Li, S. Bai, X. Wang, M. Zhong, Q. Yang and C. Li, *Angew. Chem. Int. Ed. Engl.*, 2012, **51**, 11517.

124. E. Möllmann, P. Tomlinson and W. . Hölderich, *J. Mol. Catal. A Chem.*, 2003, **206**, 253.

125. N. Madhavan and M. Weck, *Adv. Synth. Catal.*, 2008, **350**, 419.

126. S. Bai, B. Li, J. Peng, X. Zhang, Q. Yang and C. Li, *Chem. Sci.*, 2012, **3**, 2864.

127. L. Canali, E. Cowan, C. L. Gibson, D. C. Sherrington and H. Deleuze, *Chem. Commun.*, 1998, 2561.

128. L. K. Yeung and R. M. Crooks, *Nano Lett.*, 2001, **1**, 14.

129. B. W. Han, P. Kohler-redlich, C. Scheu, F. Ernst, M. Rühle, N. Grobert, M. Terrones, H. W. Kroto and D. R. M. Walton, *Adv. Mater.*, 2000, 1356.

130. Z. Chen, Z.-M. Cui, F. Niu, L. Jiang and W.-G. Song, *Chem. Commun. (Camb).*, 2010, **46**, 6524.

131. B. M. Rossbach, K. Leopold and R. Weberskirch, *Angew. Chem. Int. Ed. Engl.*, 2006, **45**, 1309.

132. Y. Lu, S. Proch, M. Schrinner, M. Drechsler, R. Kempe and M. Ballauff, *J. Mater. Chem.*, 2009, **19**, 3955.

133. Y. Hao, Y. Chong, S. Li and H. Yang, *J. Phys. Chem. C*, 2012, **116**, 6512.

134. H. Yang, L. Zhang, P. Wang, Q. Yang and C. Li, *Green Chem.*, 2009, **11**, 257.

135. A. de Meijere and F. Diderich, *Metal-Catalyzed Cross-Coupling Reactions*, Wiley-VCH, 2008.

136. J. G. de Vries, *Can. J. Chem.*, 2001, **79**, 1086.

137. R. F. Heck, *J. Am. Chem. Soc.*, 1968, **90**, 5518.

138. R. F. Heck, *J. Am. Chem. Soc.*, 1968, **90**, 5526.

139. R. F. Heck, *J. Am. Chem. Soc.*, 1968, **90**, 5531.

140. R. F. Heck, *J. Am. Chem. Soc.*, 1968, **90**, 5538.

141. R. F. Heck, *J. Am. Chem. Soc.*, 1968, **90**, 5542.

142. H. A. Dieck and F. Heck, *J. Am. Chem. Soc.*, 1973, **95**,1133.

143. R. F. Heck and J. P. Nolley, *J. Org. Chem.*, 1972, **37**, 2320.

144. N. Miyaura, K. Yamada and A. Suzuki, *Tetrahedron Lett.*, 1979, **20**, 3437.

145. A. Miyaura, Norio; Suzuki, *J. Chem. Soc. Chem. Commun.*, 1979, 866.

146. B. Ei-ichi, *J. Chem. Soc. Chem. Commun.*, 1976, 596.

147. E. Baba, Shigeru; Negishi, *J. Am. Chem. Soc.*, 1976, **98**, 6729.

148. N. Negishi, Ei-ichi; King, Anthony O.; Okukado, *J. Org. Chem.*, 1977, **42**, 1821.

149. T. J. Colacot, *Platin. Met. Rev.*, 2011, **55**, 84.

150. D. Camp, C. F. Matthews, S. T. Neville, M. Rouns, R. W. Scott and Y. Truong, *Org. Process Res. Dev.*, 2006, **10**, 814.

151. C. Torborg and M. Beller, *Adv. Synth. Catal.*, 2009, **351**, 3027.

152. R. K. Anderson, R. D. Larsen, R. Verhoeven, B. Xiang, M. Belley and M. Labelle, *J. Org. Chem.*, 2000, **65**, 3731.

153. D. H. B. Ripin, D. E. Bourassa, T. Brandt, M. J. Castaldi, H. N. Frost, J. Hawkins, P. J. Johnson, S. S. Massett, K. Neumann, J. Phillips, J. W. Raggon, P. R. Rose, J. L. Rutherford, B. Sitter, A. M. Stewart, M. G. Vetelino and L. Wei, *Org. Process Res. Dev.*, 2005, **9**, 440.

154. J. W. Raggon and W. M. Snyder, *Org. Process Res. Dev.*, 2002, **6**, 1999.

155. U. H. Methodology, *Org. Process Res. Dev.*, 2002, **6**, 811.

156. J. F. Perkins (Pfizer Ltd.) European Patent 1 0888 817 B1, 2001.

157. T. C. Wu, (Albermale) U.S. Patent 5.315.026, 1994.

158. A. Synthesis and E. Enantiomer, *J. Am. Chem. Soc.*, 1993, **115**, 11028.

159. Z. Niu, Q. Peng, Z. Zhuang, W. He and Y. Li, *Chemistry*, 2012, **18**, 9813.

160. L. Yin and J. Liebscher, *Chem. Rev.*, 2007, **107**, 133.

161. Á. Molnár, *Chem. Rev.*, 2011, **111**, 2251.

162. L. Djakovitch, K. Koehler, A. Institut and D.-G. Mu, *J. Am. Chem. Soc.*, 2001, **123**, 5990.

163. M. L. Kantam, R. Chakravarti, V. R. Chintareddy, B. Sreedhar and S. Bhargava, *Adv. Synth. Catal.*, 2008, **350**, 2544.

164. A. Monopoli, A. Nacci, V. Calò, F. Ciminale, P. Cotugno, A. Mangone, L. C. Giannossa, P. Azzone and N. Cioffi, *Molecules*, 2010, **15**, 4511.

165. B. Altava, M. I. Burguete, E. García-Verdugo, N. Karbass, S. V. Luis, A. Puzary and V. Sans, *Tetrahedron Lett.*, 2006, **47**, 2311.

166. M. I. Burguete, E. García-Verdugo, I. Garcia-Villar, F. Gelat, P. Licence, S. V. Luis and V. Sans, *J. Catal.*, 2010, **269**, 150.

167. M. Kantam, S. Roy, M. Roy, M. Subhas, P. R. Likhar, B. Sreedhar and B. Choudary, *Synlett*, 2006, **17**, 2747.

168. C.-A. Lin and F.-T. Luo, *Tetrahedron Lett.*, 2003, **44**, 7565.

169. C. Luo, Y. Zhang and Y. Wang, *J. Mol. Catal. A Chem.*, 2005, **229**, 7.

170. M.-J. Jin and D.-H. Lee, *Angew. Chem. Int. Ed. Engl.*, 2010, **49**, 1119.

171. A. Papp, G. Galbács and Á. Molnár, *Tetrahedron Lett.*, 2005, **46**, 7725.

172. A. M. Trzeciak and J. J. Ziółkowski, *Coord. Chem. Rev.*, 2007, **251**, 1281.

173. C. Yao, H. Li, H. Wu, Y. Liu and P. Wu, *Catal. Commun.*, 2009, **10**, 1099.

174. R. G. Heidenreich, J. G. . Krauter, J. Pietsch and K. Köhler, *J. Mol. Catal. A Chem.*, 2002, **182**, 499.

175. K. Köhler, M. Wagner and L. Djakovitch, *Catal. Today*, 2001, **66**, 105.

176. M. Wagner, *Top. Catal.*, 2000, **13**, 319.

177. H. Yang, X. Han, G. Li and Y. Wang, *Green Chem.*, 2009, **11**, 1184.

178. J. H. Clark, D. J. Macquarrie and E. B. Mubofu, *Green Chem.*, 2000, **2**, 53.

179. B. Karimi and D. Enders, *Org. Lett.*, 2006, **8**, 1237.

180. V. Polshettiwar and Á. Molnár, *Tetrahedron*, 2007, **63**, 6949.

181. M. Pagliaro, V. Pandarus, F. Béland, R. Ciriminna, G. Palmisano and P. D. Carà, *Catal. Sci. Technol.*, 2011, **1**, 736.

182. K. Köhler, R. G. Heidenreich, J. G. E. Krauter and J. Pietsch, *Chemistry*, 2002, **8**, 622.

183. S. Macquarrie, B. Nohair, J. H. Horton, S. Kaliaguine and C. M. Crudden, *J. Phys. Chem. C*, 2010, **114**, 57.

184. B. Nohair, S. Macquarrie, C. M. Crudden and S. Kaliaguine, *J. Phys. Chem. C*, 2008, **112**, 6065.

185. G. Zhang, H. Zhou, J. Hu, M. Liu and Y. Kuang, *Green Chem.*, 2009, **11**, 1428.

186. A. Kabalka, L. Wang, R. M. Pagni, C. M. Hair and V. Namboodiri, *Synthesis (Stuttg).*, 2002, **2**, 217.

187. P. Pfeiffer, E. Breith, E. Lubbe and T. Tsumaki, *Justus Leibigs Ann. Chem.*, 1933, **503**, 84.

188. C. Baleizao and H. Garcia, *Chem. Rev.*, 2006, **106**, 3987.

189. W. Zhang and E. N. Jacobsen, *J. Org. Chem.*, 1991, **56**, 2296.

190. W. Zhang, J. L. Loebach and S. R. Wilson, *J. Am. Chem. Soc.*, 1990,**112**, 2801.

191. S. Aerts, H. Weyten, A. Buekenhoudt, L. E. M. Gevers, I. F. J. Vankelecom, P. A. Jacobs, A. B. Sciences and K. U. Leuven, *Chem. Commun.*, 2004, 710.

192. M. Janssen and O. Synthesis, *Tetrahedron: Asymmetry*, 1997, **8**, 3481.

193. N. S. Venkataramanan, S. Premsingh, S. Rajagopal and K. Pitchumani, *J. Org. Chem.*, 2003, **68**, 7460.

194. B. Saito and T. Katsuki, *Tetrahedron Lett.*, 2001, **42**, 8333.

195. G. E. O'Mahony, A. Ford and A. R. Maguire, *J. Sulfur Chem.*, 2013, **34**, 301.

196. B. Saito and T. Katsuki, *Tetrahedron Lett.*, 2001, **42**, 3873.

197. V. K. Sivasubramanian, M. Ganesan, S. Rajagopal and R. Ramaraj, *J. Org. Chem.*, 2002, **67**, 1506.

198. W.-L. Man, W. W. Y. Lam, S.-M. Yiu, T.-C. Lau and S.-M. Peng, *J. Am. Chem. Soc.*, 2004, **126**, 15336.

199. Z. Li, K. R. Conser and E. N. Jacobsen, *J. Am. Chem. Soc.*, 1993, **115**, 5326.

200. R. B. Bedford, D. W. Bruce, R. M. Frost, W. Goodby and M. Hird, *Chem. Commun.*, 2004, 2822.

201. V. K.-Y. Lo, Y. Liu, M.-K. Wong and C.-M. Che, *Org. Lett.*, 2006, **8**, 1529.

202. M. Bakherad, A. Keivanloo, B. Bahramian and M. Hashemi, *Tetrahedron Lett.*, 2009, **50**, 1557.

203. Z. Zeng, G. Zhao, Z. Zhou and C. Tang, *European J. Org. Chem.*, 2008, **73**, 1615.

204. S. S. Kim, J. M. Kwak and S. C. George, *Appl. Organomet. Chem.*, 2007, **21**,809.

205. C. Baleizão, B. Gigante, H. García and A. Corma, *Tetrahedron*, 2004, **60**, 10461.

206. L. E. Martinez, J. L. Leighton, D. H. Carsten and E. N. Jacobsen, *J. Am. Chem. Soc.*, 1995, **117**, 5897.

207. S. E. Schaus, J. Brånalt and E. N. Jacobsen, *J. Org. Chem.*, 1998, **3263**, 403.

208. A. Watanabe, T. Uchida and T. Katsuki, *Tetrahedron Lett.*, 2002, **43**, 4481.

209. P. G. Cozzi, *Angew. Chem. Int. Ed. Engl.*, 2003, **42**, 2895.

Chapter 2

Mapping nanocavities in plugged SBA-15 with confined silver nanostructures

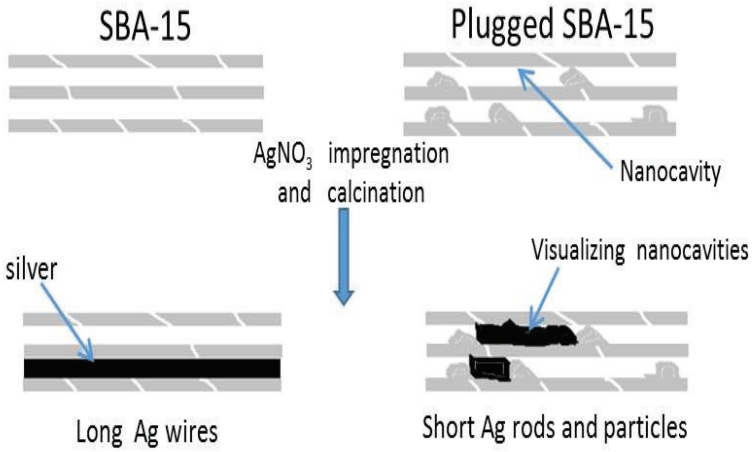

Abstract

Silver nanostructures inside the pores of SBA-15 and plugged SBA-15 were synthesized and imaged, providing for the first time quantitative information about the nanocavity dimensions and plug distributions in plugged SBA-15.

Based on: Rafael L. Oliveira , Mozaffar Shakeri , Johannes D. Meeldijk, Krijn P. de Jong and Petra E. de Jongh. Mapping nanocavities in plugged SBA-15 with confined silver nanostructures, Micro. Meso. Mater., 2015, 201, 234-239.

Introduction

The synthesis of ordered mesoporous materials (OMM) has received much attention in the last two decades.[1] OMM have large surface areas, uniform pore sizes and tunable periodic pore arrangements. These properties make them attractive for applications in various fields such as catalysis, adsorption and drug delivery.[2–6]SBA-15 is the most studied mesoporous silica, because of its facile synthesis and stability.

In 2002, a new type of SBA-15 was reported and named plugged hexagonal templated silica (PHTS) or plugged SBA-15.[7,8] These materials are synthesized using an excess of tetraethyl orthosilicate (TEOS), the silica precursor, leading to an ordered mesoporous silica with constricted pores.[9,10]By varying the synthesis parameters, the extent of the plugging can be influenced producing materials in which either all pores contain plugs ("completely plugged") or only a fraction of the pores contains plugs ("partially plugged"). In the case of PHTS materials the plugging is apparent from an ink bottle hysteresis in the N_2 physisorption isotherm, as liquid N_2 remains trapped by the narrow (plugged) entrances of the pores, resulting in delayed desorption. Moreover, these solids exhibit a remarkable mechanical and hydrothermal stability. In recent years, alternative strategies to produce PHTS materials have been proposed using different silica precursors and procedures.[11–14]

Despite the importance of PHTS materials, the exact details of their structure have remained elusive. Van der Voort et al. proposed that the cylindrical SBA-15 channels were fully plugged, and only accessible via micropores in the channel walls.[7,8] On the other hand, Ryoo et al. explained the characteristics by an appreciable mesopore surface corrugation, possibly related to incomplete formation of plugs.[15] Zhao et al. pointed out that these solids just have a fraction of ordered mesopores exhibiting porous plugs within SBA-15 mesochannels.[16]

In general, N_2 physisorption has been used to characterize porosity. Information about the size of the pores can be obtained from the adsorption branch and the accessibility of the pores (entrance sizes) can be derived from the desorption branch of the isotherm. However,

the limitation is that only entrance sizes larger than ~ 4.7 nm can be characterized.[17]For plugged SBA-15, it is generally found that the entrance size is smaller than this limit. Argon at 77K is an alternative as the capillary evaporation of argon at 77K happens at lower relative pressures extending its use to analyze a wider range of constrictions in the porous structure, limited to entrance sizes larger than ~ 3.6 nm. [18]

Other techniques such as electron tomography,[19,20] modification of the silica surface using organosilanes[21] and metal oxide impregnation[22] have also been used to study these solids. However, none of these techniques is able to measure and quantify the nature of the plugging of the PHTS. A promising option is the use of replicas which are produced by filling the mesoporous structure with a carbon or a metal precursor (Au, Pt, Pd and others) followed by thermal treatment and silica removal.[23–27]This technique has been used to study the entrance size of 3-D mesoporous silica, for example FDU-12, [28] and to identify the connections between pores in SBA-15.[29]

In this chapter, we present for the first time a study of the spatial distribution of the plugs, the dimensions and accessibility of the nanocavities in PHTS by synthesizing and imaging silver nanostructures confined inside the porous structure using TEM analysis.

Results and discussion

PHTS structure

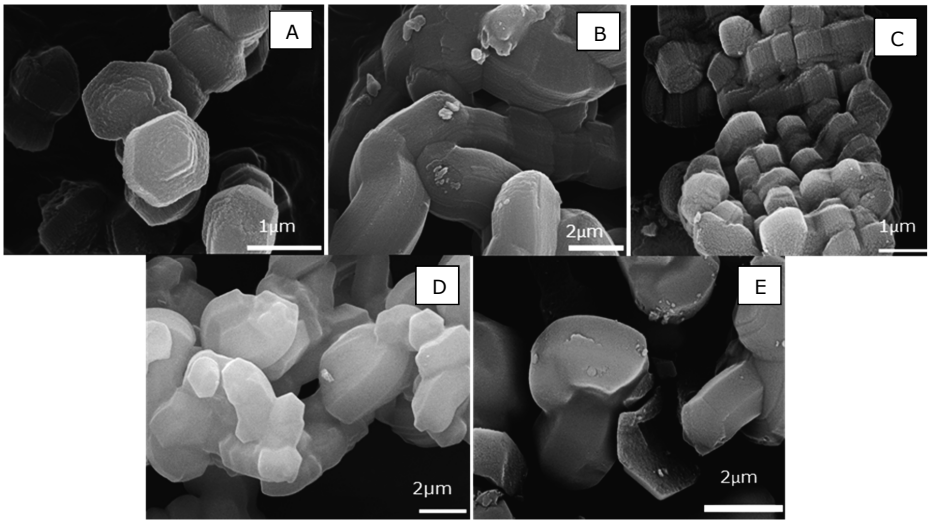

Figure 1 SEM images: (A) SBA-15, (B) PHTS-1-60, (C) PHTS-2-80, (D) PHTS-1-80, (E) PHTS-1-100

The small-angle powder XRD patterns of PHTS (Appendices, Figure A1) shows three diffraction peaks that can be assigned to the (100), (110) and (200) planes, corresponding to a hexagonal *p6mm* arrangement of the pores. The peaks have lower intensities for PHTS than for SBA-15. This can be explained by the presence of plugs inside the pores, which decrease the difference in electron density between pores and silica walls. SEM (Figure 1) showed that the plugged SBA-15 particles have a uniform morphology with sizes of 1-2 μm and the shape of the particles was affected slightly by the hydrothermal synthesis temperatures. TEM analysis (Figure 2) demonstrated the ordered pore structure of the PHTS materials. It is possible to observe that increasing the hydrothermal temperature results in larger pores. HAADF-STEM was used to study the PHTS-1-60 showing the constrictions inside the pore structure of this material (Figure 3).

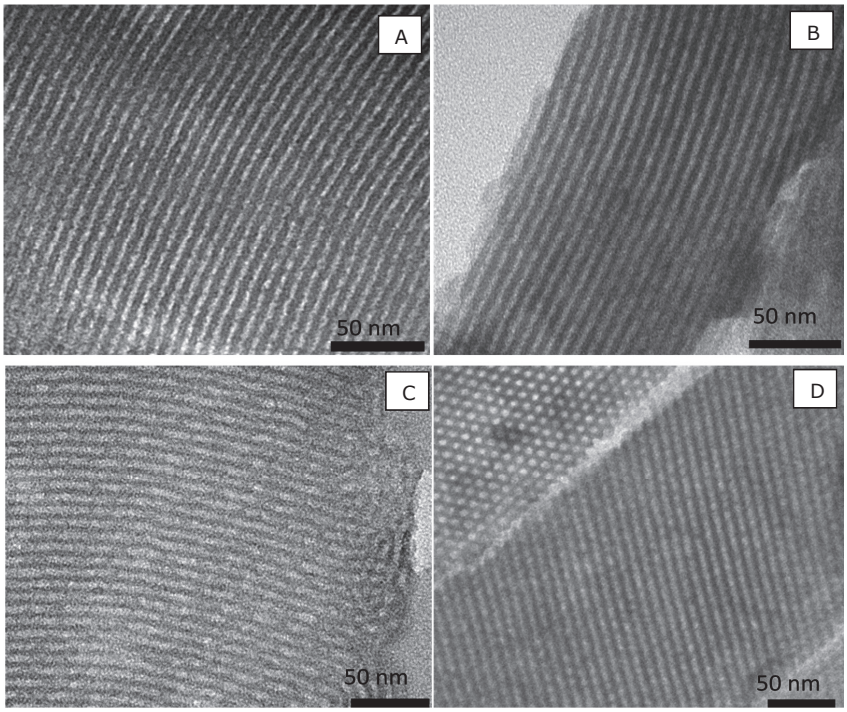

Figure 2- TEM images (A) PHTS-1-60, (B) PHTS-2-80, (C) PHTS-1-80, (D)PHTS-1-100

Nitrogen isotherms at 77 K are shown in Figure 4, the isotherms show hysteresis in the pressure range of p/p_0=0.4-0.8 indicative of the presence of mesopores. N_2

physisorption isotherms of samples PHTS-2-80 and PHTS-1-100 show 2-step desorption. The first desorption step is due to desorption from open mesopores. The second desorption step is attributed to plugged mesopores and used to calculate the fraction of plugged mesopore volume. Comparison of results for PHTS-2-80 and PHTS-1-80 shows that adding the silica precursor in two steps leads to only partially plugged materials (2-steps desorption); however, slow addition in one step resulted in completely plugged SBA-15 (1-step desorption). All N_2 desorption isotherms showed cavitation at ~0.42 relative pressure, indicating that the entrance size of some plugged mesopores is smaller than 4.7 nm.

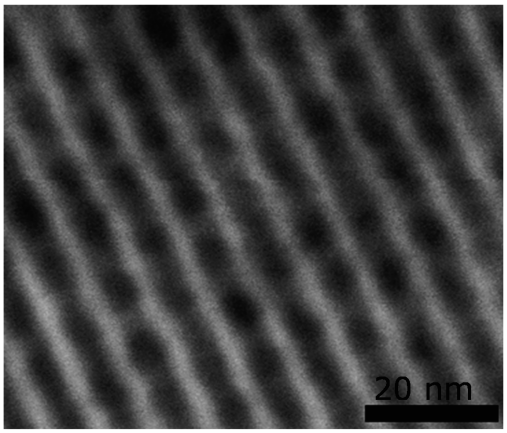

Figure 3- ***HAADF-STEM of PHTS-1-60***

We define the plugged pore volume as that part of the silica pore volume that can only be accessed via a pathway that is significantly narrower than the average pore size of the plugged SBA-15. The terminology derives from the fact that narrowing of the entrance to part of the porosity is caused by the presence of silica plugs in the mesopores, which narrow the entrance size of part of the pore volume to below 3.5-4.0 nm. The plugged pore volume can be quantitatively derived from the desorption branch of the nitrogen physisorption isotherm. If two step desorption is observed (Figure 4) the solid is called “partially plugged". It means that part of the pore volume is open (“open pore volume”), but another part of the pore volume is only accessible via an entrance smaller than 3.5-4.0 nm (“plugged pore volume”), which results in a sudden decrease in adsorbed nitrogen volume with decreasing

pressure around p/p_0=0.42. However, when one step delayed desorption is observed around p/po 0.42, this means that virtually all pore volume is only accessible via smaller (plugged) entrances, hence in this case the material is nominated as "completely plugged", as virtually all pores contain plugs.

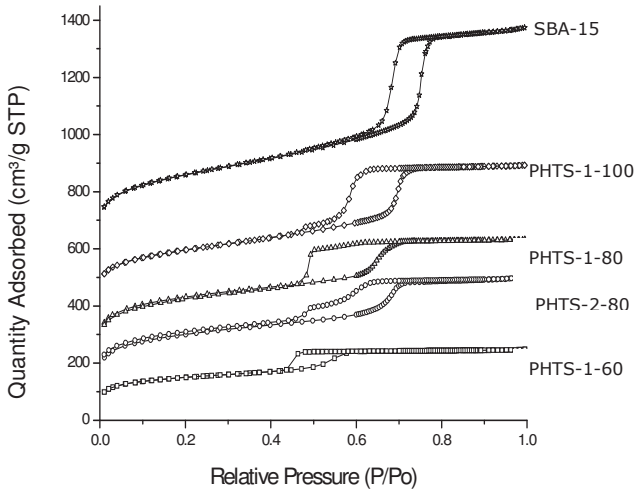

Figure 4 N_2 physisorption measured at 77 K. The N_2 isotherms were offset vertically by 100, 200, 400, 600 cm^3/g STP

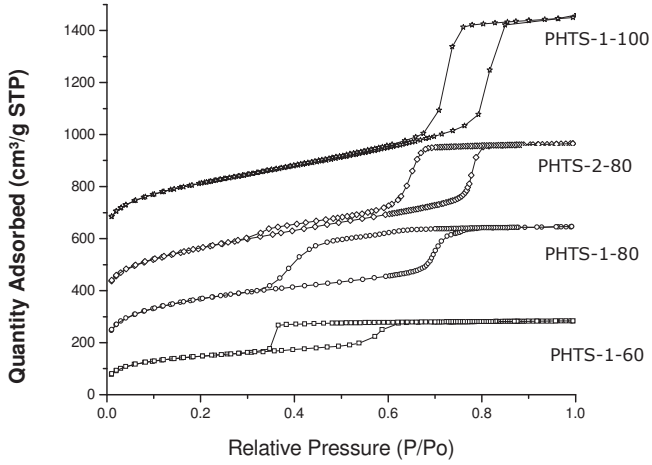

Figure 5 Ar physisorption measured at 77 K. Ar physisorption isotherms for PHTS were offset vertically 100, 200, 500 cm^3/g STP.

Ar physisorption (Figure 5) allows extending this measurement limit down to ~3.6 nm.[30] In the case of PHTS-1-80 and PHTS-2-80, Ar physisorption (Figure 5) displays a continuous gas desorption at relative pressures from 0.6 to 0.35, showing that constrictions inside the mesopores had a broad size distribution with entrance sizes from 5.6 to 3.6 nm. Thus, the PHTS-1-80 materials are accessible through mesosized entrances and not only through micropores as reported earlier.[8] For PHTS-1-60 1-step desorption was observed again, facing smaller entrance sizes which are not able to be measured by argon physisorption.

Table 1- Structural properties of samples derived from N_2 physisorption and XRD

Sample	a_o(nm)	d(nm)	S_{BET} (m^2/g)	V_{total} (cm^3/g)	V_{meso} plugged	V_{micr} (cm^3/g)
SBA-15	10.7	7.0	917	1.18	0%	0.06
PHTS-1-60	9.0	4.5	508	0.38	100%	0.10
PHTS-1-80	10.2	6.0	797	0.67	96%	0.11
PHTS-1-100	10.7	7.0	694	0.76	19%	0.05
PHTS-2-80	10.7	6.5	695	0.61	41%	0.08

a=lattice spacing, d= pore diameter from adsorption branch (BJH), S_{BET} = BET surface area, V_{total}= total pore volume, V_{meso} plugged = volume of plugged mesopores, V_{micro} = micropore volume

Table 1 provides an overview of the structural properties of the materials. If the aging temperature is raised from 60º to 100ºC, the unit cell parameter increases from 9.0 to 10.7 nm, while also the pore diameter and total pore volume increase. In general, the accessibility of the mesopores is related to the mesopore diameter. The sample PHTS-1-60, which has mesopores of ~4.5 nm, is only accessible through entrances smaller than 3.6 nm. The samples PHTS-1-80, PHTS-1-100 and PHTS-2-80 (pore diameter 6.0, 7 and 6.7 nm respectively) have partially open mesopores and larger window sizes. The micropore volume is low when the hydrothermal temperature was 100º C. It has been well documented for SBA-15 that the micropores are related to the hydrophilic nature of the PEO chains of the organic template around which silica is grown and that at 100ºC, the PEO blocks become less hydrophilic, leading to lower micropore volumes.[31]

Silver Deposition

Although gas physisorption gives information about the average properties of the samples, such as surface area and plugged porosity, it does not show where the plugs and cavities are located inside the material. Thus, to gain a better understanding of spatial distribution of constrictions and cavities in these solids, silver structures were synthesized inside the mesopores of silica, giving local information about the pore structure of these materials. Moreover, samples with different silver loadings were synthesized to verify that the use of relatively low silver volume loadings, as used in this study, did not lead to preferential silver deposition in certain mesopores.

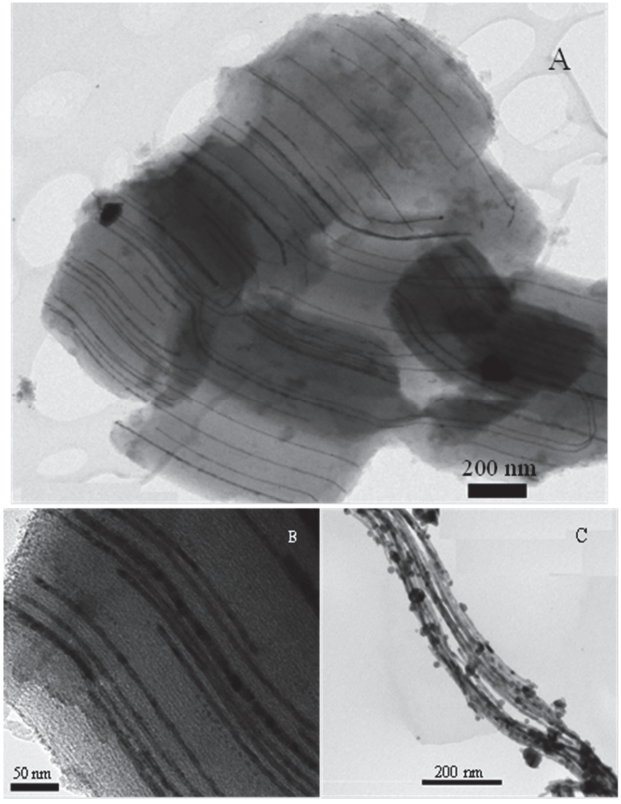

Figure 6 Silver nanowires inside SBA-15 (A, B), silver nanowires after silica removal (C)

Figure 6 shows TEM images of SBA-15 material containing silver nanowires (frame A and B) and silver nanowires obtained after silica removal (frame C). Very long silver

nanowires running over the full length of the silica particles are observed (Figure 6A), confirming the regular open mesopore structure of SBA-15. The Ag nanowires were around 7.2 nm in diameter (Figure 6B), in accordance with the pore diameter of SBA-15. Despite the pore corrugation of SBA-15 that has been reported before,[20] the silver nanowires have not broken up into smaller rods (Figure 6A). Part of the pores was filled completely, while other pores contain no Ag, which is not unexpected given the fact that after drying the silver nitrate

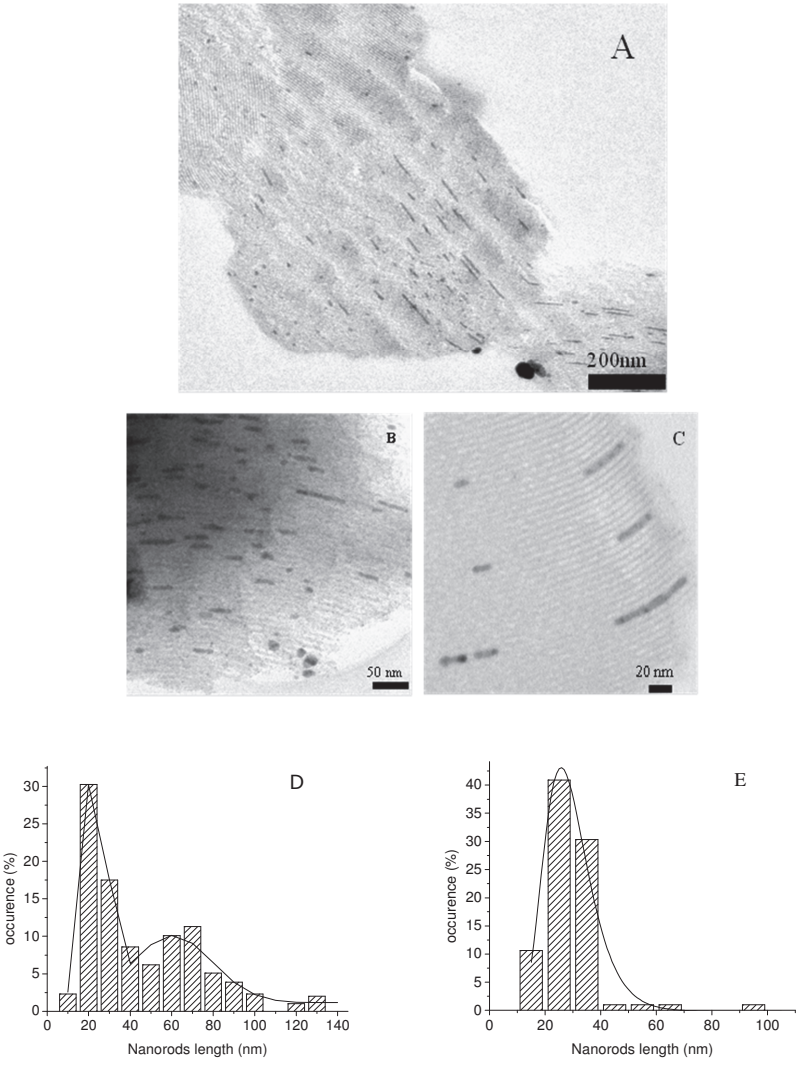

Figure 7 TEM images (A, B, C) Silver nanowires and nanorods inside PHTS-2-80 and histograms with the length distribution of Ag nanorods in PHTS-2-80(D), and PHTS-1-80(E)

corresponds to 20% of the pore volume, while conversion to silver results in another 10% volume decrease. Moreover, the redistribution of mobile intermediate phases during the thermal treatment can also explain the distribution of silver in SBA-15, as has been observed before for Ni, Co and other metals.[32,33] Furthermore after silica removal, long silver wires were obtained (frame 6C). The stability of these wires was limited, which might be due to electron beam exposure. Nevertheless, it is clear that the silver nanostructures faithfully represent the pore structure of the SBA-15 material. Hence based on this result, we decided to probe the nanocavities and pore constrictions in PHTS by imaging silver nanorods grown in the pores.

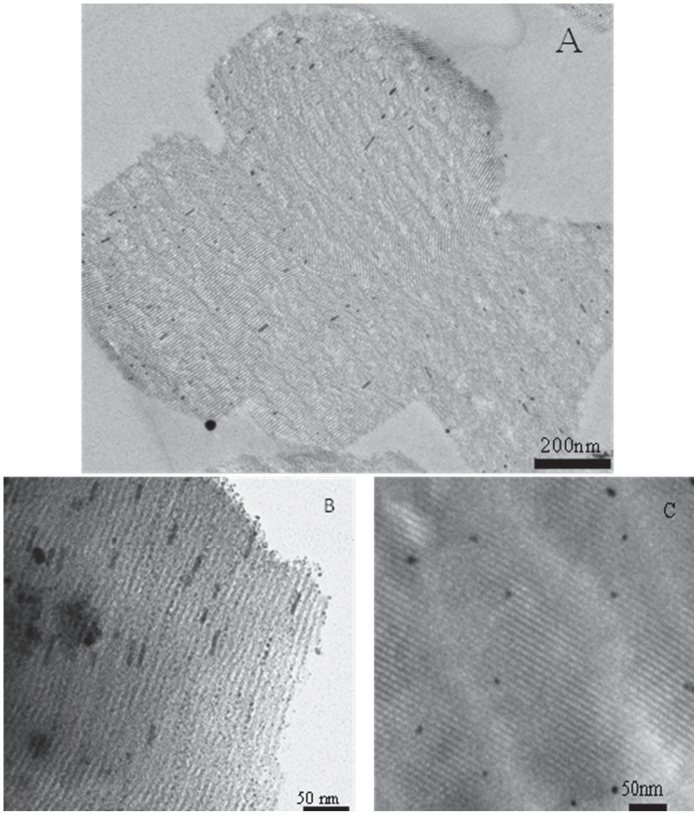

Figure 8 Silver nanorods inside PHTS-1-80 (A, B) PHTS-1-60 (C).

Ag-PHTS-2-80 (Figure 7) showed clearly shorter silver structures than Ag-SBA-15. Silver rods of 70-100 nm length were observed, showing that in some pores the distance between the constrictions was relatively long (figure 7A). In other areas of the sample even shorter silver rods with 15-30 nm of length were observed, indicating even shorter distances between the constrictions (Figure 7A, B, C). A histogram (Figure 7D) confirms a wide distribution of silver structures inside PHTS-2-80. The relatively large distances between the plugs are in accordance with the physisorption which shows 41% of mesopore volume contains plugs. Since in PHTS the nanorods are short in contrast to those in SBA-15 we conclude that in PHTS materials the constrictions are narrow enough to stop the continuous growth of the silver wires.

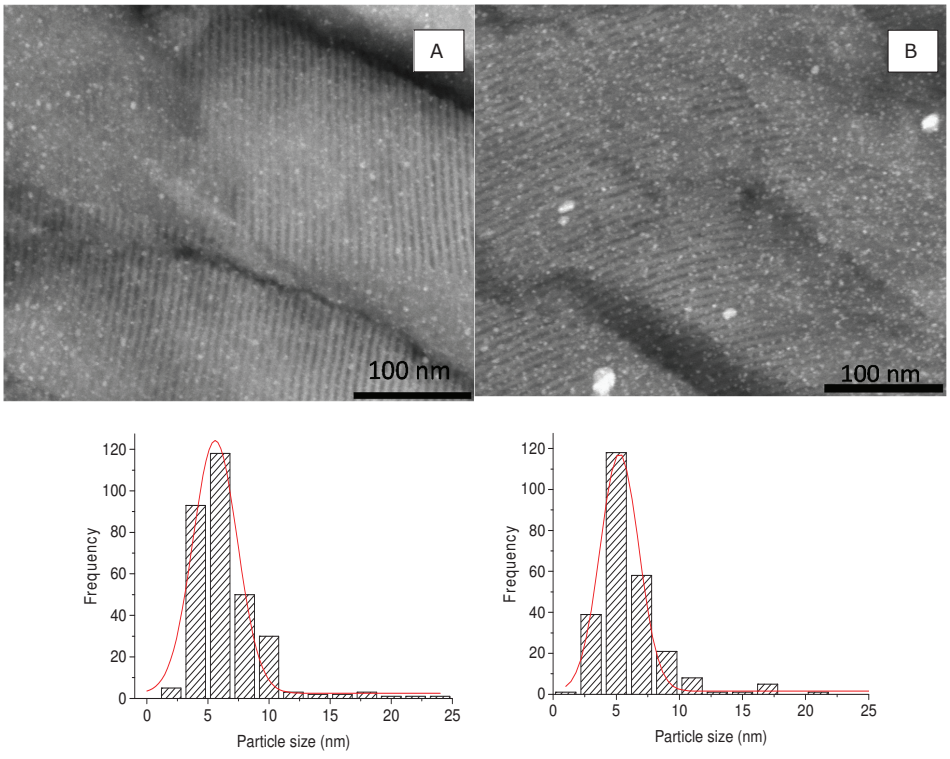

Figure 9- HAADF-STEM images of Ag-PHTS-1-60 with 2 different loading 20 w/w % (A) and 35 w/w% (B) and the histogram of particle size distribution.

Samples Ag-PHTS-1-60 and Ag-PHTS-1-80 contain much shorter silver nanorods, mainly around 10-40 nm of length, and even silver nanoparticles (Figure 8).The length of the rods is nicely in line with direct imaging of cavities (Figure 3). Frame A illustrates that for Ag-PHTS-1-80 plugs with small inter-plug distances are abundant throughout the whole material. The average rod length was 28±7.5nm (Figure 7E). For Ag-PHTS-1-60, with the smallest pores, some silver deposits were observed outside the silica structure (Appendices, Figure A2). Inside the mesoporous structure only spherical particles and short rods are observed (Figure 8C) illustrating the severe constriction of all pores. These results are in accordance with gas physisorption results which showed that PHTS-1-60 and PHTS-1-80 have 100% and 96% of their mesopore volume plugged, respectively.

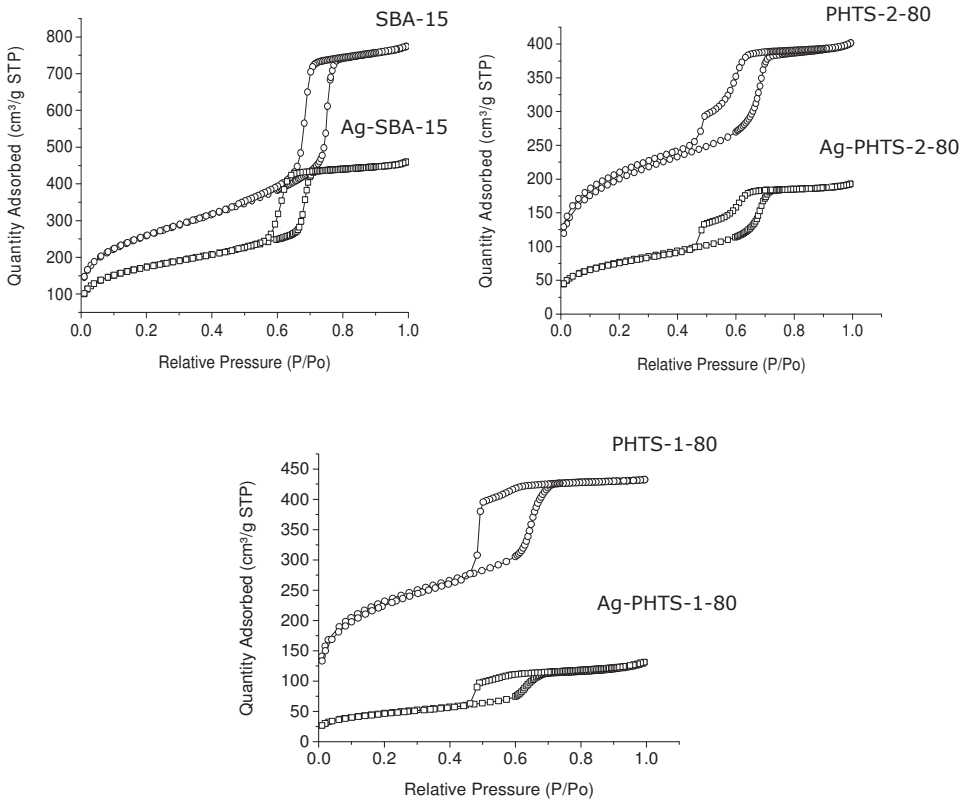

Figure 10- N_2 physisorption isotherms of SBA-15 and two different PHTS samples before and after loading with silver.

PHTS-1-60 was prepared with different silver loadings (20 and 35 w/w% Figure 9). For these two loadings, very similar Ag dimensions were observed, indicating no significant influence of loading on the silver particle size. For 20 w/w% silver the particle size was 5.5±1.8 nm and when the loading was 35w/w% the particle size was 4.9±1.3nm. This result differs from that obtained by Wang et al[34] who observed an influence of the metal loading of Au, Ag and Pt in SBA-15 on the particle size. This fact gives a strong indication that in our case imaging the Ag plugs inside the PHTS materials faithfully represents the mesopore structure.

It was observed in the case of SBA-15 that no cavities were created (Figure 10) by the addition of silver (no change in the hysteresis shape) but a large reduction of the surface area and the amount of liquid nitrogen filling the mesopores was observed. Thus, to investigate a possible damage of the SBA-15 structure, the silver was dissolved using HNO_3 (3M), and after that the porosity of the resulting silica was investigated by N_2 physisorption. The results showed no significant damage to the SBA-15 structure (Table 2), confirming that a reduction of pore volume and surface area was caused by the addition of silver in SBA-15. In all cases, the pore volume loss was larger than expected based solely on the volume of the added silver. Hence in this case most likely part of the silica porosity was probably rendered inaccessible by the silver addition.

Table 2 Structural properties of the samples as derived from N_2 physisorption

Material	BET surface area	Total pore volume	Micropore volume
SBA-15	917	1.18	0.06
Ag-SBA-15	319	0.44	0.01
SBA-15 after Ag removal*	863	1.17	0.04
PHTS-1-60	508	0.38	0.10
Ag-PHTS-1-60	236	0.2	0.03
PHTS-1-80	797	0.67	0.11
Ag-PHTS-1-80	170	0.19	0.009
PHTS-2-80	695	0.61	0.08
Ag-PHTS-2-80	265	0.29	0.015

*The silver structure of Ag-SBA-15 was dissolved in an aqueous solution of HNO_3 (3M)

Experimental section

Ordered- mesopore silica synthesis and silver deposition

Synthesis of the SBA-15

SBA-15 was synthesized following a procedure previously described.[35] In a polypropylene bottle 250 ml, 2.0 g of P123 blockcopolymer was dissolved in a mixture of 15 g of water and 60 g of 2M HCl. This solution was stirred at 35 ºC overnight. Then, 4.0 g of TEOS was added dropwise to this solution under vigorous stirring. After 5 min of stirring, the mixture was kept under static conditions at 35 ºC for 20 hours followed by 24 hours at 80 ºC. The solid product was collected by filtration, washed with distilled water, dried at 60 ºC during 48 h and calcined at 550 ºC in static air during 6 hours.

Synthesis of the PHTS Materials

Samples were designated PHTS-A-B, A indicating in how many steps TEOS was added and B indicating the hydrothermal treatment temperature.

PHTS-1-60, PHTS-1-80, PHTS-1-100

In a polypropylene bottle 250 ml, 2.0 g of P123 blockcopolymer was dissolved in a mixture of 15 g of water and 60 g of 2M HCl. This solution was stirred at 35 ºC overnight. Then, 8.5 g of TEOS was added dropwise during 15 minutes to this solution under vigorous stirring. After 5 min of stirring, the mixture was kept under static condition at 35º C for 20 hours followed by 24 hours at different temperature (60º, 80º and 100ºC). The solid product was collected by centrifugation, washed with distilled water, dried at 60ºC during 48h and calcined at 550ºC in static air during 6 hours.

Synthesis of the PHTS-2-80

In a polypropylene bottle 250 ml, 2.0 g of P123 blockcopolymer was dissolved in a mixture of 15 g of water and 60 g of 2M HCl. Then, 4.25 g of TEOS was added to this solution under vigorous stirring. The solution was kept stirring for 30 minutes, then, 4.25 g of

TEOS was added dropwise in this solution. The mixture was kept under static condition at 35º C for 20 hours followed by 24 hours at 80º C. The solid product was collected by centrifugation, washed with distilled water, dried at 60ºC during 48h and calcined at 550ºC in static air during 6 hours.

Deposition of the silver nanowires

Silver structures on SBA-15 were synthesized using using a two-solvent technique.[36,37] In this methodology, 300 mg of mesoporous silica was first dried at 120 ºC for 12 hours to remove physisorbed water. Then, 5 ml of n-hexane was added to the dried mesoporous silica and this suspension was stirred vigorously during 10 minutes.

After this procedure, 2 ml of 1.25 M $AgNO_3$ aqueous solution was added to this suspension dropwise. Then, the suspension was stirred during 4 hours at room temperature, the composite was centrifuged, dried at 80 ºC for 6 hours to remove n-hexane and then heated to 350 ºC with a temperature increase rate of 2 ºC/min, and calcined at 350 ºC in stagnant air during 2 hours.

The synthesis of Ag-PHTS-1-60 with a lower metal loading was done using exactly the same procedure described above, but changing the volume of the silver nitrate solution (1ml). The metal loadings were determined by AAS (Mikroanalytisches Laboratorium Kolbe, Germany).

Freestanding silver nanowires were obtained by dissolving the SBA-15. In this procedure, 50 mg of Ag-SBA-15 was added to a solution of 3.0 M of NaOH (1.0 ml), then, this mixture was stirred during 24 hours. After this period, the silver wires were retrieved by centrifugation and washed with distillated water and ethanol.

Structural analysis

XRD analysis

Long range pore ordering was confirmed with low-angle X-ray diffraction. Patterns were obtained at room temperature from 0.5 to 8° 2θ with a -AXS D2 Phaser powder X-ray diffractometer, in Bragg-Brentano mode, equipped with a Lynxeye detector using Co–$K_{\alpha 12}$

radiation, with λ = 1.79 Å, operated at 30kV, 10 mA. To provide reproducible results and minimize effects of sample preparation the average over three individual small angle XRD measurements was used. XRD patterns of silver were recorded for all solids between 10 and 100° 2θ using the same equipment.

N_2 and Ar Physisorption

N_2 and Ar Physisorption measurements were performed at 77 K using a Micromeritics Tristar 3000. The samples were dried before the measurement under an N_2 flow at 250 °C for at least 12 h. The total microporous and mesoporous volume (V_p) was determined using the t-plot method. The pore size distribution of the mesoporous silica supports was calculated from the adsorption branch of the isotherm by BJH analysis. The maximum of the pore size distribution was taken as the average pore diameter.

The percentage of plugged mesopore volume that was calculated from the differential or cumulative pore volume as a function of the pore size distribution (BJH analysis of the desorption branch) by defining the peak as 3.5-4.0 nm as plugged pores as shown in figure below. The areas of the peaks (plugged and open) were integrated and the percentage of plugged pores was determined by the formula:

$$\text{Percentage of plugged pores} = \frac{\text{area of the peak related to plugged pores}}{\text{Total area (plugged + open pores)}}$$

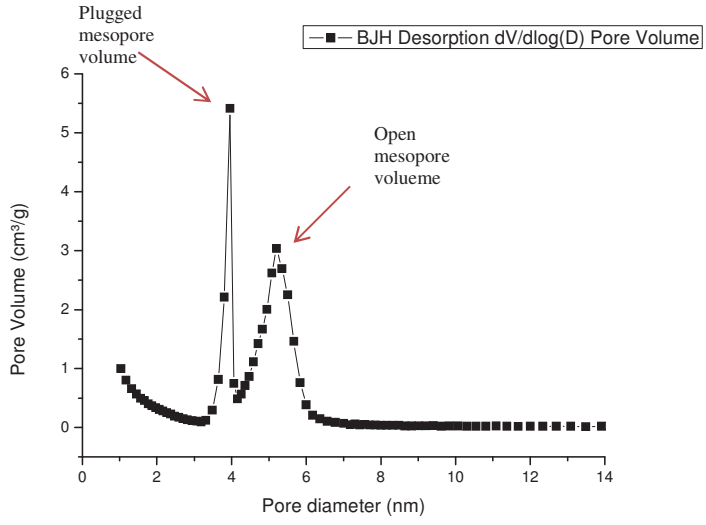

Figure 11- BJH pore size distribution from desorption branch

SEM and TEM analysis

The morphology and sizes of the silica particles were determined with a Tecnai FEI XL 30SFEG Scanning Electron Microscope (SEM). Transmission electron microscopy was performed using a microscope FEI Tecnai20F, operated at 200 kV equipped with CCD camera.

The samples were embedded in epoxy resin (Epofix, EMS) and cured at 60ºC overnight. Then, they were cut into thin sections with a nominal thickness of 60 nm using a Diatome Ultra knife, 4 mm wide and 35° clearance angle, mounted on a Reichert–Jung Ultracut E microtome. The sections float on water after cutting, were picked up and deposited onto a carbon coated polymer grid and left to dry.

The histograms of particle size distribution were obtained from observing about 500 particles in representative micrographs of different areas.

Conclusions

Visualizing silver nanostructures confined in the pores of SBA-15 and plugged SBA-15 allows a detailed characterization of the porosity in these materials. For SBA-15, Ag nanowires extended over the full pore length. Plugged SBA-15 materials were prepared with a variation in the degree of constriction of the pores. Especially a lower hydrothermal treatment temperature resulted in a higher degree of plugging, with virtually all pores containing plugs. The length of the enclosed nanocavities was determined, and varied from 10 to 100 nm, depending on the synthesis procedure. These results demonstrate the suitability of visualization of pore-confined metal nanostructures to characterize the nature of complex porosities such as in nanocavities-containing materials.

Acknowledgments

The authors thank the Dutch National Research School Combination Catalysis Controlled by Chemical Design (NRSC-Catalysis) for the financial supporting and Marjan Versluijs-Helder for the SEM analysis.

References

1. V. Meynen, P. Cool and E. F. Vansant, *Microporous Mesoporous Mater.*, 2009, **125**, 170.

2. M. Shakeri, R. J. M. Klein Gebbink, P. E. de Jongh and K. P. de Jong, *Angew. Chemie*, 2013, **125**, 11054.

3. J. Sun and X. Bao, *Chemistry*, 2008, **14**, 7478.

4. I. I. Slowing, J. L. Vivero-Escoto, C.-W. Wu and V. S.-Y. Lin, *Adv. Drug Deliv. Rev.*, 2008, **60**, 1278.

5. B. J. Melde, B. J. Johnson and P. T. Charles, *Sensors*, 2008, **8**, 5202.

6. L. P. Mercuri, L. V Carvalho, F. a Lima, C. Quayle, M. C. a Fantini, G. S. Tanaka, W. H. Cabrera, M. F. D. Furtado, D. V Tambourgi, J. D. R. Matos, M. Jaroniec and O. a Sant'Anna, *Small*, 2006, **2**, 254.

7. P. Van der Voort, P. I. Ravikovitch, K. P. De Jong, a V Neimark, a H. Janssen, M. Benjelloun, E. Van Bavel, P. Cool, B. M. Weckhuysen and E. F. Vansant, *Chem. Commun. (Camb).*, 2002, 1010.

8. P. Van Der Voort, P. I. Ravikovitch, K. P. De Jong, M. Benjelloun, E. Van Bavel, A. H. Janssen, A. V Neimark, B. M. Weckhuysen and E. F. Vansant, *J. Phys. Chem. B*, 2002, **123**, 5873.

9. E. Van Bavel, P. Cool, K. Aerts and E. F. Vansant, *J. Phys. Chem. B*, 2004, **108**, 5263.

10. M. Mandal and M. Kruk, *Chem. Mater.*, 2012, **24**, 149.

11. W. Wang, W. Shan and H. Ru, *J. Mater. Chem.*, 2011, **21**, 17433.

12. B.-H. Min, E.-Y. Jeong, M. Thommes and S.-E. Park, *Chem. Commun. (Camb).*, 2011, **47**, 4673.

13. E. Van Bavel, P. Cool, K. Aerts and E. F. Vansant, *J. Porous Mater.*, 2005, **12**, 65.

14. J. Lee, Y. Park, P. Kim, H. Kim and J. Yi, *J. Mater. Chem.*, 2004, **14**, 1050.

15. M. Kruk, M. Jaroniec, S. H. Joo and R. Ryoo, *J. Phys. Chem. B*, 2003, **107**, 2205.

16. Y. Wan and D. Zhao, *Chem. Rev.*, 2007, **107**, 2821.

17. J. Groen, J. Perez-Ramirez, *Appl. Catal. A Gen.*, 2004, **268**, 121.

18. M. Kruk and M. Jaroniec, Chem. Mater. 2002, **13**, 3169.

19. A. H. Janssen, P. Van Der Voort, J. Koster and K. P. De Jong, *Chem. Commun.*, 2002, 1632.

20. C. J. Gommes, H. Friedrich, M. Wolters, P. E. De Jongh and K. P. De Jong, *Chem. Mater.*, 2009, **21**, 1311.

21. M. Shakeri, R. J. M. Klein Gebbink, P. E. de Jongh and K. P. de Jong, *Microporous Mesoporous Mater.*, 2013, **170**, 340.

22. V. Meynen, Y. Segura, M. Mertens, P. Cool and E. F. Vansant, *Microporous Mesoporous Mater.*, 2005, **85**, 119.

23. L. M. Worboys, P. P. Edwards and P. A. Anderson, *Chem. Commun.*, 2002, 2894.

24. H. J. Shin, R. Ryoo, M. Kruk and M. Jaroniec, *Chem. Commun.*, 2001, **1**, 349.

25. M. H. Huang, A. Choudrey and P. Yang, *Chem. Commun.*, 2000, 1063.

26. M. Tiemann, *Chem. Mater.*, 2008, **20**, 961.

27. Y.-J. Han, J. M. Kim and G. D. Stucky, *Chem. Mater.*, 2000, **12**, 2068.

28. J. Fan, C. Yu, F. Gao, J. Lei, B. Tian, L. Wang, Q. Luo, B. Tu, W. Zhou and D. Zhao, *Angew. Chem. Int. Ed. Engl.*, 2003, **42**, 3146.

29. R. Ryoo, C. H. Ko, M. Kruk, V. Antochshuk and M. Jaroniec, *J. Phys. Chem. B*, 2000, **104**, 11465.

30. T. M. Eggenhuisen, G. Prieto, H. Talsma, K. P. de Jong and P. E. de Jongh, *J. Phys. Chem. C*, 2012, **116**, 23383.

31. P. F. Fulvio, S. Pikus and M. Jaroniec, *J. Mater. Chem.*, 2005, **15**, 5049.

32. R. L. Oliveira, P. K. Kiyohara and L. M. Rossi, *Green Chem.*, 2010, **12**, 144.

33. J. R. a Sietsma, J. D. Meeldijk, J. P. den Breejen, M. Versluijs-Helder, a J. van Dillen, P. E. de Jongh and K. P. de Jong, *Angew. Chem. Int. Ed. Engl.*, 2007, **46**, 4547.

34. Z. Wang, Y. Xie and C. Liu, *J. Phys. Chem. C*, 2008, **112**, 19818.

35. A. Sayari, B. Han and Y. Yang, *J. Am. Chem. Soc.*, 2004, **100**, 14348.

36. X. Huang, W. Dong, G. Wang, M. Yang, L. Tan, Y. Feng and X. Zhang, *J. Colloid Interface Sci.*, 2011, **359**, 40.

37. J. van der Meer, I. Bardez-Giboire, C. Mercier, B. Revel, A. Davidson and R. Denoyel, *J. Phys. Chem. C*, 2010, **114**, 3507.

Chapter 3

Stabilization of Palladium Catalysts for the Heck reaction by Support Functionalization and Solvent Selection

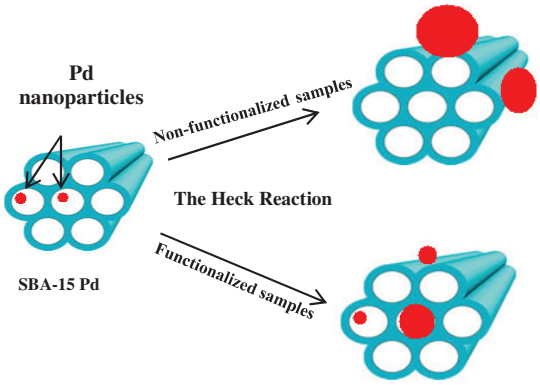

Abstract

Pd nanoparticles were synthesized on nonfunctionalized and functionalized SBA-15 grafted with thiol or amine groups. The resulting materials were used as catalysts to study the influence of these functional groups for a similar Pd particle size approximately 2 nm on the Heck reaction that uses iodide substrates. The non-functionalized catalysts lost their activity quickly because of Pd leaching and particle growth. However, if a mixed solvent that consisted of toluene and DMF was used and thiol groups were grafted on SBA-15, we were able to reduce the Pd leaching and particle growth to thus obtain a more stable catalyst in which an important role of the ligands was to recapture Pd. However, heterogeneity tests, such as a hot filtration test and poisoning experiments, gave a strong indication that Pd still leached from the support and that homogeneous Pd species were mainly responsible for the activity. Pd on S-functionalized SBA-15 was able to catalyze the Heck reaction using different substrates to achieve good activity and selectivity in most cases.

Based on: R. L. Oliveira, J. B. F. Hooijmans, P. E. de Jongh, R. J. M. Klein Gebbink, K. P. de Jong. Stabilization of Palladium Catalysts for the Heck reaction by Support Functionalization and Solvent Selection, ChemCatChem, 2014, 6, 1-9.

Introduction

C-C bond formation reactions are among the most important transformations in organic chemistry. Traditionally, these reactions are performed using strongly basic reagents such as Grignards and lithiated carbon nucleophiles, however, these reagents lead to a considerable amount of waste and low selectivity.[1] In 1968, Heck invented a new route to form C-C bonds using homogeneous Pd catalysts.[2–4] The Heck reaction offers several advantages, such as reactants available commercially, mild reaction conditions, high selectivity, and the use of small amounts of Pd. Nonetheless, the homogeneous catalysts suffer from low stability, high cost, and poor recyclability.

In the last decades, the application of heterogeneous Pd catalysts for C-C coupling reactions has received a lot of attention because these can be separated easily from the reaction mixture to result in their more efficient reuse.[5–12]However, leaching, poisoning, and particle growth have remained a challenge for heterogeneous catalysts, which result in a loss of activity and limited recyclability in some cases.

The most common heterogeneous catalysts are metal nanoparticles supported on carbon, alumina or silica. In general, the catalytic activity is influenced by the nature of the support.[13,14] Among these supports, ordered mesoporous silica has been applied for C-C coupling reactions.[15–17] These materials have large specific surface areas, uniform pore sizes, and tunable periodic pore arrangements. All these properties make them very interesting for metal particles encapsulation and catalysis application.[16–25]For example, Bao et al. showed that confined particles in SBA-15 were more stable and did not grow as severely as unconfined particles on silica gel.[26]

In general, nanoparticles supported on mesoporous silica are confined in mesopores, which prevent their agglomeration. Traditionally, supported metal nanoparticles have been encapsulated in mesoporous materials by incipient wetness impregnation (IWI) and sol-gel processes. However, these methodologies display a lack of control of the particle size and in

many cases result in particles with a bimodal size distribution or a mixture of nanowires and nanoparticles.[27–29]The methodologies used to deposit metal particles on different supports have been reviewed.[30–32]

The synthesis of nanoparticles by ligand-assisted methods has been used as an alternative to produce heterogeneous catalysts for liquid-phase reactions.[33] In this methodology, materials such as silica and polymers are modified with N-, S-, and P-containing groups that are able to anchor metal complexes or nanoparticles.[34–38] Moreover, the substitution of silanol by other functional groups facilitates the adsorption of metal precursors and the control of the particle size.[39–41]

These ligand-assisted methods have been applied to produce catalysts active for C-C coupling reactions.[42–46]Shimizu et al. immobilized Pd on FSM-16 modified with 3-mercaptopropylsiloxane and reported a detailed characterization of this material using extended X-ray absorption fine structure (EXAFS) analysis, which showed the interaction between the ligand and the metal.[47] Kaliaguine et al. functionalized the surface of SBA-16 and KIT-6 with thiol groups and used these solids to immobilize Pd complexes; the obtained materials presented a high activity for C-C coupling, however, the silica structure collapsed after some cycles.[48,49]Dutta and Sarkar modified the surface of silica gel with polyethylene glycol to produce a catalyst that could be recycled five times without loss of activity.[50]

Ji et al.[51]and Richardson et al.[52]used different types of modified silica to study the active species of the catalyst, that is, leached or supported metal, using different techniques, such as hot filtration, poly(4-vinylpyridine) (PVPy) poisoning, and three-phase tests, and concluded that leached species were responsible for the activity. However, Crudden et al. [53] used the same catalysts and tests and concluded that the Heck reaction takes place at the surface of the catalysts. The true nature of the active species continues to be a controversial topic of discussion.

The influence of the nature of the solvent in the Heck reaction was reported previously.[54,55] In general, polar solvents such as DMF and *N*-methylpyrrolidone (NMP) give a higher yield than nonpolar solvents for both homogeneous and heterogeneous catalysts.

However, if DMF and NMP are used in heterogeneous systems, severe Pd leaching is often reported. On the other hand, nonpolar solvents often bring about longer reaction times and require higher amounts of Pd.

Despite the development of these new catalysts, no rigorous comparison has been reported of the activity of Pd nanoparticles with similar sizes synthesized on unmodified and modified supports to further understand the influence of functional groups on the support surface. In this chapter, we report the synthesis of Pd nanoparticles on nonfunctionalized SBA-15 using IWI and ion adsorption. Furthermore, Pd nanoparticles of a similar size immobilized on SBA-15 grafted with amino or thiol groups have been studied. We compared the activity, recyclability, and stability in the Heck reaction. Moreover, Pd particle growth, the nature of the active species (leached or supported), and the influence of the solvent were examined.

Results and Discussion

Catalyst synthesis and characterization

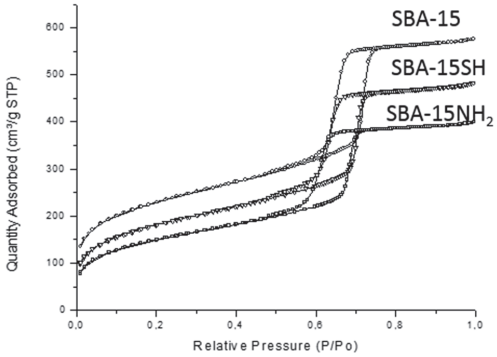

Figure 1- N_2 physisorption of the SBA-15 and functionalized SBA-15

SBA-15 was selected as a support because it has high porosity, surface area, stability, and a high concentration of silanol groups, which permits us to obtain a good metal dispersion and distribution of functional groups during the functionalization step. A postsynthetic functionalization technique[56] was used to graft two different functional groups that contain amine (SBA-15NH_2) or thiol (SBA-15SH) on the silica surface. N_2 physisorption isotherms of samples before and after the functionalization are shown in Figure1. The functionalized samples displayed a decrease in the specific surface area and pore volume (Table 1), which confirms the functionalization of external and internal walls of SBA-15. Although we used the same molar amount of ligand precursor during the functionalization step, the amine-functionalized sample showed a greater decrease of the surface area. This phenomenon was probably caused by amine groups that autocatalyze the functionalization reaction.[57,58] Elemental analysis showed that SBA-15NH_2 contained 3.0 wt% of N and SBA-15SH contained 1.9 wt% of S.

Table 1 . Porosity of synthesized materials from nitrogen physisorption

Materials	BET (m^2/g)	Pore volume (cm^3/g)	Pore diameter D(nm)*	Density of S or N ($\mu mol.m^{-2}$)
SBA-15	774	0.77	6.8	-
SBA-15SH	588	0.62	6.6	1.0
SBA-15NH_2	394	0.45	5.6	5.4

*BJH analysis from adsorption branch

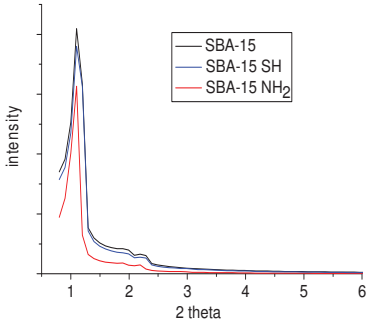

Figure 2 Small angle XRD of SBA-15 and functionalized SBA-15

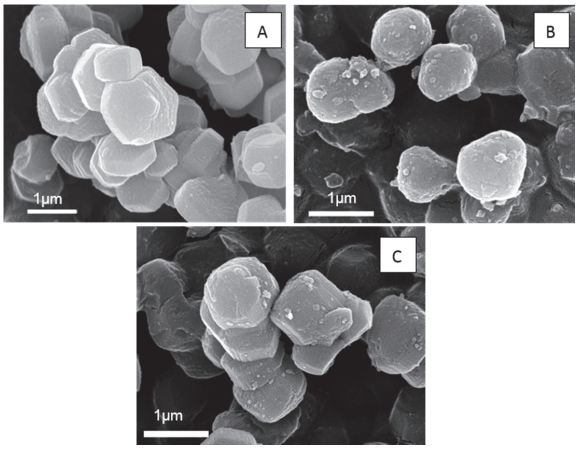

Figure 3 Scanning electron microscopy images, (A) SBA-15; (B) SBA-15 NH_2; (C) SBA-15SH

FTIR spectroscopy and thermogravimetric analysis (TGA) were performed to confirm the incorporation of functional groups on the silica surface (Appendices, Figures A3 and A4).The low-angle XRD pattern (Figure 2) confirmed that all samples exhibited the characteristic diffraction lines of *P6mm*, which indicates no loss of the structure, but in the case of SBA-15NH_2 a lower intensity of the peaks was observed. SEM analysis (Figure 3) of SBA-15 before and after functionalization shows that the material retains the same morphology.

The Pd nanoparticles were synthesized on nonfunctionalized SBA-15 by IWI or ion adsorption (Experimental Section) followed by an oxidation treatment and a reduction procedure. The resulting Pd nanoparticles were observed by dark-field scanning transmission electron microscopy (STEM; Figure 4). In the case of IWI, the particles had a relatively broad particle size distribution with an average size of 4.5 nm (Pd-4.5). The ion adsorption method gave particles with a narrower particle size distribution with an average size of 1.9 nm (Pd-1.9). Pd was also deposited on N- or S-functionalized SBA-15 using a modified methodology described by Ying et al.[59] For both supports, particles with a relatively narrow size distribution were observed. In the case of SBA-15SH particles with an average size of 1.8 nm (Pd-S-1.8) were observed, and for SBA-15NH_2 particles of 1.5 nm (Pd-N-1.5) were

seen. A Gaussian function was used to fit the particle size distribution for all materials (Figure 4 and Table 2).

Table 2 Metal loading and particle size distribution of synthesized materials

Catalyst	w/w% Pd[a]	Pd particle size (nm)
Pd- 1.9	1.55	1.9±0.5
Pd-4.5	1.52	4.5±1.0
Pd-S-1.8	1.54	1.8±0.5
Pd-N-1.5	1.57	1.5±0.4

[a] determined by AAS (Atomic absorption spectroscopy)

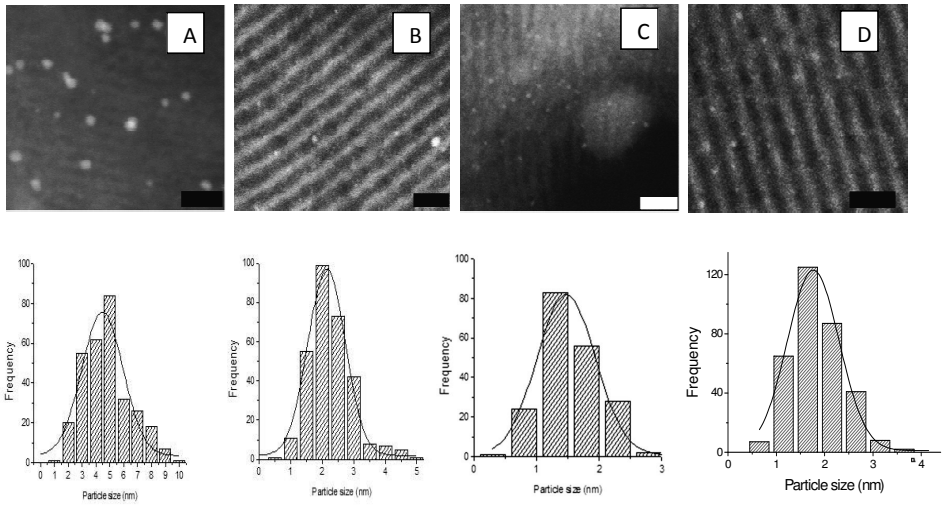

Figure 4 Dark field STEM images and the histograms of catalysts (A) Pd-4.5(B) Pd-1.9 (C) Pd-N-1.5 (D) Pd-S- 1.8; scale bars 20 nm

Catalyst test for Heck reaction

Influence of solvent and detection of leached species

The Heck reaction between iodobenzene and butylacrylate was used as a model reaction (Scheme 1). The influences of solvents and bases were examined first using catalyst Pd-4.5 (Table 3). The highest conversion was obtained if DMF and NMP were used as solvents, and triethylamine was a more suitable base than piperidine. However, if we used DMF or NMP and triethylamine, a black solution was obtained after the catalysis, which

indicates the formation of Pd black in solution (Appendices, Figure A5). The hot filtration test confirmed that the black liquid contained active species that resulted from Pd leaching. Elemental analysis showed a high concentration of the Pd in the liquid after the catalyst separation, and values that correspond to 71% (DMF) and 80% (NMP) of the Pd present in the solid originally were obtained.

If toluene was used as a solvent, a colorless solution was observed after the reaction and a much lower conversion of iodobenzene was obtained (Appendices Figure A5; Table 3, entry 3). The hot filtration test showed a negative result, which implies that there are no active Pd species in the solution. However, inductively coupled plasma (ICP) analysis still revealed Pd in low concentration in the solution (Table 3). Probably, the leached species were deactivated during the test; the limitation of the hot filtration test and its limited reproducibility have been reported before.[51,60]

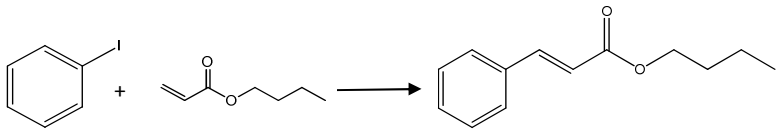

Scheme 1 The Heck reaction between iodobenzene and butyl acrylate

Table 3- Results of Heck coupling reaction of iodobenzene and butylacrylate using different bases and solvents

Entry	Solvent	Base	Conversion (%)	Time (h)	Pd leaching (%)
1	DMF	triethylamine	90	1	71
2	NMP	triethylamine	90	1	80
3	toluene	triethylamine	44	24	6
4	Toluene + 10%V/V DMF	triethylamine	60	12	19
5	DMF	piperidine	40	1	72
6	NMP	piperidine	74	1	68
7	toluene	piperidine	35	24	5

[a] Reaction conditions: 2.25 mmol of iodobenzene, 3.4 mmol of butyl acrylate, 20 mg of supported Pd-4.5 (0.13 mol% of palladium relative to iodobenzene), 2.14 mmol of base, 2.2 mL of solvent , 100ºC; determined by GC (hexamethylbenzene, internal standard).

A mixture of toluene with 10% v/v DMF (Table 3, entry 4) was also tested as a solvent. The mixture with DMF enhanced the conversion of iodobenzene compared to that in pure toluene. The hot filtration test showed a positive result, and elemental analysis showed the presence of a lower concentration of Pd in the liquid than that for pure DMF (Table 3, entries 1 and 4).

Insoluble PVPy (2% cross-linked) was used by Yu et al.[61]as a trap to confirm the presence of leached Pd. In the current work, we used insoluble PVPy to complement the hot filtration test and elemental analysis. For all cases studied, the catalytic activity was ceased by the addition of PVPy (350 equivalents of pyridine sites to total Pd).This indicates that Pd was liberated from the surface of the support and that these leached species were responsible for most of the catalytic performance.

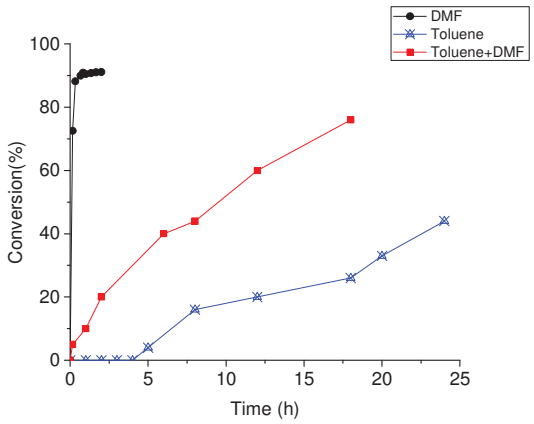

Figure 5- Plots of iodobenzene conversion with time in the Heck reaction using different solvents

Conditions: 2.25 mmol of iodobenzene, 3.4 mmol of butyl acrylate, 20 mg of supported catalyst (0.13 mol% of palladium), 2.14 mmol of Et_3N, 2.2 mL of solvent (DMF or toluene) or 2.0mL toluene+ 0.2mL DMF, 100ºC; determined by GC (hexamethylbenzene, internal standard)

A plot of conversion versus time of the reaction using DMF, toluene, and a mixture of solvents is shown in Figure 5. The plots indicate that 90% of iodobenzene was converted in 20 min if DMF is the solvent. However, if toluene was the solvent, a long induction period

and a much slower reaction rate were observed. In the case of a mixture of DMF and toluene, no induction time was observed and the reaction rate was higher than that in pure toluene. Some authors suggested that the higher activity for the Heck reaction if DMF or NMP are used as the solvent is related to more severe Pd leaching because of the stronger coordination of leached Pd.[54,55,62] The mixture of solvents used in this work suppressed the leaching of Pd with consequent moderation of the reaction rate.

Effect of Pd particle size and functional groups on activity and recyclability

The catalytic tests for all Pd catalysts were performed in DMF and in a mixture of toluene and DMF as described previously (Table 4). The comparison between nonfunctionalized samples was used to analyze the influence of Pd particle size in the Heck reaction, and the comparison between Pd-1.9 and functionalized catalysts provided a direct size influence of the functional groups in the Heck reaction, which excludes the effect of Pd particle and distribution.

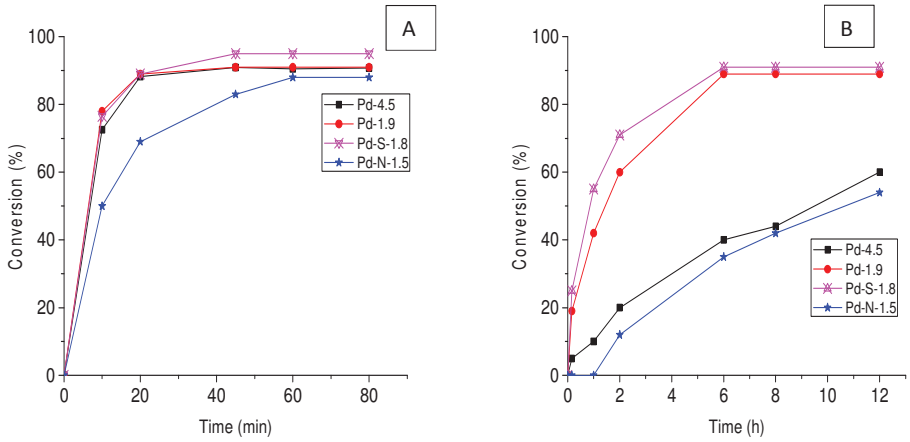

Figure 6-Plots of iodobenezene conversion with time on the Heck reaction for different catalysts (A) DMF as solvent (B) toluene+10% V/V DMF

Conditions: 2.25 mmol of iodobenzene, 3.4 mmol of butyl acrylate, 20 mg of supported catalyst (0.13 mol% of palladium), 2.14 mmol of base, 2.2 mL of solvent (DMF or toluene) or 2.0mL toluene+ 0.2mL DMF, 100ºC; determined by GC (hexamethylbenzene, internal standard)

If DMF is used as the solvent, the nonfunctionalized solids and Pd-S-1.8 presented very high conversion (≥90%) and the reaction rate was almost the same in all cases (Figure 6 A), which shows no effect of particle size and thiol groups but a much stronger effect of the solvent on Pd leaching. However, a slightly lower conversion was observed for Pd-N-1.5. Possibly the higher amount of amine groups overcoordinated the metal and decreased its catalytic performance. In all cases, a severe loss of metal was observed, however, functionalized samples showed a lower concentration of metal in the solution (Table 4).

If a mixed solvent was applied, Pd-S-1.8 and Pd-1.9 showed the highest conversion. Probably, the small particles are dissolved more easily than larger particles of Pd-4.5, which causes the faster formation of Pd species in the solution through oxidative addition. The kinetics studies revealed almost the same reaction rate for Pd-S-1.8 and Pd-1.9 and a much lower rate for Pd-4.5 and Pd-N-1.5 (Figure 6 B). The hot filtration tests showed positive results in all cases studied, and the conversion decreased tremendously if PVPy was added to the reactor (Table 4), which confirms the contribution of leached species to the conversion of iodobenzene.

Table 4 Heck reaction performance for synthesized catalysts

Catalyst	Solvent	Conversion (%)	Pd leaching (%)	Conversion (%) PVPy test
Pd 4.5	DMF	90	71	3.0
Pd 1.9	DMF	91	64	2.0
Pd-S-1.8	DMF	95	33	2.4
Pd-N-1.5	DMF	83	30	1.2
Pd 4.5	Toluene+DMF	60	6	2.0
Pd 1.9	Toluene+DMF	89	5.1	3.0
Pd-S-1.8	Toluene+DMF	91	0.5	2.8
Pd-N-1.5	Toluene+DMF	54	0.7	0

[a] Reaction conditions: 2.25 mmol of iodobenzene, 3.4 mmol of butyl acrylate, 20 mg of supported catalyst (0.13% of palladium), 2.14 mmol of base, 2.2 mL of solvent , 100ºC, 1 hour (DMF) and 12 hours (toluene+ DMF); determined by GC (hexamethylbenzene, internal standard)

Elemental analysis showed the presence of Pd in the liquid in all cases. However, the metal leaching was less severe for the mixed solvents than for pure DMF. Again, the nonfunctionalized samples faced a higher loss of Pd than functionalized solids (Table 4). Probably, functional groups on SBA-15 were able to recapture the Pd leached to the solution, which thus avoids a large amount of metal in the solution.

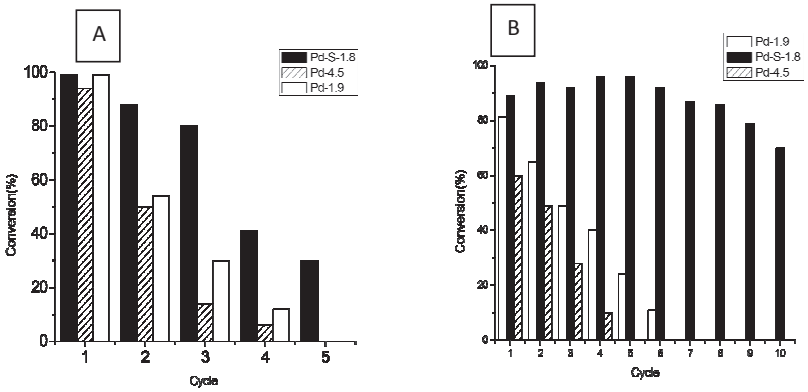

Figure 7 Recyclability of Pd-S-1.8, Pd-4.5 and Pd-1.9 using DMF (A) and toluene+10V/V DMF (B).

Reaction conditions: 2.25 mmol of iodobenzene, 3.4 mmol of butyl acrylate, 20 mg of supported catalysts (0.13 mol% of palladium), 2.14 mmol of base, 2.2mL of DMF or 2.0 mL toluene + 0.2mL DMF, 100ºC, 0.5 hour and 12 hours (toluene+ DMF); determined by GC (hexamethylbenzene, internal standard)

The recyclability of Pd-4.5, Pd-1.9 and Pd-S-1.8 is shown in Figure 7. If DMF was used as the solvent, a gradually decreased activity was observed after each cycle (Figure 7A).The decreasing conversion can be explained by leaching of metal to the solution after each cycle. Pd-S-1.8 had a higher stability than the nonfunctionalized catalysts because of a lower degree of Pd leaching after catalysis. If the mixed solvent system was used (Figure 7B), the nonfunctionalized solids lost their activities gradually as observed previously. On the other hand, Pd-S-1.8 could be recycled ten times with only a slight decrease in activity after six cycles, which shows that the combination of functional groups and the mixed solvent decreased the metal leaching and enhanced the lifetime of this catalyst.STEM images of the

recovered catalysts after the first cycle are shown in Figure 8. For all catalysts, the structure of SBA-15 was still present, and no considerable damage to its structure is observed. However, the Pd particle size and distribution changed drastically for nonfunctionalized samples (Figure 8 A and B) as large metal particles were observed on the outer surface of SBA-15 particles, which shows a redistribution of particles through Ostwald ripening. In this ripening process, atoms or clusters are detached from the surface of small Pd particles and the deposition of these species takes place on larger particles.

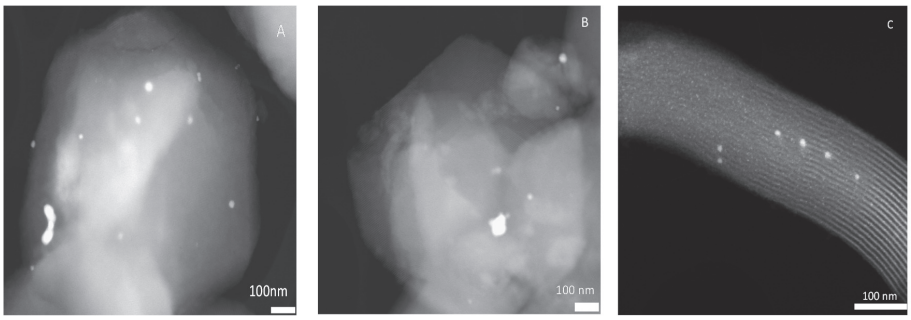

Figure 8 Dark field STEMimages of recovered catalysts (A) Pd-1.9, (B) Pd-4.5, (C) Pd-S-1.8

Particle growth was less severe in the case of Pd-S-1.8. Some Pd nanoparticles were observed at the outer surface but most of the particles were confined in the SBA-15 mesopores, although particle growth inside the mesopores was observed (Figure 8 C). These results indicate clearly that thiols on the SBA-15 surface are crucial to decrease the metal leaching and to slow particle growth by controlling Pd redeposition.

Tolerance of organic functional groups

The Heck reaction has high organic functional group tolerance especially if homogeneous catalysts are used. This tolerance is very important for the application of catalysts in fine chemistry in which molecules with different organic functional groups are used. The ability of Pd-S-1.8 to convert different substrates was studied (Table 5).

Electron-deficient, electron-neutral, and electron-rich aryl iodides reacted with butylacrylate to generate the corresponding cross-coupling products with no formation of byproducts. The compounds with an electron-withdrawing group, such as cyano, amine, and carbonyl groups, gave a higher conversion. 1-Iodo-2-methylbenzene had the lowest conversion, which shows the influence of the steric effect (entry 2).

Table 5 Heck reaction of aryl iodides with butyl acrylate promoted by Pd-S-1.8

Entry	Compound	Product	Conversion (%)
1		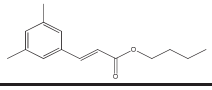	86
2		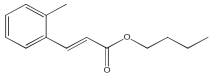	41
3		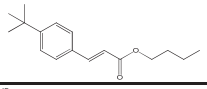	85
4		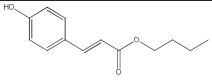	85
5		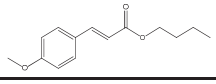	86
6		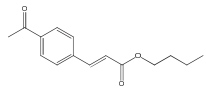	95
7		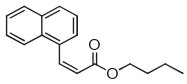	86
8		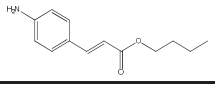	100
9		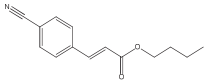	99

Reaction conditions: 2.25 mmol of iodobenzene, 3.4 mmol of butyl acrylate, 20 mg of supported catalyst (0.13 mol% of Pd), 2.14 mmol of triethylamine, 2.0 mL of toluene and 0.2mL of DMF, 100ºC, 12 hours; determined by GC (hexamethylbenzene, internal standard)

Conclusions

Solvents were shown to have a large effect on metal leaching and on the reaction rates of the Heck reaction. In general, a high degree of metal leaching was related to fast substrate conversion. The hot filtration test, poly(4-vinylpyridine) poisoning, and Pd analysis gave a strong indication that soluble species influenced the final conversion of iodobenzene considerably.

The Pd particle size had little effect on the activity and recyclability of the Heck reaction especially if DMF was used as the solvent. A mixed solvent of toluene and DMF was important to decrease metal leaching. The combination of a mixed solvent and thiol groups grafted on SBA-15 was very efficient to limit Pd leaching and particle growth, which permitted this catalyst to be recycled ten times with only a slight loss of its activity. Clearly, the functionalized catalysts were more stable than the nonfunctionalized catalysts, which lost their activity gradually because of metal leaching and Pd particle growth. Furthermore, the Pd on S-functionalized SBA-15 catalyst (Pd-S-1.8) was able to catalyze the Heck reaction with different substrates to achieve good activity and selectivity in almost all cases.

Experimental Section

Chemicals

Triblock copolymer poly(ethylene oxide)–poly(propylene oxide)–poly(ethylene oxide) (P123), tetraethyl orthosilicate (TEOS) 99%, (3-mercaptopropyl) triethoxysilane 80%, (3-aminopropyl)triethoxysilane 97%, 2% cross-linked PVPy, butyl acrylate 99%, piperidine 99%, triethylamine 99%, and tetraamminepalladium(II) nitrate solution 10 wt% in water were purchased from Sigma--Aldrich. Palladium acetate ($Pd(OAc)_2$, 47.1% Pd) was purchased from Degussa, and iodobenzene 98% and other aryl halides were purchased from Acros Organics.

Catalysts preparation and catalysis experiments

SBA-15 synthesis

SBA-15 was synthesized following the a procedure described previously.[63] In a 250 mL polypropylene bottle P123 block copolymer (2.0g, 0.35mmol) was dissolved in a mixture of water (15g) and HCl (60g, 2M). This solution was stirred at 35°C overnight. TEOS (4.0g, 19.2mmol) was added dropwise to this solution under vigorous stirring. After 5min of stirring, the mixture was kept under static conditions at 35°C for 20 hours, then 24 hours at 80°C. The solid product was collected by filtration, washed with distilled water, dried at 60°C for 24 hours, and calcined at 550°C in static air for 6 hours.

Functionalization of the silica surface

SBA-15 (500 mg) was dried at 140°C under vacuum for 12 hours. The solid was dispersed in dried toluene (20 mL) under nitrogen. Then, (3-aminopropyl)triethoxysilane (0.93 mL, 4 mmol) or (3-thiopropyl)triethoxysilane (1.2 mL, 4 mmol) was added to the mixture dropwise over 5 minutes under vigorous stirring. Then, the mixture was heated at 110°C and stirred for 24 hours under nitrogen. The obtained materials were collected by filtration and washed once with toluene and twice with ethanol and dried at 60°C for 24 hours.

Incipient Wetness Impregnation

In this methodology, the metal precursor is dissolved in an aqueous solution, which is used to fill the pores of the support, followed by drying and calcination. In this procedure, SBA-15 (500 mg) was dried at 140°C under vacuum for 12 hours. Then, an aqueous solution of $[Pd(NH_3)_4(NO_3)_2]$ (0.59 mL, 0.12M, 0.071mmol) was added to the solid with stirring. The obtained material was dried at 60°C for 24hours in static air. After drying, the catalyst precursor was inserted in a microreactor and heated to 200°C at a heating rate of $10°C min^{-1}$. During this period, the solid was exposed to an O_2 flow ($30mL.min^{-1}$) for 30 minutes. The

reduction of particles was performed by heating the sample to 400°C at a rate of 10°C.min^{-1} and flow rate of 30mL.min^{-1} of a mixture of N_2 and H_2 (1:1, v/v).

Ion adsorption

In this methodology, an attractive electrostatic interaction between the metal precursor and support prevailed.[64] The solid was synthesized using a modification of the methodology described by Zou et al. [65] In this process, SBA-15 (500 mg) was added to deionized water (1 mL), and the pH of the solution was adjusted to 8 through the dropwise addition of a solution of NH_4OH (1 M). Then, an aqueous solution of $[Pd(NH_3)_4(NO_3)_2]$ (0.59 mL, 0.12M, 0.071 mmol) was added to this solid with stirring. The pH was readjusted to 8 using $NH_4OH_{(aq)}$, and the mixture was stirred for 12 hours. The solid was recovered by centrifugation and washed with water. The same calcination treatment described above for IWI was used for this material.

Synthesis of Pd nanoparticles on the functionalized support

The protocol was based on the modification of a procedure reported by Ying et al.[23] Functionalized SBA-15 (250 mg) was dried under vacuum at 140°C for 12 hours. After drying, the solid was dispersed in dry toluene (5 mL) under N_2. Palladium(II) acetate (8 mg, 0.036 mmol) was dissolved in dichloromethane (1 mL) and then added slowly to the dispersion. The dispersion was then heated to 60°C and stirred for 24 hours. The solids were collected by centrifugation, washed once with toluene and once with ethanol, and dried at 60°C. To reduce the Pd, Pd-loaded SBA-15 (100 mg) was dispersed in water (1 mL). Then, $NaBH_4$ (1 mL, 0.2M, 0.2 mmol) was added rapidly under vigorous stirring. After 20min, the dispersion was diluted with water to 35mL, centrifuged, washed thoroughly with water, and dried at 60°C.

Catalyst test

In a typical Heck reaction, a mixed solution of iodobenzene (2.25 mmol), butylacrylate (3.47 mmol), base (2.15 mmol), hexamethylbenzene (internal standard for GC

analysis, 1.1 mmol), and solvent (2.2 mL) was prepared under nitrogen (Schlenk technique), and catalyst (20 mg, 0.1 mol% of Pd relative to iodobenzene) was added. The mixture was stirred for a given time and at a given temperature. After the catalytic reaction, the solid catalysts were recovered by centrifugation, washed with ethanol (35 mL), and dried under vacuum. For recycling experiments, a new solution mixture described above was added to the solid.

A small fraction of the liquid samples were taken, diluted with toluene, and analyzed by GC with flame ionization detection (FID). GC analysis was performed by using a PerkinElmer Clarus 500 equipped with a 30 m capillary column with 5 % phenyl/95 % methylpolysiloxane as the stationary phase (AT5) using the following parameters: initial temperature 50 °C, temperature ramp 10°Cmin^{-1}, final temperature 250°C, injection volume 0.5 μL.

Hot filtration test and PVPy poisoning test

A Heck reaction was allowed to run for 30 minutes in DMF, 3 hours for a mixture of solvents, and 14 hours for toluene. Then, the solids were collected by filtration under a static vacuum by using a swivel frit filter connected to an empty flask, and the filtrate was kept at reaction temperature. The conversion was monitored by GC.

The catalyst poison was added to the Schlenk flask before the addition of the reaction solution. PVPy was used at 350equiv. of pyridine sites to total of Pd.

Characterization

XRD

Long-range pore ordering was confirmed with by low-angle XRD. Patterns were obtained at RT from 2θ= 0.5-8° by using a Bruker-AXS D2 Phaser powder X-ray diffractometer in Bragg-Brentano mode equipped a Lynxeye detector using $CoK_{\alpha 12}$ radiation, λ=1.79Å, operated at 30 kV and 10 mA.

TEM

TEM was performed by using an FEI Tecnai20F system operated at 200kV equipped with a charge coupled device (CCD) camera. The samples were prepared by embedding the solid in an epoxy resin (Epofix, EMS) and cured at 60 °C overnight. Then, they were cut into thin sections with a nominal thickness of 60 nm by using a Diatome Ultra knife, 4mm wide and 35° clearance angle, mounted on a Reichert-Jung Ultracut E microtome. The sections that float on water after cutting were picked up by a Pt loop, put on a carbon-coated polymer grid, and left to dry.

The histograms of particle sizes were obtained from the measurement of approximately 500 particles found using representative images.

N_2 physisorption

N_2 physisorption measurements were performed at -196.15ºC using a Micromeritics Tristar 3000. The samples were dried before measurement under an N_2 flow at 250°C (SBA-15) and 150°C (functionalized materials) for at least 12 h. The pore size distribution of the mesoporous silica materials was calculated from the adsorption branch of the isotherm by Barrett-Joyner-Halenda (BJH) analysis. The maximum of the pore size distribution was reported.

Elemental analysis

S contents of the silica were determined by inductively coupled plasma atomic emission spectroscopy (ICP-AES) by using a Metrohm IC Plus 883. Pd contents of the solid samples and in the liquids from catalysis experiments were analyzed by atomic absorption spectroscopy (AAS) by using an AAS AANALYST200 instrument (PerkinElmer). N contents were measured by using a Vario-EL (Elementar) system equipped with a CHNOS-Analyzer.

TGA

TGA was performed by using a PerkinElmer Pyris 1 apparatus, a typical S/D sample quantity of 5 mg under an air flow of 10 mL .min^{-1}. A heating rate of 5°C.min^{-1} from 50-700°C was used.

IR spectroscopy

IR spectra were measured by using a PerkinElmer System 2000 FTIR instrument. The functionalized samples were dried at 130 °C and bare SBA-15 was dried at 210°C under vacuum before the measurement.

Acknowledgements

The authors are grateful to the Dutch National Research School Combination Catalysis (NRSC-Catalysis) for financial support and Marjan Versluijs-Helder and Hans Meeldijk for SEM and TEM analysis, respectively.

References

1. J. G. de Vries, *Can. J. Chem.*, 2001, **79**, 1086.
2. R. F. Heck, *J. Am. Chem. Soc.*, 1968, **5542**, 5542.
3. R. F. Heck, *J. Am. Chem. Soc.*, 1968, **90**, 5531.
4. R. F. Heck and J. P. Nolley, *J. Org. Chem.*, 1972, **37**, 2320.
5. A. Balanta, C. Godard and C. Claver, *Chem. Soc. Rev.*, 2011, **40**, 4973.
6. L. Djakovitch, K. Koehler, A. Institut and D.-G. Mu, *J. Am. Chem. Soc.*, 2001, **123**, 5990.
7. A. Papp, G. Galbács and Á. Molnár, *Tetrahedron Lett.*, 2005, **46**, 7725.
8. Y. Wan and D. Zhao, *Chem. Rev.*, 2007, **107**, 2821.
9. A. Biffis, M. Zecca and M. Basato, *J. Mater. Chem. A*, 2001, **173**, 249.
10. B. R. Vaddula, A. Saha, J. Leazer and R. S. Varma, *Green Chem.*, 2012, **14**, 2133.
11. E. J. García-Suárez, P. Lara, A. B. García, M. Ojeda, R. Luque and K. Philippot, *Appl. Catal. A Gen.*, 2013, **468**, 59.

12. T. Ishida, Y. Onuma, K. Kinjo, A. Hamasaki, H. Ohashi, T. Honma, T. Akita, T. Yokoyama, M. Tokunaga and M. Haruta, *Tetrahedron*, 2014, **70**, 6150.

13. K. Köhler, M. Wagner and L. Djakovitch, *Catal. Today*, 2001, **66**, 105.

14. M. Wagner, *Top. Catal.*, 2000, **13**, 319.

15. X. Ma, Y. Zhou, J. Zhang, A. Zhu, T. Jiang and B. Han, *Green Chem.*, 2008, **10**, 59.

16. P. Han, X. Wang, X. Qiu, X. Ji and L. Gao, *J. Mol. Catal. A Chem.*, 2007, **272**, 136.

17. O. Verho, A. Nagendiran, E. V. Johnston, C. Tai and J.-E. Bäckvall, *ChemCatChem*, 2013, **5**, 612.

18. M. Shakeri, R. J. M. Klein Gebbink, P. E. de Jongh and K. P. de Jong, *Angew. Chem. Int. Ed. Engl.*, 2013, **52**, 10854.

19. Y. Hao, Y. Chong, S. Li and H. Yang, *J. Phys. Chem. C*, 2012, **116**, 6512.

20. S.-Y. Chen, T. Yokoi, C.-Y. Tang, L.-Y. Jang, T. Tatsumi, J. C. C. Chan and S. Cheng, *Green Chem.*, 2011, **13**, 2920.

21. F. F. de Sousa, A. C. Oliveira, J. M. Filho, G. S. Pinheiro, M. Giotto, N. a. Barros, H. S. a. Souza and A. C. Oliveira, *Chem. Eng. J.*, 2013, **228**, 442.

22. N. C. Mehendale, J. R. a. Sietsma, K. P. de Jong, C. A. van Walree, R. J. M. K. Gebbink and G. van Koten, *Adv. Synth. Catal.*, 2007, **349**, 2619.

23. M. Wolters, L. J. W. van Grotel, T. M. Eggenhuisen, J. R. a. Sietsma, K. P. de Jong and P. E. de Jongh, *Catal. Today*, 2011, **163**, 27.

24. A. H. de Morais Batista, F. F. de Sousa, S. B. Honorato, A. P. Ayala, J. M. Filho, F. W. de Sousa, A. N. Pinheiro, J. C. S. de Araujo, R. F. Nascimento and A. Valentini, *J. Mol. Catal. A Chem.*, 2010, **315**, 86.

25. L. Escamilla-Perea, R. Nava, B. Pawelec, M. G. Rosmaninho, C. L. Peza-Ledesma and J. L. G. Fierro, *Appl. Catal. A Gen.*, 2010, **381**, 42.

26. J. Sun, D. Ma, H. Zhang, X. Liu, X. Han, X. Bao, G. Weinberg, N. Pfänder and D. Su, *J. Am. Chem. Soc.*, 2006, **128**, 15756.

27. M. H. Huang, A. Choudrey and P. Yang, *Chem. Commun.*, 2000, 1063.

28. U. Junges and B. Krutzschc, *J. Chem. Soc. Chem. Commun.*, 1995, 2283.

29. T. Kang, Y. Park and J. Yi, *J. Mol. Catal. A Chem.*, 2006, **244**, 151.

30. J. Sun and X. Bao, *Chemistry*, 2008, **14**, 7478.

31. R. J. White, R. Luque, V. L. Budarin, J. H. Clark and D. J. Macquarrie, *Chem. Soc. Rev.*, 2009, **38**, 481.

32. M. L. Toebes, J. a. van Dillen and K. P. de Jong, *J. Mol. Catal. A Chem.*, 2001, **173**, 75.

33. N. J. S. Costa and L. M. Rossi, *Nanoscale*, 2012, **4**, 5826.

34. R. L. Oliveira, D. Zanchet, P. K. Kiyohara and L. M. Rossi, *Chemistry*, 2011, **17**, 4626.

35. R. L. Oliveira, P. K. Kiyohara and L. M. Rossi, *Green Chem.*, 2009, **11**, 1366.

36. R. L. Oliveira, P. K. Kiyohara and L. M. Rossi, *Green Chem.*, 2010, **12**, 144.

37. M. Shakeri, C. Tai, E. Göthelid, S. Oscarsson and J.-E. Bäckvall, *Chemistry*, 2011, **17**, 13269.

38. O. P. Khatri, K. Adachi, K. Murase, K. Okazaki, T. Torimoto, N. Tanaka, S. Kuwabata and H. Sugimura, *Langmuir*, 2008, **24**,7785.

39. M. Guerrero, N. J. S. Costa, L. L. R. Vono, L. M. Rossi, E. V. Gusevskaya and K. Philippot, *J. Mater. Chem. A*, 2013, **1**, 1441.

40. D. K. Yi, S. S. Lee, G. C. Papaefthymiou, J. Y. Ying, B. Way, T. Nanos, R. V June, V. Re, M. Recei and V. October, *Chem. Mater.*, 2006, **18**,614.

41. L. M. Rossi, I. M. Nangoi and N. J. S. Costa, *Inorg. Chem.*, 2009, **48**, 4640.

42. N. J. S. Costa, P. K. Kiyohara, A. L. Monteiro, Y. Coppel, K. Philippot and L. M. Rossi, *J. Catal.*, 2010, **276**, 382.

43. J. Webb, S. Macquarrie, K. Mceleney and C. Crudden, *J. Catal.*, 2007, **252**, 97.

44. J. H. Clark, D. J. Macquarrie and E. B. Mubofu, *Green Chem.*, 2000, **2**, 53.

45. A. Modak, J. Mondal and A. Bhaumik, *Green Chem.*, 2012, **14**, 2840.

46. V. Polshettiwar, C. Len and A. Fihri, *Coord. Chem. Rev.*, 2009, **253**, 2599.

47. K. Shimizu, S. Koizumi, T. Hatamachi, H. Yoshida, S. Komai, T. Kodama and Y. Kitayama, *J. Catal.*, 2004, **228**, 141.

48. B. Nohair, S. Macquarrie, C. M. Crudden and S. Kaliaguine, *J. Phys. Chem. C*, 2008, **112**, 6065.

49. S. Macquarrie, B. Nohair, J. H. Horton, S. Kaliaguine and C. M. Crudden, *J. Phys. Chem. C*, 2010, **114**, 57.

50. S. C. Reactions, P. Dutta and A. Sarkar, *Adv. Synth. Catal.*, 2011, **353**, 2814.

51. Y. Ji, S. Jain and R. J. Davis, *J. Phys. Chem. B*, 2005, **109**, 17232.

52. J. Richardson and C. Jones, *J. Catal.*, 2007, **251**, 80.

53. C. M. Crudden, M. Sateesh, R. Lewis and C. Kl, *J. Am. Chem. Soc.*, 2005, **127**, 10045.

54. F. Zhao, B. M. Bhanage, M. Shirai and M. Arai, *J. Mol. Catal. A Chem.*, 1999, **142**, 7.

55. K. Köhler, R. G. Heidenreich, J. G. E. Krauter and J. Pietsch, *Chemistry*, 2002, **8**, 622.

56. D. Br, *Nanoscale*, 2010, **2**, 887.

57. P. Trens, R. Denoyel and J. Rouquerol, *Langmuir*, 1995, **11**, 551.

58. S. Murthy, *J. Colloid Interface Sci.*, 1988, **126**, 387.

59. N. Erathodiyil, S. Ooi, A. M. Seayad, Y. Han, S. S. Lee and J. Y. Ying, *Chemistry*, 2008, **14**, 3118.

60. J. a. Widegren and R. G. Finke, *J. Mol. Catal. A Chem.*, 2003, **198**, 317.

61. K. Yu, W. Sommer, M. Weck and C. W. Jones, *J. Catal.*, 2004, **226**, 101.

62. M. Dams, L. Drijkoningen, B. Pauwels, G. Van Tendeloo, D. E. De Vos and P. A. Jacobs, *J. Catal.*, 2002, **236**, 225.

63. A. Sayari, B. Han and Y. Yang, *J. Am. Chem. Soc.*, 2004, **100**, 14348.

64. L. Jiao and J. R. Regalbuto, *J. Catal.*, 2008, **260**, 329.

65. R. D. Gonzalez and N. Orleans, *Catal. Lett.*, 1992, **12**, 73.

Chapter 4

Palladium nanoparticles confined in thiol-functionalized ordered mesoporous silica for more stable Heck and Suzuki catalysts

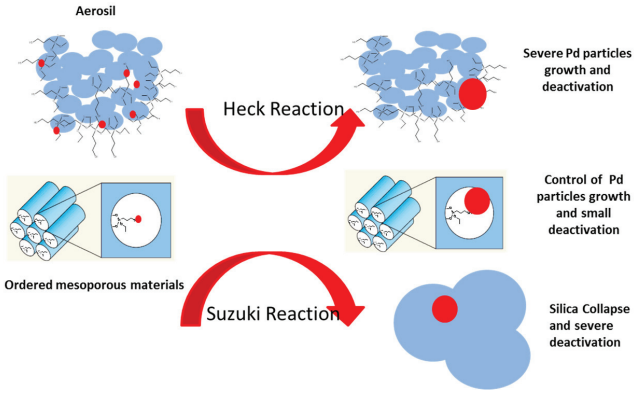

Abstract

Palladium nanoparticles of similar size of ~2 nm were synthesized on different silica-based materials all functionalized with thiol groups i.e., Aerosil-380, SBA-15, Plugged SBA-15 and m-MCF. The resulting materials were used to study the influence of confinement of Pd nanoparticles in functionalized silica support on the Heck and the Suzuki reaction. In the case of the Heck reaction, for all catalysts it was proven that leached Pd species were responsible for activity. However, the catalysts based on ordered mesoporous silica were still able to restrict Pd particle growth giving rise to an enhanced stability. For the Suzuki reaction, stronger alkaline conditions were required and catalysts based on plugged SBA-15 showed a higher stability than those based on SBA-15 and m-MCF which both collapsed after the first cycle. At almost identical Pd particle size, ordered mesoporous materials enhance stability and particle growth is slowed down but not fully suppressed.

Based On: R. L. Oliveira, Wuliyasu He, Robertus J. M. Klein Gebbinkb, Krijn P. de Jong. Palladium nanoparticles confined in thiol-functionalized ordered mesoporous silica for more stable Heck and Suzuki catalysts, Catal. Sci. Tech., 2015, 5, 1919-1928.

Introduction

Ordered mesoporous silica (OMS) such as SBA-15 and MCM-41 has attracted increased interest in the last two decades because of their unique properties such as controllable pore size, large internal surface area and narrow pore size distribution. Due to these properties, numerous applications of OMS in different fields have been reported such as sensors[1–3], drug delivery systems[4–6], chromatography[7,8] and catalysis[9–16]. In catalysis, however, siliceous materials do not have sufficient intrinsic activity and a lot of effort has been done to introduce active species in their pores such as organometallic complexes, molecules with alkaline and acidic properties and metal particles.[17–20]

Silica has been used as support to many different metal nanoparticles. [21–26] However, OMS has been shown very interesting because of the possibility to study the effect of confinement of nanoparticles on their stability. Hao et al. compared the catalytic activity of gold nanoparticles immobilized on SBA-16 and commercial silica gel on the oxidative esterification of alcohols, concluding that the cages of SBA-16 were efficient to prevent the growth of Au, as consequence Au/SBA-16 showed a longer life time.[27] Prieto et al. observed the same phenomena for methanol synthesis using Zn promoted Cu nanoparticles immobilized in SBA-16 and silica gel.[28] In another example, Sun et al. proved that silver nanoparticles confined in SBA-15 have a higher thermal stability than particles immobilized on silica gel surface. [29]

Despite the vast literature about mesoporous materials in catalysis, these materials face big limitations, i.e.s their limited mechanical and hydrothermal stability. Many efforts have been done to produce OMS with a higher stability, for example, Kisler et al. functionalized MCM-41 surface with alkyl groups and proved that its hydrothermal stability increased significantly. [30] Pham et al. coated SBA-15 structure with a thin carbon film and reported that the synthesized material has a higher hydrothermal stability than SBA-15. [31] Van der Voort et al. modified the SBA-15 synthesis and produced a new material called plugged SBA-15, this material showed a higher mechanical and a thermal stability when compared to other OMS, due to the pillaring effect. [32–34]

Plugged SBA-15 was synthesized using an excess of tetraethyl orthosilicate (TEOS), the silica precursor, leading to an ordered mesoporous silica with constricted pores. By varying the synthesis parameters, the extent of plugging can be influenced. Further studies on plugged SBA-15 showed that entrance sizes and cavities length can be tuned by changing synthetic parameters. [35,36] Another interesting OMS is modified mesocellular foam (m-MCF) that was recently synthesized by Shakeri et al.. [37] The procedure is based on P.SBA-15 synthesis, but in this case they introduced a swelling agent (mesitylene) during the synthesis which caused the formation of larger cages. A very interesting characteristic of this material is its narrow entrance sizes and large cages. Moreover, they also showed using electron tomography that the cages are connected with 9-12 neighboring cavities resulting in a highly interconnected network.

Palladium nanoparticles have been widely immobilized on different supports and have been applied as catalyst for many reactions such as oxidation, reduction, C-C cross coupling and others, [38–47] among C-C coupling reactions, the Suzuki and the Heck reactions are the most explored examples. Nevertheless, Pd nanoparticles immobilized on inorganic matrixes suffer from leaching and particle growth due to Ostwald ripening, resulting in a limited recyclability. [48–51] Recently, a lot of work has been done to produce more efficient heterogeneous catalysts for C-C cross coupling reactions. For examples, Pagliaro et al. entrapped Pd nanoparticles using a sol-gel procedure, producing leach-proof nanostructures; these materials could be recycled seven times without losing activity. [52] Budroni et al. also entrapped Pd nanoparticles in a sponge-like silica and reported that leached species were partially responsible for the conversion. [53] Park et al. immobilized Pd nanoparticles in silica nanotubes producing efficient nano-reactors for the Suzuki reaction, and they reported an insignificant Pd leaching and concluded the surface nature of the Suzuki reaction. [54]

A lot of reports in literature have shown that supports with functional groups containing sulfur, nitrogen, phosphorous can lead to more stable catalysts for C-C cross coupling. [55–61] Recently, our group reported that SBA-15 with thiol grafted on its surface produced a more stable catalyst than Pd immobilized on bare SBA-15.[62] In another example,

Ma et al. used an ionic liquid to stabilized palladium nanoparticles on SBA-15 surface. They reported a higher stability of this material when compared with Pd impregnated on pristine SBA-15. [63]

In this chapter, Pd nanoparticles of the almost the same size were synthesized on different silica supports, i.e., Aerosil-380, SBA-15, Plugged SBA-15, m-MCF all modified with thiol ligands. These materials were used to study the effect of the confinement of functionalized silica on the activity and the recyclability of the Heck and the Suzuki reaction. The leaching of Pd, growth of Pd particles and the stability of silica supports were examined to explain possible reasons for deactivation of the catalysts.

Results and discussion

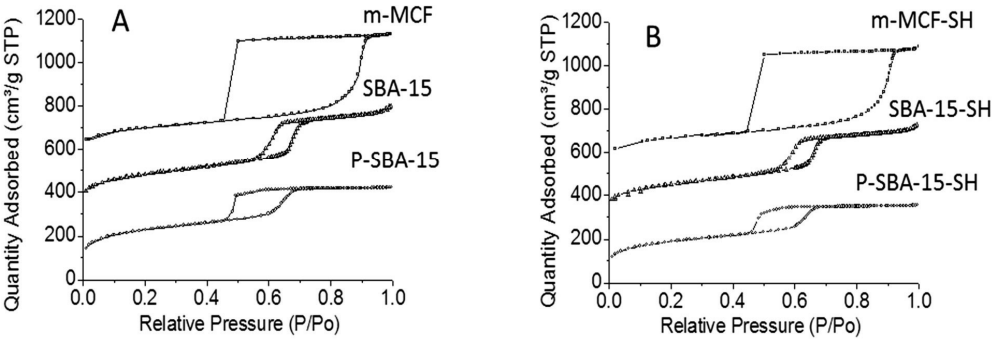

Figure 1-N2 physisorption at 77K of ordered mesoporous silica (A) and functionalized ordered mesoporous silica (B) the isotherms were offset by 300 cm^3/g (SBA-15) and 500 cm^3/g (m-MCF)

The nitrogen sorption isotherms of the synthesized silica materials are type IV following the IUPAC classification (Figure 1A) since they show one step capillary condensation in the adsorption branch, corresponding to filling of the uniform mesoporous by N_2 molecules. The isotherm shows a typical parallel hysteresis of the open mesopores of SBA-15. In the case of plugged SBA-15, which consists of well-ordered mesoporous silica with constrictions and nanocavities in the pores, N_2 physisorption showed an ink-bottle hysteresis typical for cage-like materials, where desorption is delayed until P/Po around 0.47. For m-MCF materials the isotherms showed a broader ink-bottle hysteresis compared to P-

SBA-15 confirming the larger cavities inside this material (22 nm in the case of m-MCF and 6 nm for P-SBA-15).

Argon physisorption at 77K is an alternative to study the entrance size of these materials due to the capillary evaporation which happens at lower relative pressures, extending its use to analyze smaller entrance sizes. Ar physisorption of plugged SBA-15 and m-MCF (Appendices Figure A6) showed that the entrance size of the cavities had a broad size distribution from 5.6 to 3.6 nm in the case of P- SBA-15 and all entrance sizes were smaller than 3.6 nm for m-MCF.

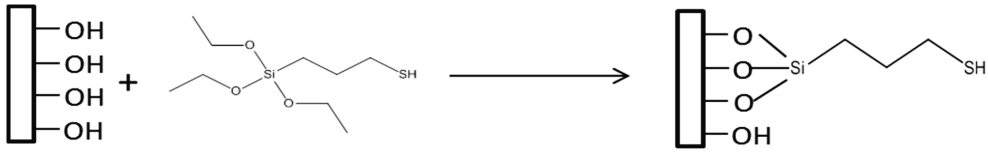

Scheme 1 Functionalization of silica surface with thiol groups

Table 1 Structure and composition of silica supported Pd catalysts

Material	Surface Area (m^2/g)	Pore volume ($cm^3.g$)	S loading (w/w%)	SH density ($\mu mol.m^{-2}$)	Pd loading (w/w%)	S:Pd molar ratio
SiO_2-SHPd	280	2.32	1.2	1.3	1.48	2.7
SiO_2-aSHPd	210	1.47	2.5	3.7	1.54	5.4
SBA-15SHPd	660	0.53	2.7	1.3	1.6	5.6
P-SBA-15SHPd	619	0.52	2.43	1.2	1.55	5.2
m-MCFSHPd	534	0.72	2.61	1.5	1.57	5.5

The thiol groups were grafted on the surface of silica materials using a post synthetic procedure (Scheme 1). Figure 1B shows the isotherms from N_2 physisorption of materials after thiol functionalization. It is observed that functionalized samples displayed a decrease in the specific surface area and pore volume, suggesting functionalization of internal and probably of external walls of OMS materials (Table A1, Appendices). The same phenomena were observed for Aerosil samples (designation SiO_2), silica composed by spheres packed together (N_2 physisorption in Figure A7, Appendices). In the case of SiO_2, two different methodologies were used (Table 1, designated after Pd loading as SiO_2SHPd and SiO_2aSHPd), permitting to obtain materials with different thiol loadings.

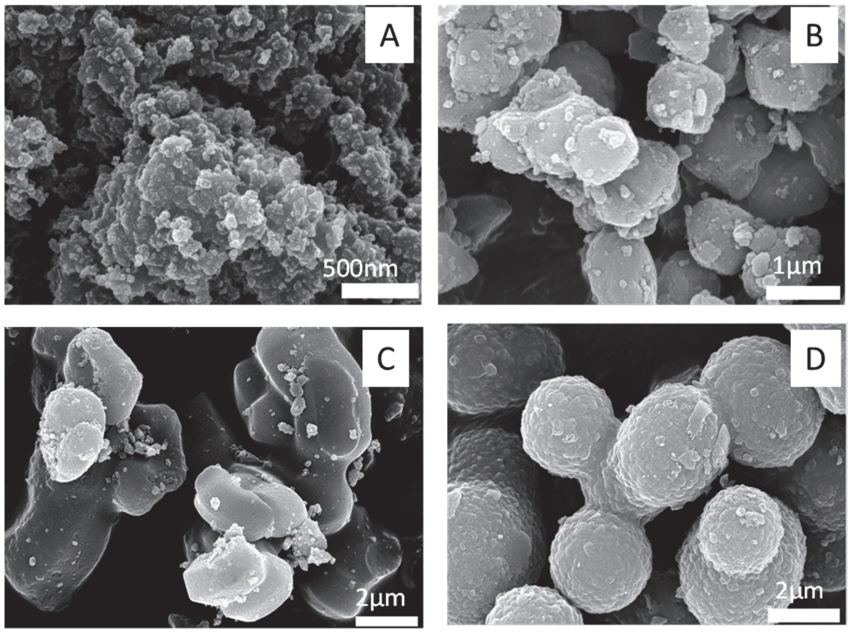

Figure 2 SEM images (A) SiO_2-SH (Aerosil) (B) SBA-15SH (C) P. SBA-15 SH (D) m-MCF-SH

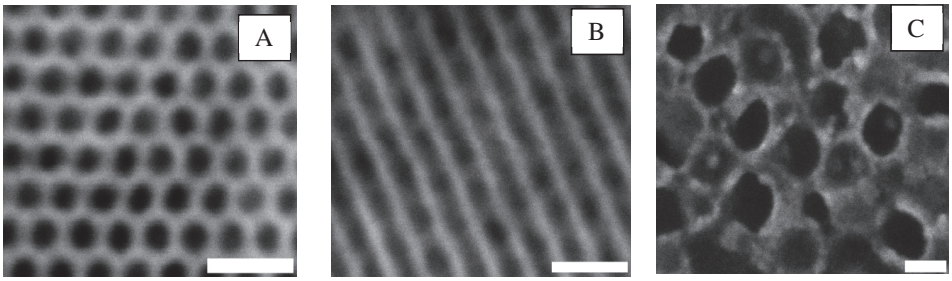

Figure 3 TEM images (A) SBA-15-SH (B) P. SBA-15 SH (C) m-MCF-SH Scale bars: 20 nm

By comparison of SEM images of functionalized samples (Figure 2) and the original supports (images not shown) revealed no changes in the morphology after the functionalization procedure. STEM-HAADF analysis (Figure 3) showed that materials kept the same regularity in pore structure. The open pore structure of SBA-15, the constrictions and nanocavities inside plugged SBA-15 and the cages of m-MCF are shown in Figure 3 A, B, C respectively.

After the synthesis of the hybrid supports, palladium was deposited on functionalized silica using a methodology described recently by our group.[62] TEM analysis (Figure 4) showed that for all cases the structure of silica was unchanged and Pd particles with a very narrow size distribution were observed with an average size of 2.0±0.5 nm. This facilitates the comparison of the catalytic performance of the materials while excluding the influence of the particle size. Table 1 showed the structural properties of the obtained materials. XRD patterns of the fresh catalysts are shown in the Appendices A8 showing a very broad peak around 2θ=50º from which we could not derive a crystallite size.

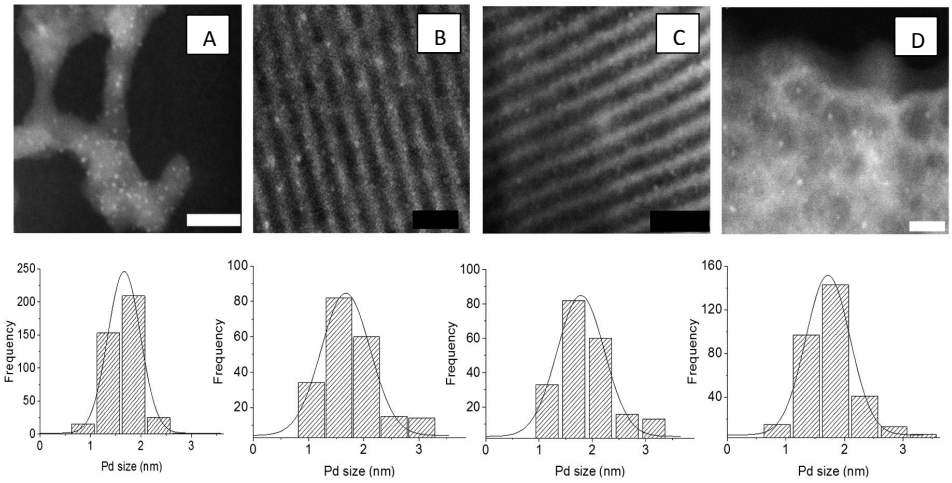

Figure 4 TEM images (A) SiO_2-SHPd, (B) SBA-15-SHPd, (C) P.SBA-15SHPd, (D) m-MCF-SHPd and the corresponding histograms on the bottom. Scale bars are 20 nm

The Heck reaction

Table 2 shows the conversion on the Heck reaction between iodobenzene and butyl acrylate (Scheme 2) and the Pd leached after the separation of the catalysts, in all cases butyl cinnamate was the only product formed. All OMS based catalysts gave rise to similar conversion and metal leaching. However, SiO_2-SHPd showed a slightly higher metal leaching. Please note that a mixture of solvents (toluene + DMF) was used as previously reported.[62]

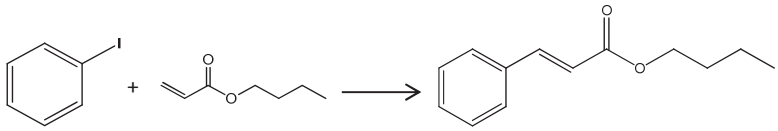

Scheme 2 The Heck reaction between iodobenzene and butyl acrylate

Table 2 The catalytic performance of all synthesized materials and Pd leaching after the Heck reaction

Samples	Conversion (%)	Pd leaching(%)
SBA-15SHPd	88	0.8
P- SBA-15SHPd	88	0.9
m-MCFSHPd	89	0.7
SiO_2-SHPd	85	2.4
SiO_2-aSHPd	5	-

Reaction conditions: 2.25 mmol of iodobenzene, 3.4 mmol of butyl acrylate, 20 mg of supported catalyst (0.1mol% of palladium), 2.14 mmol of Et_3N, 2.0mL toluene+ 0.2mL DMF, 100ºC, 12 hours reaction time.

The loading of thiol groups on the surface of aerosil was increased, permitting it had the same thiol loading and molar ratio between Pd and S as on OMS materials (SiO_2-aSHPd, Table 1). However, this sample showed almost no activity, probably caused by the over-coordination of palladium. As aerosil has a lower specific surface area, the density of thiol per m^2 was much higher (Table 1), this fact might be causing poisoning of the Pd species. Moreover, Pd leaching was lower for this solid compared to OMS, indicating a stronger interaction between Pd and the ligands on this material. This result is in agreement with an earlier report by Jones et al.,[64] that an excess of thiol groups was able to poison Pd species, resulting in a loss of the activity on the Heck reaction.

Hot filtration test and PVP test were used to investigate the nature of the reactive species, i.e., surface or leached Pd (Table A2, appendices). In all cases, hot filtration showed that leached metal species had a strong influence on the activity for the Heck reaction. Moreover, when PVPy was added, the conversion dropped tremendously confirming the results obtained with the hot filtration tests. This fact might explain why all fresh materials with the same density of thiol displayed almost the same reaction rate (Figure A9, appendices).

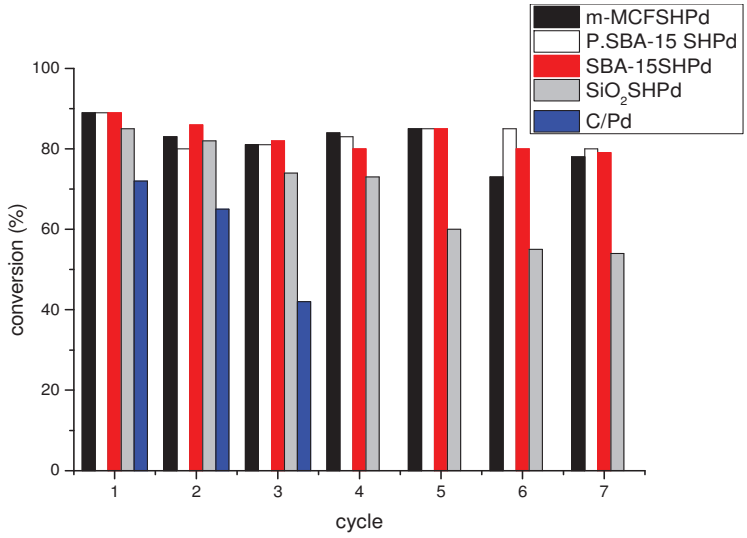

Figure 5 Recyclability of synthesized materials for the Heck reaction

Reaction conditions: 2.25 mmol of iodobenzene, 3.4 mmol of butyl acrylate, 20 mg of supported catalyst (0.13mol% of palladium), 2.14 mmol of base, 2.0mL toluene+ 0.2mL DMF, 100ºC, 12 hours (toluene+ DMF)

The recyclability of the catalysts are shown in Figure 5, a commercial Pd/C, one of the most used catalyst for these reactions, was also used to compare its stability with synthesized materials. In the case of Pd/C, the catalyst suffered from high metal leaching (20% of original Pd amount), as a consequence no conversion was observed after three cycles, showing a limited stability of this material for the Heck reaction under applied conditions. SiO_2-SHPd started to face a considerable decrease on the activity after four cycles, however, this catalyst showed a higher stability than Pd/C. The solids based on OMS could be used 7 times with only a slight reduction of the activity in line earlier publications.[62] However, here it is shown that Pd in OMS is more stable than Pd on activated carbon or non-porous silica (Aerosil).

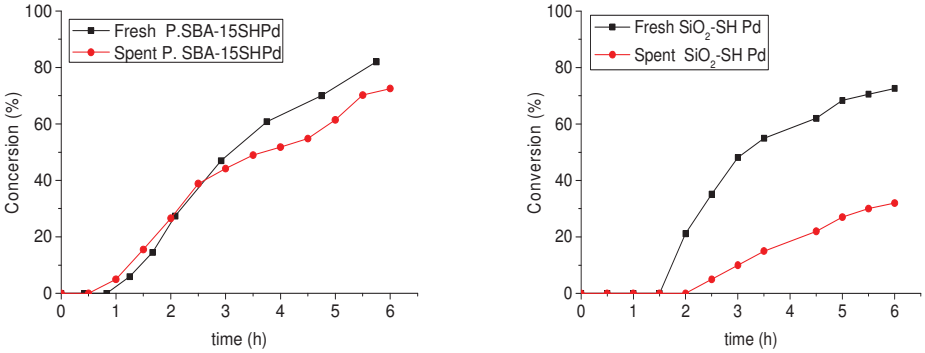

Figure 6 Plot of product yield versus time for the Heck reaction with fresh and spent (after four reaction cycles) SiO_2SHPd and P.SBA-15SHPd

Reaction conditions: 22.5 mmol of iodobenzene, 34 mmol of butyl acrylate, 20 mg of supported catalyst (0.01mol% of palladium), 21.4 mmol of Et_3N, 20mL toluene+ 2mL DMF, 100ºC

Figure 6 shows conversion versus time plots of the fresh and the spent catalysts after four cycles for P.SBA-15SHPd and SiO_2SHPd. The experiments were run at a lower palladium concentration (0.01 mol% of Pd related to iodobenzene). In the case of P.SBA-15SHPd, almost the same reaction rate for fresh and spent catalyst is noted. However, SiO_2SHPd sample displayed a considerable decrease of the reaction rate for the spent catalyst. To reveal the reason for deactivation, the spent catalysts (after four cycles) were studied by X-ray diffraction (XRD) and transmission electron microscopy (TEM). XRD analysis (Appendices A8) showed new lines due to changes on enhanced palladium crystallinity for all catalysts, the new pattern lines corresponded to Pd metal with face centered cubic structure. These results differ from Shimizu et al.[65] which reported no change in palladium crystallinity after the C-C cross coupling reaction using FDU as support. The obtained results give a strong indication that during the catalytic performance the palladium species leached into the solution and were re-deposited on silica surface, leading to particle growth (Ostwald ripening) and enhanced crystallinity of Pd.

TEM analyses of the spent catalysts and histograms of Pd particle size distribution (after 4 cycles) are shown in Figure 7. The structure of Plugged SBA-15 and m-MCF were still recognized, but the palladium particle size had grown slightly, and the majority of metal particles were still found confined in the silica pore structure (Figure 6 B, C). In the case of SiO_2-SHPd, particles grew severely (Figure 6A), very large metal particle from 10-160 nm in diameter were found on the external surface of silica aggregates. These results give a strong indication that the combination of thiol groups and confinement of Pd particles in mesopores had restricted the Pd growth in the case of P.SBA-15 and m-MCF, producing more stable catalysts than SiO_2-SHPd where confinement effects were limited.

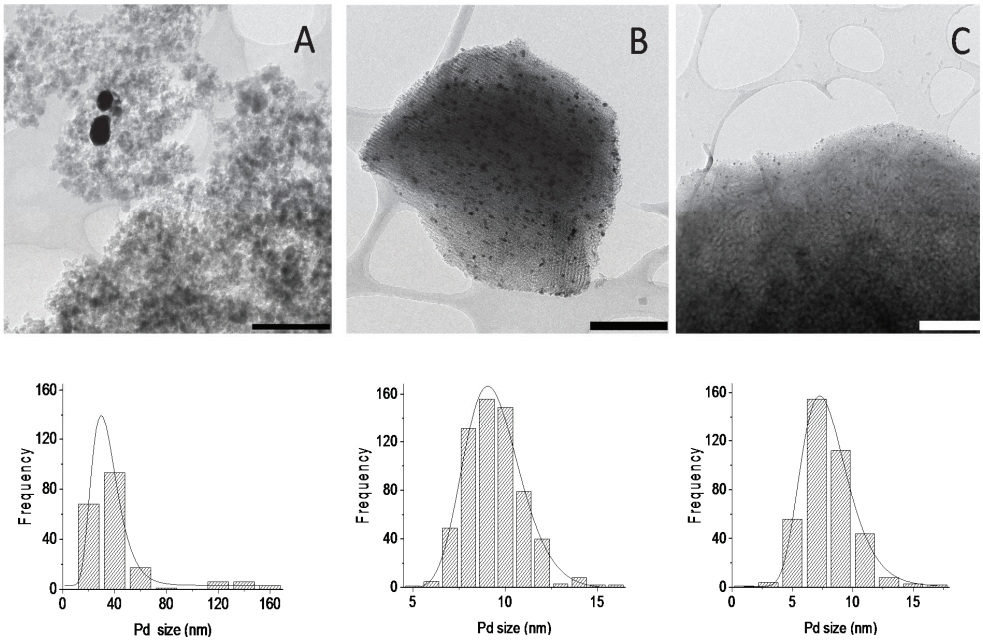

Figure 7 Spent catalysts after four cycle (A) SiO_2-SHPd (B) P. SBA-15 SHPd (C) m-MCFSHPd, scale bars 200 nm, and derived Pd particle size distributions.

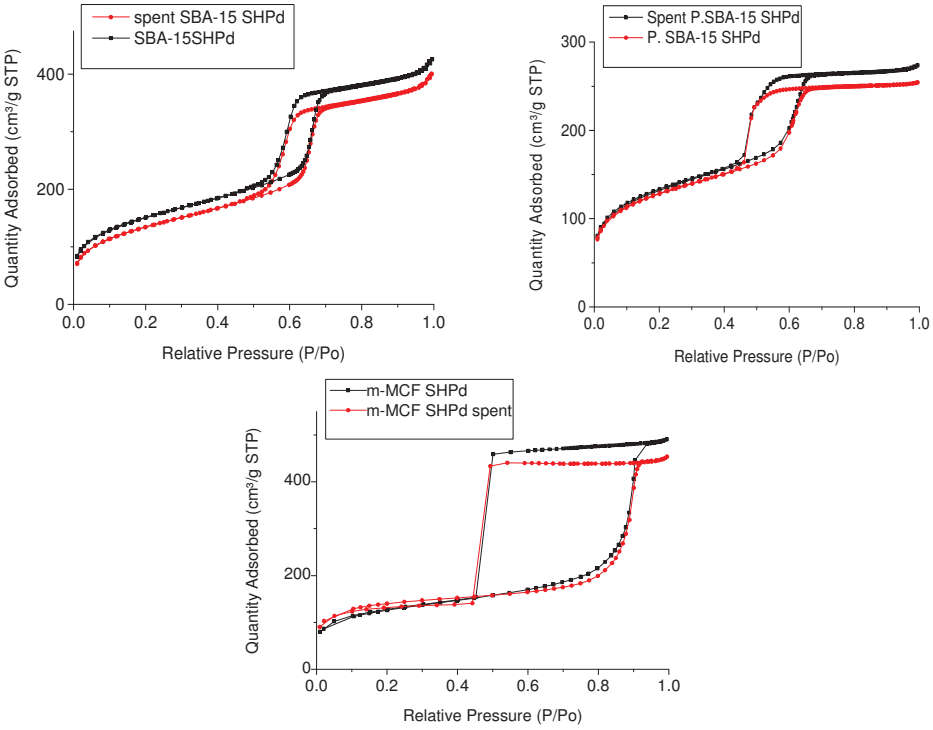

Figure 8 N_2 isotherms at 77K of fresh and spent OMS materials after the Heck reaction

As shown by hot filtration and PVP test, Pd species leached from the support and brought about the catalytic process in solution. Thus, the recapturing process is very important to reduce the formation of large particles and to extend catalyst life time. Despite having the same density of thiol groups per unit of surface area, the Pd particles grew much more severely on Aerosil, we think that the mesopores of OMM provide a concave surface structure with more effective functionalization and, moreover, the confinement of Pd nanoparticles helps to readsorb Pd species and thereby decrease the palladium particle growth. In the case of Areosil, the convex surface structure may provide less effective functionalization, on the one hand, and the fact that Pd nanoparticles are not effectively confined inside pores that results in faster growth of Pd particles via Ostwald ripening, on the other hand.

The porosity of spent catalysts was also investigated by N_2 physisorption to examine the stability of OMS under Heck reaction conditions (Figure 8). Isotherms of fresh and spent catalysts showed that the support materials kept almost the same porosity after 4 cycles, showing no damage to the silica structure under the applied conditions.

Suzuki reaction

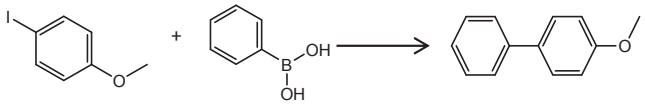

Scheme 3 The Suzuki reaction between 4-iodoanisole and phenylboronic acid

Table 3 Results of Suzuki reaction of 4-iodoanisole and phenylboronic acid using different bases and solvents for P.SBA-15SHPd

Entry	Solvent	Base	Conversion (%)	T ºC
1*	10%V/V DMF/toluene	Et_3N	2	100
2	DMF	Et_3N	8	100
3	Ethanol	Et_3N	5	60
4	Ethanol	n-butylamine	7	60
5	DMF	$Na_3PO_4.12H_2O$	30	60
6	DMF/toluene	$Na_3PO_4.12H_2O$	21	60
7	Ethanol	$Na_3PO_4.12H_2O$	80	60
8	Ethanol	K_2CO_3	41	60
9	Ethanol	Na_3PO_4	45	60

Conditions: 4-iodoanisole (2.4 mmol), phenylboronic acid (2.88 mmol), base (2.4 mmol), 20 mg of P.SBA-15SHPd (0.12 mol % of Pd), 3 hours. *12 hours

The reaction between 4-iodoanisole and phenylboronic acid was used as a model reaction (Scheme 3). Table 3 shows the performance of P-SBA-15SHPd when different solvents and bases were used. In the case of the Suzuki reaction, Et_3N showed to be inefficient when compared to $Na_3PO_4.12H_2O$ and K_2CO_3.Anhydrous Na_3PO_4 was also used as base, but a lower conversion was observed, indicating the influence of water in this reaction as reported before.[66] Moreover, ethanol showed to be a better solvent compared to pure DMF and a mixture of DMF and toluene.

The recyclability of the catalysts was carried out using the conditions described in Table 3 entry 7. The commercial Pd/C catalyst was used for comparing its performance with

silica-supported catalysts. All catalysts suffered a considerable deactivation after each cycle (Figure 9). SBA-15SHPd suffered the strongest deactivation when compared to the other materials. As observed for the Heck reaction, Pd/C suffered again from severe leaching, leading a short life time.

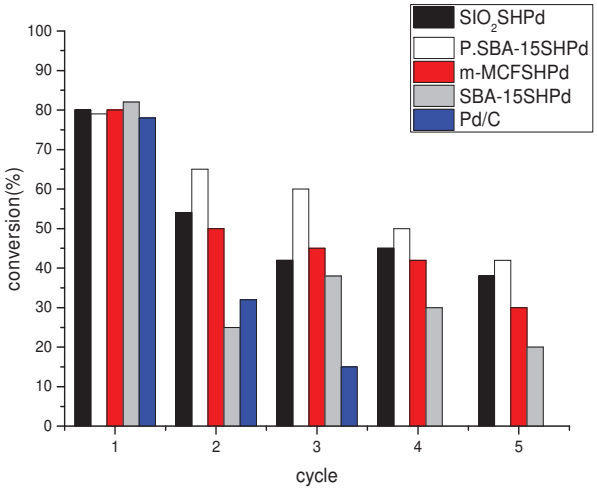

Figure 9 Recyclability of synthesized materials for the Suzuki reaction

Conditions: 4-iodoanisole (2.4 mmol), phenylboronic acid (2.88 mmol), $Na_3P0_4.12H_2O$ (2.4 mmol), 20 mg of P-SBA-15SHPd (0.12 mol % of Pd), 70ºC, 3 hours.

The stability of the supports was examined to address a possible explanation for this extensive deactivation. Figure 10 shows the low angle XRD pattern for the spent (1 cycle) P-SBA-15SHPd and SBA-15SHPd. The peaks which correspond to the *p6mm* configuration are not detected for SBA-15, indicating the pores had collapsed during catalysis. Probably the alkaline condition applied during the Suzuki reaction was responsible for pore collapse. Plugged SBA-15 preserved its structure after the first cycle (Figure 10) as the peaks which correspond to the pore configuration were still visible. This is a clear indication of the higher stability of P-SBA-15 when compared to SBA-15 due to its robust structure and wall thickness. TEM was also used to confirm these results, no well- structured pores were

observed on the spent SBA-15 sample, and on the other hand, the pore structure was still observed for P-SBA-15 (Appendices, A10).

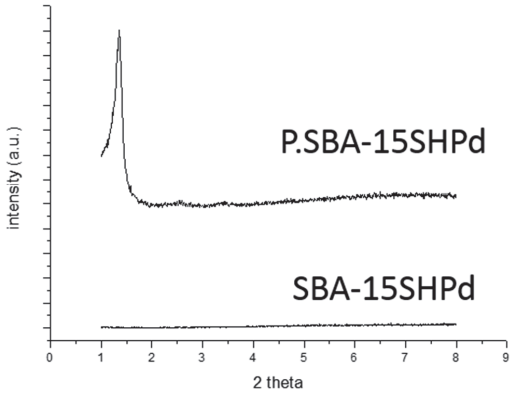

Figure 10 Low angle XRD from SBA-15-SHPd and P.SBA-15SHPd used for the Suzuki reaction (1 cycle)

Table 4 Structural characteristic of catalysts after the Suzuki reaction after 1st cycle

Material	BET surface area (m^2/g)	Pore volume ($cm^3.g$)	Pd leaching (%)*
SBA-15SHPd	15	0.004	24
P.SBA-15SHPd	154	0.16	5
m-MCFSHPd	50	0.07	15
SiO_2SHPd	100	0.16	6

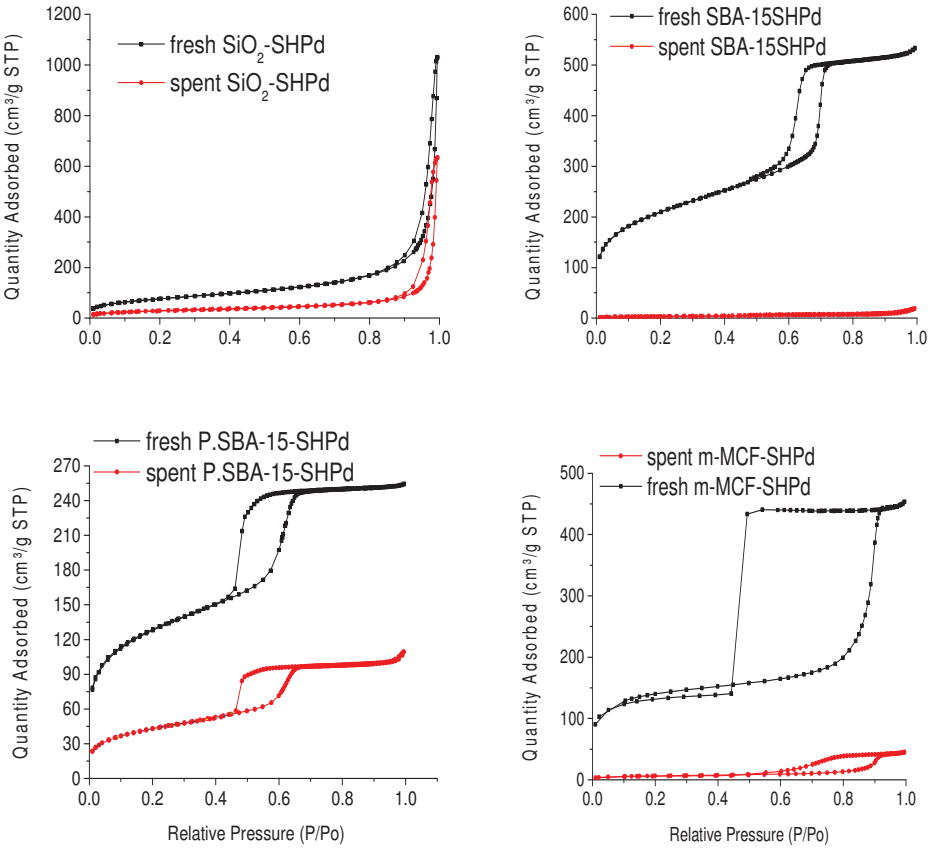

Figure 11 N_2 isotherms of fresh and spent OMS materials after the Suzuki reaction

The porosity of spent materials after first cycle was also investigated by N_2 physisorption (Figure 11), all materials faced a strong loss of surface area and pore volume (Table 4). However, plugged SBA- 15 showed to be the more resistant material compared to other mesoporous materials SBA-15 and m-MCF. In the case of P.SBA-15, the surface area decreased but not as severe as for SBA-15 and m-MCF, a clear ink-bottle hysteresis could still be seen (Figure 11).This can also explain the higher metal leaching from SBA-15SHPd when compared to SiO_2SHPd and P.SBA-15SHPd (Table 4). Probably the destruction of the pores resulted on the reduction of accessibility of the thiol groups, as a consequence limiting the recovery of the palladium species by the ligands. It is also interesting to point out that

P.SBA-15SHPd showed the best recyclability when compared to the other studied supports (Figure 9). For the Suzuki reaction, the collapse of the silica structure might be considered as the main factor for the deactivation of silica-based catalysts. As shown in Table 4, SBA-15 lost 24% of Pd originally deposited on SBA-15, however, the catalyst suffered a larger reduction on activity after the first cycle (from 80% to 26%) which cannot be just explained just by leaching.

Conclusion

In summary, the structural stability of Pd species was influenced by the thiol-functionalized silica structure. Here, we report for the first time that for the Heck reaction, the combined effects of functionalization and confinement of Pd nanoparticles in the cavities of ordered mesoporous silica P.SBA-15 or m-MCF was efficient to limit the Ostwald ripening avoiding the formation of large Pd particles that was observed with non-porous silica. Despite having the same Pd particles size distribution, the materials based on OMS showed a better recyclability when compared to non-porous silica due to the prevention of formation of large Pd particles. The hot filtration and PVP tests showed that homogeneous species contributed considerably to the final conversion. Stabilization of heterogeneous Heck Pd catalyst, therefore, cannot be realized by suppression of leaching. Rather, re-adsorption by functionalization in combination with restriction of Pd particle growth by confinement is effective to extend catalyst life time.

In the case of the Suzuki reaction, the use of stronger alkaline conditions promotes a considerable damage to silica supports. This fact resulted in a limited recyclability of all synthesized materials. However, SBA-15 showed to be the most fragile structure, which collapsed during the first cycle, resulting in a poor recyclability when compared to P.SBA-15. The plugs and the most robust structure of P.SBA-15 permitted the material to display a higher stability for the Suzuki reaction, providing an improvement on the recyclability results.

Experimental

Synthesis and catalytic performance

Chemicals

Triblock copolymer poly(ethylene oxide)–poly(propylene oxide)–poly(ethylene oxide) (P123), tetraethyl orthosilicate 99%, (3-mercaptopropyl)-triethoxysilane 80%, 2% cross-linked poly(4-vinylpyridine) (PVPy), butyl acrylate 99%, piperidine 99%, triethylamine 99%, tetraamminepalladium(II) nitrate solution 10w/w% in water and 5wt % Pd on Carbon (product number 20568-0) were purchased from Sigma-Aldrich. Palladium acetate ($Pd(OAc)_2$, 47.1% Pd) and Aerosil-380 were purchased from Degussa and iodobenzene 98%, 4-iodoanisole 98% and n-butylamine 99% were purchased from Acros Organics

Ordered Mesoporous Silica

SBA-15 and plugged SBA-15 (hereafter referred to as P-SBA-15) were synthesized following a procedure previously described. [36]

For m-MCF synthesis, 4 grams of copolymer Pluronic P123 was dissolved in an aqueous acidic solution (150 ml; 1.6 M) in a 500 mL polypropylene bottle at room temperature overnight. Then, 3 grams of TMB (mesitylene) was added to the reaction mixture at 35 °C dropwise and stirred vigorously during 2 h. After this period, 17 grams of TEOS was slowly added to the mixture ($1.5 mL.min^{-1}$) and stirred vigorously during 5 minutes. After this period, the mixture was kept under static condition at 35ºC for 20 hours followed by 24 hours at 80ºC. The solid product was collected by filtration, washed with distilled water, dried at 60ºC during 24h and calcined at 550ºC in static air during 6 hours.

Functionalization of silica surface

500 mg of SBA-15, P-SBA-15, m-MCF and aerosil-380 was dried at 140ºC under vacuum during 12 hours. After this, the solid was dispersed in 20mL of dried toluene under nitrogen. Then, 2.0 mL of (3-thiopropyl)triethoxysilane (MPTES) was added to the mixture dropwise over 5 minutes under vigorous stirring. Then, the mixture was heated at 110ºC and

stirred during 24 hours under nitrogen. The obtained materials were filtered off and washed 1 time with toluene, 2 times with ethanol and dried at 60ºC during 24 hours.

Aerosil-380 was also functionalized using a different methodology. In this procedure, 500 mg of silica was dried at 140ºC as previously described. Then, the silica was dispersed in 20 mL of dried toluene. Then, 300µL glacial CH_3COOH and 1.5 mL of MPTES were added subsequently to the reaction mixture dropwise. The mixture was reacted at 110ºC under N_2 for 24 hours. The solid was collected and washed as previously described.

Impregnation of Pd

250 mg of functionalized silica support was dried under vacuum at 140º C during 12 hours. After drying, the solid was dispersed in 5mL dry toluene under N_2. 8mg of palladium(II) acetate was dissolved in 1 mL dichloromethane and then added slowly to the dispersion. The dispersion was then heated to 60ºC and stirred during 24h. The solids were collected by centrifugation, washed once with toluene and once with ethanol and finally dried at 60ºC. For reduction of palladium, 100mg of Pd-loaded silica was dispersed in 1mL water. Then, 1mL of 0.1M $NaBH_4$ was added rapidly under vigorous stirring. After 20 minutes, the dispersion was diluted with water to 35 mL, centrifuged, washed thoroughly with water and dried at 60ºC under stagnant air.

Catalyst tests

The Heck reaction

In a typical Heck reaction, a mixed solution of iodobenzene (2.25 mmol), butylacrylate (3.47 mmol), NEt_3(2.15mmol), hexamethylbenzene (internal standard for GC analysis, 1.1mmol) and 2.0 mL of toluene and 0.2 mL of DMF were added to a Schlenk, followed by addition of 20 mg of catalyst (0.1 mol% of palladium relative to iodobenzene). Then, the mixture was stirred for a given time and temperature.

After reaction, solid catalysts were recovered by centrifugation and washed with ethanol (35 mL) and dried under vacuum. For recycling experiments, a new solution mixture described above was added to the solid.

The Suzuki reaction

In a typical reaction, a mixed solution of 4-iodoanisole (2.4 mmol), phenylboronic acid (2.88 mmol), base (2.4 mmol,) and solvent (4 mL) were added to a Schlenk , followed by addition of 20 mg of catalyst (0.1 mol% of palladium relative to 4-iodoanisole). Then, the mixture was reacted at desired temperature and time. For a recycle experiment, the catalyst was recovered by centrifugation and the solid was washed with ethanol/water (1/1, 2 × 40 mL), ethanol (30 mL) and dried at 60˚C overnight. Then, a new solution mixture described above was added to the solid and allows to react during the same period of time. As just one product was observed, the conversions were obtained by external calibration.

GC analysis

A small fraction of the liquid samples were taken and diluted with toluene and analyzed by GC-FID. CG analysis was performed using a PerkinElmer Clarus 500, equipped with a 30m capillary column with 5% phenyl/ 95% methylpolysiloxane as stationary phase(AT5), using the following parameters: initial temperature 50ºC, temperature ramp 10ºC min^{-1}, final temperature 250ºC, injection volume 0.5µL.

Hot filtration test and PVPy poison test

A Heck reaction was allowed to run during 3 hours for a mixture of solvents. Then, the solids were filtered off under static vacuum using a swivel frit filter connected with an empty flask, the filtrate was kept at reaction temperature, the conversion was monitored by GC.

The catalyst poison was added to the Schlenk flask before the addition of reaction solution. Poly(4-vinylpyridine) (2% cross-linked) (PVPy) was used in 350 equivalents of pyridine sites to total of palladium.

Characterization

Electron Microscopy

The morphology and sizes of the silica particles were determined with a Tecnai FEI XL 30SFEG Scanning Electron Microscope (SEM). Transmission electron microscopy was performed using a microscope FEI Tecnai20F, operated at 200 kV equipped with CCD camera.

The samples were embedded in epoxy resin (Epofix, EMS) and cured at 60ºC overnight. Then, they were cut into thin sections with a nominal thickness of 60 nm using a Diatome Ultra knife, 4 mm wide and 35° clearance angle, mounted on a Reichert–Jung Ultracut E microtome. The sections float on water after cutting, were picked up and deposited onto a carbon coated polymer grid and left to dry. The histograms of particle size distribution were obtained from observing about 500 particles in representative micrographs of different areas.

Gas physisorption

N_2 and Ar physisorption measurements were performed at 77 K using a Micromeritics Tristar 3000. The samples were dried before the measurement under a N_2 flow at 250 °C for at least 12 h. The functionalized samples were dried at 130ºC during at least 12 h. The total microporous and mesoporous volume (V_p) was determined using the t-plot method. The pore size distribution of the mesoporous silica supports was calculated from the adsorption branch of the isotherm by BJH analysis. The maximum of the pore size distribution was taken as the average pore diameter.

XRD analysis

Long range pore ordering was confirmed with low-angle X-ray diffraction. Patterns were obtained at room temperature from 0.5 to 8° 2θ with a AXS D2 Phaser powder X-ray diffractometer, in Bragg-Brentano mode, equipped with a Lynxeye detector using Co−$K_{\alpha 12}$ radiation, with λ = 1.790 Å, operated at 30kV, 10 mA. XRD patterns of palladium were recorded for all solids between 10 and 100° 2θ using the same equipment.

Elemental Analysis

S contents of the silica was determined by Inductively Coupled Plasma-Atomic Emission Spectroscopy (ICP-AES) using a Metrohm IC Plus 883. Pd contents of the solid samples and in the liquids from catalysis experiments were analyzed by Atomic Absorption Spectroscopy (AAS) using an AAS, AANALYST200 Perkin Elmer.

Acknowledgments

The authors acknowledge support from European Research Council (ERC) advanced grant no. 338846 and the Dutch National Research School Combination Catalysis (NRSCC).

References

1. L.-L. Li, H. Sun, C.-J. Fang, J. Xu, J.-Y. Jin, C.-H. Yan, *J. Mater. Chem.*, 2007, **17**, 4492.
2. R. Métivier, I. Leray, B. Lebeau, B. Valeur, *J. Mater. Chem.*, 2005, **15**, 2965.
3. D.-H. Lin, Y.-X. Jiang, Y. Wang, S.-G. Sun, *J. Nanomater.*, 2008, **2008**, 1.
4. S. Wang, *Micro. Meso. Mater.*, 2009, **117**, 1.
5. I. I. Slowing, J. L. Vivero-Escoto, C.-W. Wu, V. S.-Y. Lin, *Adv. Drug Deliv. Rev.*, 2008, **60**, 1278.
6. M. Vallet-Regí, F. Balas, D. Arcos, *Angew. Chem. Int. Ed. Engl.*, 2007, **46**, 7548.
7. X. Liu, L. Li, Y. Du, Z. Guo, T. T. Ong, Y. Chen, S. C. Ng and Y. Yang, *J. Chromatogr. A*, 2009, **1216**, 7767.
8. H. Wan, L. Liu, C. Li, X. Xue, X. Liang, *J. Colloid Interface Sci.*, 2009, **337**, 420.
9. L. Escamilla-Perea, R. Nava, B. Pawelec, M. G. Rosmaninho, C. L. Peza-Ledesma, J. L. G. Fierro, *Appl. Catal. A Gen.*, 2010, **381**, 42.

10. H. Yang, L. Zhang, W. Su, Q. Yang, C. Li, *J. Catal.*, 2007, **248**, 204.

11. T.-W. Kim, M.-J. Kim, F. Kleitz, M. M. Nair, R. Guillet-Nicolas, K.-E. Jeong, H.-J. Chae, C.-U. Kim, S.-Y. Jeong, *ChemCatChem*, 2012, **4**, 687.

12. M. Shakeri, R. J. M. Klein Gebbink, P. E. de Jongh, K. P. de Jong, *Angew. Chemie*, 2013, **125**, 11054.

13. M. C. G. Albuquerque, I. Jiménez-Urbistondo, J. Santamaría-González, J. M. Mérida-Robles, R. Moreno-Tost, E. Rodríguez-Castellón, A. Jiménez-López, D. C. S. Azevedo, C. L. Cavalcante Jr., P. Maireles-Torres, *Appl. Catal. A Gen.*, 2008, **334**, 35.

14. S. Das, A. Goswami, N. Murali, T. Asefa, *ChemCatChem*, 2013, **5**, 910.

15. A. Taguchi, F. Schüth, Micro. Meso. Mater. 2005, **77**, 1.

16. Y.-S. Kim, X.-F. Guo, G.-J. Kim, *Chem. Commun. (Camb).*, 2009, 4296.

17. H. Yang, L. Zhang, P. Wang, Q. Yang, C. Li, *Green Chem.*, 2009, **11**, 257.

18. H. Yang, X. Han, Z. Ma, R. Wang, J. Liu, X. Ji, *Green Chem.*, 2010, **12**, 441.

19. S.-Y. Chen, T. Yokoi, C.-Y. Tang, L.-Y. Jang, T. Tatsumi, J. C. C. Chan, S. Cheng, *Green Chem.*, 2011, **13**, 2920.

20. J. Fan, X. Jiang, H. Min, D. Li, X. Ran, L. Zou, Y. Sun, W. Li, J. Yang, W. Teng, G. Li, D. Zhao, *J. Mater. Chem. A*, 2014, **2**, 10654.

21. R. L. Oliveira, P. K. Kiyohara, L. M. Rossi, *Green Chem.*, 2010, **12**, 144.

22. R. L. Oliveira, P. K. Kiyohara, L. M. Rossi, *Green Chem.*, 2009, **11**, 1366.

23. Z. Wang, Q. Liu, J. Yu, T. Wu, G. Wang, *Appl. Catal. A Gen.*, 2003, **239**, 87.

24. E. M. Fixman, M. C. Abello, O. F. Gorriz, L. A. Arrúa, *Appl. Catal. A Gen.*, 2007, **319**, 111.

25. Z. Huang, F. Cui, H. Kang, J. Chen, X. Zhang, C. Xia, *Chem. Mater.*, 2008, **20**, 5090.

26. R. L. Oliveira, D. Zanchet, P. K. Kiyohara, L. M. Rossi, *Chemistry*, 2011, **17**, 4626.

27. Y. Hao, Y. Chong, S. Li, H. Yang, *J. Phys. Chem. C*, 2012, **116**, 6512.

28. G. Prieto, M. Shakeri, K. P. de Jong, P. E. de Jongh, *ACS Nano*, 2014, **8** 2522.

29. J. Sun, D. Ma, H. Zhang, X. Liu, X. Han, X. Bao, G. Weinberg, N. Pfänder, D. Su, *J. Am. Chem. Soc.*, 2006, **128**, 15756.

30. J. M. Kisler, M. L. Gee, G. W. Stevens, A. J. O. Connor,*Chem. Mater.*, 2003, **15**, 619.

31. H. N. Pham, A. E. Anderson, R. L. Johnson, K. Schmidt-Rohr and A. K. Datye, *Angew. Chem. Int. Ed. Engl.*, 2012, **51**, 13163.

32. P. Van Der Voort, P. I. Ravikovitch, K. P. De Jong, M. Benjelloun, E. Van Bavel, A. H. Janssen, A. V Neimark, B. M. Weckhuysen, E. F. Vansant, *J. Phy. Chem. B,* 2002, **123**, 5873.

33. P. Van der Voort, P. I. Ravikovitch, K. P. De Jong, a V Neimark, a H. Janssen, M. Benjelloun, E. Van Bavel, P. Cool, B. M. Weckhuysen, E. F. Vansant, *Chem. Commun. (Camb).*, 2002, 1010.

34. E. B. Celer, M. Kruk, Y. Zuzek, M. Jaroniec, *J. Mater. Chem.*, 2006, **16**, 2824.

35. M. Shakeri, R. J. M. Klein Gebbink, P. E. de Jongh, K. P. de Jong, *Micro. Meso. Mater.*, 2013, **170**, 340.

36. R. L. Oliveira, M. Shakeri, J. D. Meeldijk, K. P. de Jong, P. E. de Jongh, *Micro. Meso.Mater.*, 2015, **201**, 234.

37. M. Shakeri, L. Roiban, V. Yazerski, G. Prieto, J. M. K. Gebbink, P. E. De Jongh, K. P. De Jong, *ACS Catal.*, 2014, 4, 3791.

38. F. Yin, S. Ji, P. Wu, F. Zhao, C. Li, *J. Catal.*, 2008, **257**, 108.

39. B. Karimi, S. Abedi, J. H. Clark, V. Budarin, *Angew. Chem. Int. Ed.*, 2006, **45**, 4776.

40. X. Zhang, H. Yin, J. Wang, L. Chang, Y. Gao, W. Liu, Z. Tang, *Nanoscale*, 2013, **5**, 8392.

41. G. Chen, S. Wu, H. Liu, H. Jiang, Y. Li, *Green Chem.*, 2013, **15**, 230-235.

42. P.M. Ulberman, N. J. S. Costa, K. Philippot, R. C. Carmona, A. A. dos Santos, L. M. Rossi, *Green Chem.*, 2014, 16, 4566.

43. T. Ishida, Y. Onuma, K. Kinjo, A. Hamasaki, H. Ohashi, T. Honma, T. Akita, T. Yokoyama, M. Tokunaga, M. Haruta, *Tetrahedron*, 2014, **70**, 6150.

44. D. D. L. Martins, H. M. Alvarez, L. C. S. Aguiar, O. A. C. Antunes, *Appl. Catal. A Gen.*, 2011, **408**, 47.

45. N. J. S. Costa, P. K. Kiyohara, A. L. Monteiro, Y. Coppel, K. Philippot, L. M. Rossi, *J. Catal.*, 2010, **276**, 382.

46. D. Das, A. Sayari, *J. Catal.*, 2007, **246**, 60.

47. A. Gruber, D. Zim, G. Ebeling, A. Monteiro, J. Dupont, *Org. Lett.*, 2000, **2**, 1287.

48. K. Köhler, R. G. Heidenreich, J. G. E. Krauter, J. Pietsch, *Chemistry*, 2002, **8**, 622.

49. G. Zhang, H. Zhou, J. Hu, M. Liu, Y. Kuang, *Green Chem.*, 2009, **11**, 1428.

50. B. Nohair, S. Macquarrie, C. M. Crudden, S. Kaliaguine, *J. Phys. Chem. C*, 2008, **112**, 6065.

51. S. Macquarrie, B. Nohair, J. H. Horton, S. Kaliaguine, C. M. Crudden, *J. Phys. Chem. C*, 2010, **114**, 57.

52. M. Pagliaro, V. Pandarus, F. Béland, R. Ciriminna, G. Palmisano, P. D. Carà, *Catal. Sci. Technol.*, 2011, **1**, 736.

53. G. Budroni, a Corma, H. Garcia, A. Primo, *J. Catal.*, 2007, **251**, 345.

54. G. Park, S. Lee, S. J. Son, S. Shin, *Green Chem.*, 2013, **15**, 3468.

55. J. H. Clark, D. J. Macquarrie, E. B. Mubofu, *Green Chem.*, 2000, **2**, 53.

56. B. Karimi, D. Enders, *Org. Lett.*, 2006, **8**, 1237.

57. V. Polshettiwar, Á. Molnár, *Tetrahedron*, 2007, **63**, 6949.

58. D. Zhang, J. Xu, Q. Zhao, T. Cheng, G. Liu, *ChemCatChem*, 2014, **10**, 2998.

59. A. El Kadib, K. McEleney, T. Seki, T. K. Wood, C. M. Crudden, *ChemCatChem*, 2011, **3**, 1281.

60. L. Wang, S. Shylesh, D. Dehe, T. Philippi, G. Dörr, A. Seifert, Z. Zhou, M. Hartmann, R. N. Klupp Taylor, M. Jia, S. Ernst, W. R. Thiel, *ChemCatChem*, 2012, **4**, 395.

61. L. M. Rossi, L. L. R. Vono, F. P. Silva, P. K. Kiyohara, E. L. Duarte, J. R. Matos, *Appl. Catal. A Gen.*, 2007, **330**, 139.

62. R. L. Oliveira, J. B.F. Hooijmans, P.E. deJongh, R. J. M. Klein Gebbink, K. P. de Jong, *ChemCatChem*, 2014,**6**, 3223.

63. X. Ma, Y. Zhou, J. Zhang, A. Zhu, T. Jiang, B. Han, *Green Chem.* 2008, **10**, 59.

64. J. Richardson, C. *J.* Jones, *Catal.* 2007, **251**, 80.

65. K. Shimizu, S. Koizumi, T. Hatamachi, H. Yoshida, S.Komai, T. Kodama, Y. Kitayama, *J. Catal.* 2004, **228**, 141.

66. J. Webb, S. Macquarrie, K. Mceleney, C. Crudden, *J. Catal.*, 2007, **252**, 97.

Chapter 5

Encapsulation of chiral Fe(salen) in mesoporous silica structures for use as catalysts to produce optically active sulfoxides

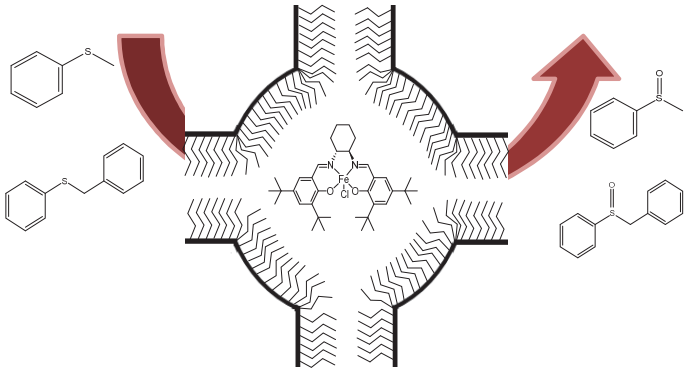

Abstract

Solid catalysts which are heterogeneous at macroscopic scale but homogeneous at microscopic level were prepared by the encapsulation of Fe(salen) by a "ship in a bottle" approach. This approach permits to synthesize inside the nanocages of SBA-16 and m-MCF a "free" Fe(salen) complex, having conformational freedom and behaving as a complex in solution. These materials were used as catalysts for asymmetric oxidation of sulfides. The entrance size of SBA-16 and m-MCF was precisely tuned by changing synthesis parameters and the silylation of silica surface with n-propyl groups, this control of entrance sizes resulted in materials with different Fe(salen) loading. Chiral Fe(salen) trapped in the m-MCF materials showed higher activity than the complex immobilized in SBA-16. The activity and enantioselectivity of catalysts based on m-MCF are almost the same of the homogeneous counterpart, although the heterogenized catalysts presented a limited recyclability due to its stability.

Based on: Rafael L. Oliveira, Tom Nijholt, Mozaffar Shakeri, Robertus J. M. Klein Gebbink and Krijn P. de Jong. Encapsulation of chiral Fe(salen) in mesoporous silica structures for use as catalysts to produce optically active sulfoxides. ChemCatChem submitted

Introduction

Asymmetric oxidation of sulfides is an important method to produce optically active sulfoxides. These sulfoxides are widely used as chiral auxiliaries in asymmetric synthesis[1–3] and as bioactive molecules in the pharmaceutical industry, for examples, drugs for the treatments of platelet aggregation, neurodegenerative disorders, peptic ulcer diseases and others.[4–8] In the last decades, several methods to produce enantiopure sulfoxides have been described; the use of biocatalysts and chiral metal complexes are the most applied methodologies.[9–18]

Chiral metal complexes based on titanium, vanadium and manganese have been extensively investigated.[19–29] In contrast, chiral iron complexes have been less explored for this reaction. Recently, many efforts have been done to produce iron complexes for asymmetric oxidation of sulfides[30–37] since iron shows advantages such as low toxicity and its earth abundance. Bryliakov et al. showed that Fe(salen) complexes can be used as catalysts for the asymmetric oxidation of sulfides, however, reasonable stereoselectivity was only obtained when iodosylbenzene was used as external oxidant.[38] Egami et al. synthesized an Fe(salan) complex that showed good yield and stereoselectivity when H_2O_2 was used as oxidant.[39]

Despite the catalytic performance of some chiral metal complexes, most of them have not been applied on an industrial scale yet. The major problems are the difficulty in the separation, recycling and contamination with metal of the desired products. Heterogeneous catalysts have attracted much attention due to their advantages, easy separation from the products and recyclability.[40–42] Thus, a lot of energy has been spent on the immobilization of metal complexes on solid supports, such as silica, polymers and carbon.[43–49] However, heterogeneous catalysts can suffer from degradation of the immobilized complexes and metal leaching, limiting their recyclability.[50,51] For example, Basset et al. studied a silica-supported zirconium complex applied on transesterification of acrylates and observed a considerable deactivation of the catalyst due to exchange of ligands during catalytic performance and also leaching of zirconium.[52]

Chiral complexes can be immobilized on solid matrixes using various methods, such as grafting, electrostatic interaction, sol-gel methods and encapsulation through the "ship in the bottle" approach.[53,54] In the "ship in the bottle" approach, metal complexes are usually synthesized inside porous materials such as zeolites.[55–59] The potential advantage of this approach is that the complex does not suffer modification, having the possibility to keep the same catalytic activity of the homogeneous counterpart. However, zeolites present some limitations as support due to their small cage sizes and restricted window sizes, resulting often in materials with lower activity and stereoselectivity. Ordered mesoporous silica (OMS) has been shown as an alternative due to their larger entrances sizes and pore structures, permitting encapsulated complexes with more conformational freedom and to behave as a free complex in solution .[60–63] The most applied OMS for the "ship in the bottle" synthesis is SBA-16, nevertheless, it is difficult to obtain this material with large cage sizes (> 7 nm) and small entrance sizes (~ 2nm). Recently our group reported the synthesis of a new silica material called modified mesocellular foam (m-MCF), which combines large cage sizes (15-22 nm) and narrow entrance sizes (1.8-3.7nm), showing properties very interesting for application in the "ship in the bottle" approach.[64]

In this contribution, we encapsulated an Fe(salen) complex in modified m-MCF and SBA-16 materials with different entrances and cage sizes. The m-MCF and SBA-16 surfaces were functionalized with n-propyl groups with allows us to tune their entrances and cage sizes. The obtained hybrid materials were used to study the influence of their structure on the loading of the Fe(salen) complex and the catalytic properties for sulfoxidation, using asymmetric oxidation of thioanisole with different oxidants as a model reaction.

Results and discussion

Synthesis and characterization of support materials (m-MCF and SBA-16)

N_2 physisorption isotherms of pristine ordered mesoporous materials (m-MCF and SBA-16) are displayed in Figure 1. The isotherms can be classified as type IV following the IUPAC classification since they show one step capillary condensation in the adsorption

branch (Figure 1), corresponding to filling of the uniform mesopores by N_2 molecules. In all cases, ink-bottle hysteresis was observed, showing that liquid N_2 remained trapped by the narrow entrances of the pores, resulting in delayed desorption at a relative pressure around 0.45. This fact does not permit the exact determination of entrances sizes of these materials since liquid nitrogen is not stable below a relative pressure of 0.45.

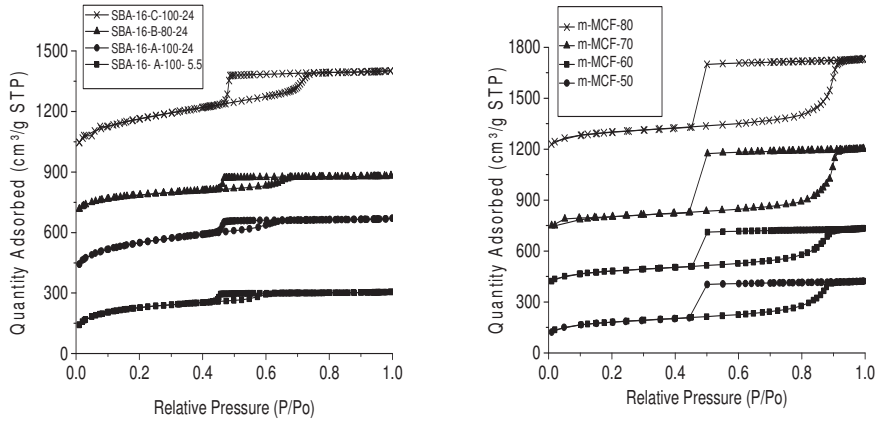

Figure 1- Nitrogen adsorption isotherms for pristine SBA-16 (left) and m-MCF (right). The isotherms were offset vertically by 300, 600 and 900 for SBA-16 materials and by 300, 600, 1100 for m-MCF.

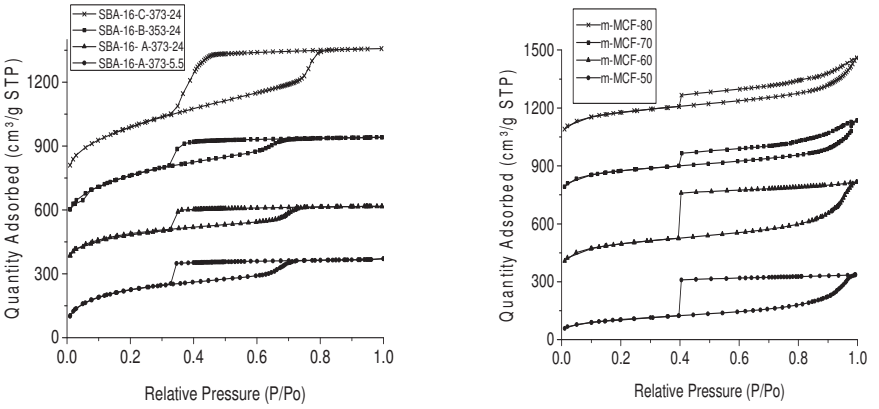

Figure 2- Argon adsorption isotherms for pristine SBA-16 (left) and m-MCF (right). The isotherms were offset vertically by 300, 500 and 700 for SBA-16 materials and by 300, 700, 1000 for m-MCF.

Argon physisorption at 77K is an alternative to study the entrance size of these materials due to the capillary evaporation of argon which takes place at lower relative pressures, extending its use to analyze smaller entrance sizes down to 3.8 nm. Argon physisorption isotherms of synthesized materials are shown in Figure 2, from the obtained hysteresis of synthesized m-MCF and SBA-16, it is possible to conclude that the majority of entrance sizes are smaller than 3.8 nm. However, the sample SBA-16-C-373-24 showed a small fraction of entrance sizes around 3.8 nm.

A method based on the post-synthetic functionalization of silica surface with alkoxysilanes with different carbon chain length was applied for determining the entrance size of synthesized materials.[66,70] After this functionalization, the obtained hybrid materials were examined by nitrogen physisorption to study the accessibility of the pores for N_2 molecules; see the appendices for details (Figures A11 and A12 show the isotherms of synthesized materials after the functionalization with different organosilanes) and the derived values of entrance size in Table 1.

Table 1- Structural properties of pristine materials from N2 physisorption and surface modification

Material	Surface area (m^2/g)	Pore volume (cm^3/g)	Cage size (nm)*	Entrance size (nm)**
SBA-16-A-373-5.5	769	0.49	5.0	2.0
SBA-16-A-373-24	875	0.56	5.0	2.5
SBA-16-B-353-24	634	0.43	6.5	2.8
SBA-16-C-373-24	911	0.77	7.5	3.2
m-MCF-50	619	0.65	16	2.0
m-MCF-60	623	0.66	16.5	2.0
m-MCF-70	685	0.92	20.8	2.5
m-MCF-80	689	0.96	21.2	2.8

*determined by BJH analysis from adsorption branch **determined by post-synthetic treatments

Table 1 shows the structural properties of the synthesized silica materials (m-MCF and SBA-16). The increase of cage size resulted almost always in an increase of the entrance sizes especially for SBA-16 materials. However, we were able to reduce the entrance sizes of

SBA-16 materials by decreasing the hydrothermal treatment time, this fact is in good agreement with results reported by Li et al[60] and Jaroniec et al..[70] The obtained materials were examined by SEM (Appendices, Figures A13 and A14) and TEM (Figure 3) to assess the ordered structure of pristine SBA-16 and m-MCF.

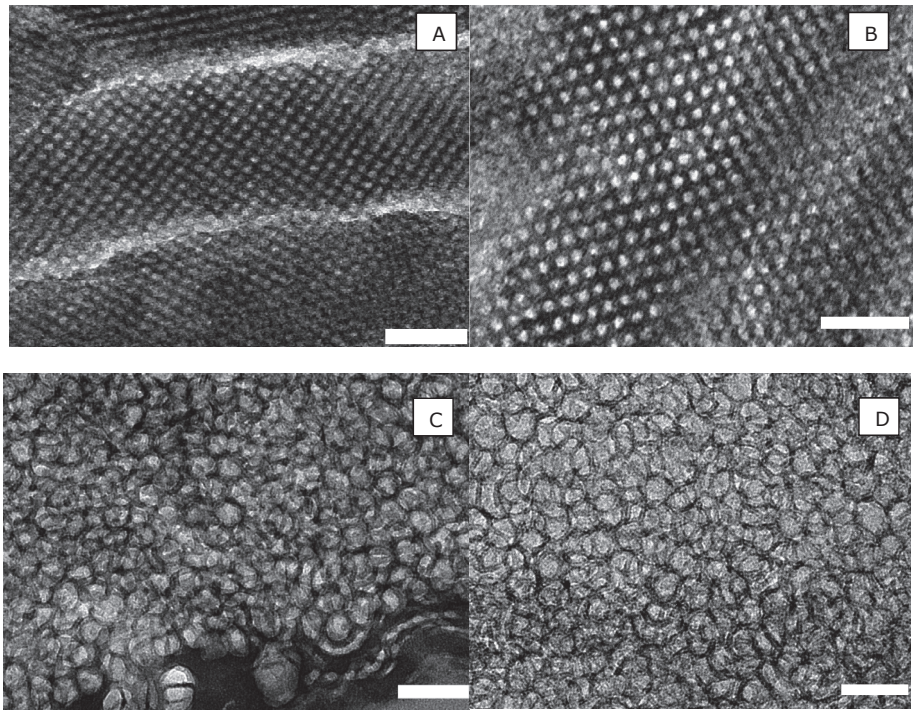

Figure 3- TEM images of pristine host materials (A) SBA-16-B-353-24 (B) SBA-16-C-373-24 (C) MCF-50 (D) MCF-70. All scale bars 50nm.

Ship in the bottle approach

A post synthetic functionalization with n-propyl groups of silica materials (Table 2) was carried out to narrow the entrance sizes and allow a better dispersion of solid materials in organic solvents (Appendices Figure A15) due to the increase of hydrophobicity (organic solvents are commonly used as solvents for salen complexes synthesis and as solvents on sulfoxidation reactions). Moreover, the functionalization decreases the acidity of silica that might cause degradation of the trapped salen complex. After the functionalization, N_2

physisorption was used to characterize these materials (Table 2), showing a decrease of the porosity, surface area and pore size compared to pristine SBA-16 and m-MCF (isotherms in appendices, Figure A16).

Table 2-Structural properties of functionalized m-MCF and SBA-16 materials from N2 physisorption

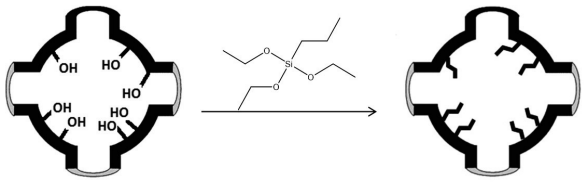

MATERIAL	BET SURFACE AREA (M^2/G)	PORE VOLUME (CM^3/G)	CAGE SIZE (NM)*
F-SBA-16-A-373-5.5	368	0.23	4.3
F-SBA-16-A-373-24	455	0.29	4.5
F-SBA-16-B-353-24	341	0.24	5.3
F-SBA-16-C-373-24	500	0.40	6.8
F-M-MCF-50	332	0.43	14
F-M-MCF-60	313	0.41	16
F-M-MCF-70	379	0.64	21
F-M-MCF-80	376	0.65	21

*determined by BJH analysis from adsorption branch

IR spectroscopy was used to assess the presence of alkyl groups on silica. Peaks at 2850-2970 cm^{-1} which correspond to C-H stretch vibrations of alkyl groups were observed. Moreover, the intensity of the peak at 3740cm^{-1} which corresponds to the stretching mode of free silanol groups almost disappeared (Appendices, Figure A17), showing a successful grafting of the organosilanes on the silica surface. TGA analyses were used to confirm the decomposition of alkyl groups grafted on silica surface (Appendices, Figure A18). This fact suggests a successful functionalization of the external and internal walls of the silica (the functionalized materials are designated F. m-MCF and F. SBA-16).

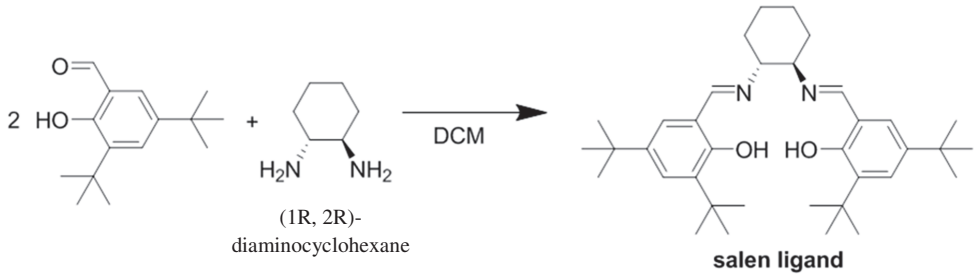

Scheme 1 Schiff base reaction witch takes place inside cages of synthesized materials

A salen ligand was selected as a model which allows to obtain reasonable loadings in the cages of different materials.[60,61,64] Scheme 1 shows the reaction (Schiff base reaction) which took place inside the cage structure of F-m-MCF and F-SBA-16 (for more details see the Experimental section). IR spectroscopy was used to confirm the formation of the salen ligand inside m-MCF-60, as a new peak at 1632 cm^{-1} appeared which corresponds to C=N bond formation (Appendices, Figure A19 B) and the absence of the peaks at 1582cm^{-1} and at 1760 cm^{-1} which correspond to primary amine, and carbonyl groups of aldehyde in the spectrum, conforming the successful formation and encapsulation of salen ligand in m-MCF-60.

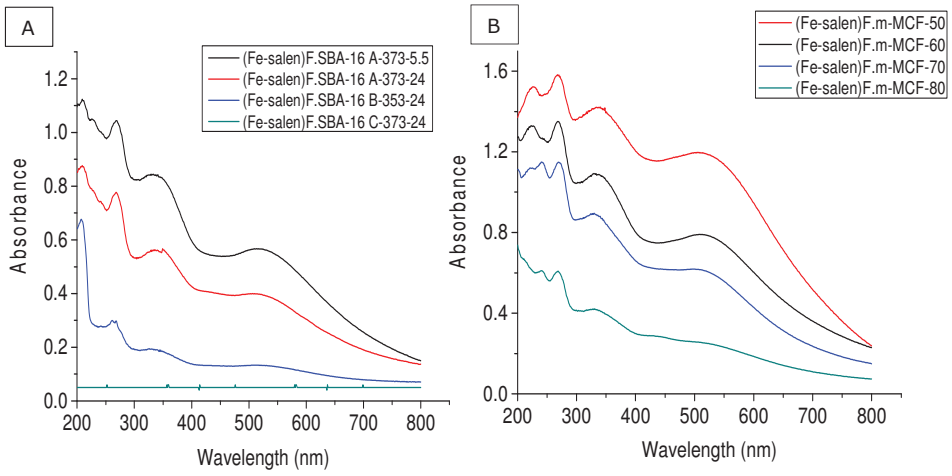

Figure 4 UV-vis spectra of Fe(salen) complex immobilized in cage-like materials base on F.SBA-16 (A) and F.m-MCF(B)

Upon complexation with iron, a color change from yellow to red was observed of the solid material, giving a strong indication that the Fe(salen) complex was formed inside functionalized m-MCF and SBA-16. UV-vis spectra of all materials (m-MCF and SBA-16) are shown in Figure 4. In almost all cases four bands were observed; the bands at 220 and 280 nm are attributed to π-π* located predominantly on the phenyl ring and the peak at 312-350 nm to C=N.[48,71-73] The expected d-d transition at 522-565 nm of Fe(salen) was also observed further confirming its formation inside silica materials. The homogeneous complex was also synthesized and physically mixed with m-MCF-60, this mixture showed the same peaks as observed for materials synthesized by "ship in the bottle" (Appendices, Figure A 20).

The intensities of the characteristic bands of Fe(salen) decreased with increase of the pore entrance sizes and these intensities are related with their concentration inside the silica structures (Figure 4). In the case of F.SBA-16-C-373-24 which has entrance size around 3.2 nm, no characteristic UV-vis bands were observed, suggesting no encapsulation of the complex, due to the large entrance sizes. A higher concentration of salen complex inside the materials is observed when the entrance sizes are smaller than 2 nm (F.m-MCF-50, F.m-MCF-60 and F.SBA-16-A-373-5.5). Table 3 shows the iron content in the materials measured by inductively coupled plasma (ICP) which are in line with the UV-vis spectra results. In general, higher concentration of Fe(salen) complexes is encapsulated in the m-MCFs than in the SBA-16 materials. For example, m-MCF-50 contained 4 times more iron than F.SBA-16-A-373-5.5, showing advantages of m-MCF for this approach.

The IR spectrum of F.m-MCF-60 after complexation of iron is shown in Appendices Figure A19. It is known that the band which correspond to C=N displays a redshift of 3-12 cm^{-1} after complexation, which corresponds to participation of the azomethine and phenolic oxygen of the ligand binding to Fe ions.[72] However, only a part of this band shows this shift in the studied case, indicating an incomplete complexation of Fe with the salen ligand, in other words, not all salen ligands present in m-MCF-60 are participating in the complexation of iron.

Table 3 Iron loading in the synthesized materials

Material	Fe loading (w/w%)
F.SBA-16-A-373 5.5	0.19
F.SBA-16-A-373-24	0.14
F.SBA-16-B-353-24	0.06
F.SBA-16-C-373-24	< 0.005
F. m-MCF-50	0.85
F.m-MCF-60	0.70
F.m-MCF-70	0.50
F.m-MCF-80	0.26

Asymmetric oxidation of sulfides

The asymmetric oxidation of thioanisole was used as a model reaction (Table 4). This reaction was run in different solvents, using different oxidants, and Fe(salen) immobilized in F-m-MCF-60 or pure Fe(salen) as catalysts. In all cases, a high selectivity to methylsulfinyl-benzene (Table 4, 1a) was observed with a very small fraction of the substrate being further oxidized to methylsulfonyl-benzene (1b). Iodosylbenzene (PhIO) was the only oxidant which gave rise to enantioselectivity, in agreement with results reported by Talsi et al. that Fe(salen) complex is able to form specific active sites with PhIO by a Lewis acid activation of iodosylbenzene to form the oxygen-transfer species.[38]

If acetonitrile and dichloromethane were used as solvents, low conversions of thioanisole were observed when PhIO was the oxidant. On the other hand, the conversion were higher using H_2O_2 (Table 4 entries 2, 4,5,7), which is probably related with the limited solubility of PhIO in these solvents. Thus, methanol was selected as a solvent due to higher solubility of PhIO. In this case, a remarkable increase of the conversion was observed (Table 4, entry 11). Sodium hypochlorite was also used as an oxidant agent, but low conversions were observed as was reported before for sulfoxidation of thioanisole using homogeneous Fe(salen) complex as a catalyst.[38]

The homogeneous Fe(salen) complex was also tested as catalyst for comparison (Table 4). The homogeneous counterpart showed only slightly higher activity than the immobilized complex in the cages of F.m-MCF-60 for thioansole as substrate. This is much more favorable than some results previously reported,[74,75] for example, Ogunwumi et. al.

reported that immobilized Mn salen complex in zeolites suffered big reduction on the activity when compared with homogeneous counterpart.[57] Table 4 also shows that the homogeneous catalyst presented somewhat higher enantioselectivity when compared to immobilized system.

Table 4- Oxidation of thioanisole using Fe(salen) immobilized in F-m-MCF-60 with different solvents and oxidations

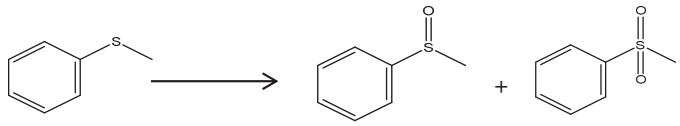

1a 1b

Entry	Solvent	Oxidant	Conversion (%)[a]	Selectivity (%)[b]	ee(%)[c]
1[d]	CH3CN	PhIO	68	99	64
2	CH3CN	H_2O_2	65	99	0
3	CH3CN	NaOCl	8	98	0
4	CH3CN	PhIO	11	99	55
5	CH_2Cl_2	H_2O_2	40	99	0
6	CH_2Cl_2	NaOCl	8	99	0
7	CH_2Cl_2	PhIO	10	99	56
8[d]	CH3OH	PhIO	92	98	66
9	CH3OH	H_2O_2	94	95	0
10	CH3OH	NaOCl	20	98	0
11	CH3OH	PhIO	90	98	57
12[e]	CH3OH	PhIO	65	99	62

[a] Determined with GC-FID, [b] selectivity to 1a, [c] determined by chiral HPLC analysis, [d] homogeneous Fe(III) salen complex uses as catalyst, [e] the reaction was run at 0ºC during 10 hours. Reaction conditions: 4 mL of solvent, 0.4 mmol of thioanisole, oxidant (0.65 mmol) and catalyst (1 mol% Fe), 20ºC, 4 hours.

The comparison between the activity of Fe(salen) complex immobilized in F-m-MCF and F-SBA-16 was also explored. Despite the same entrance sizes, higher conversion values were observed when Fe(salen) complex was immobilized in F-m-MCF (Table 5, entries 2-5), probably the large cage size of these materials allow more freely moving Fe(salen) complexes with concomitant higher activities. The conversions observed with the larger

substrate benzyl phenyl sulfide were considerable lower in the case of F-SBA-16 and F-m-MCF-60 when compared to F-m-MCF-70. Probably, the combination of larger cages and in particular entrance sizes of F-m-MCF-70 facilitates the diffusion of this substrate and PhIO producing a more suitable catalyst. Moreover, even for the catalyst based on F-m.MCF-70, the oxidation of benzyl phenyl sulfide was slightly lower than the conversion of thioanisole. This data shows that the conversion values can be optimized through tuning the silica structure (entrance size and cage size).

Table 5 Sulfoxidation using Fe(salen) and Fe(salen) immobilized in F.m-MCF and F.SBA-16

Entry	Material	Substrate	Conversion (%)[a]	Selectivity (%)[b]	ee(%)[c]
1	Fe-salen complex	PhSMe	92	98	66
2	Fe-F-m-MCF-60	PhSMe	90	98	57
3	Fe-F-SBA16-A-373-5.5	PhSMe	60	98	55
4	Fe-F-m-MCF-70	PhSMe	91	97	55
5	Fe-F-SBA-16-A-373-24	PhSMe	65	98	56
6	Fe-salen complex	$PhCH_2SPh$	94	98	74
7	Fe-F-m-MCF-60	$PhCH_2SPh$	43	93	62
8	Fe-F-SBA16-A-373-5.5	$PhCH_2SPh$	25	98	60
9	Fe-F-m-MCF-70	$PhCH_2SPh$	80	95	63
10	Fe-F-SBA16-A-373-24	$PhCH_2SPh$	40	98	61

[a] Determined with GC-FID [b] Selectivity to corresponding sulfoxide [c] Determined by chiral HPLC analysis Reaction conditions: 4 mL of MeOH, 0.4 mmol of substrate, PhIO (0.65 mmol), catalyst (1 mol% Fe), 20ºC, 4 hours.

To determine the nature of the catalytic species for the reaction, a hot filtration test was performed for the oxidation of thioanisole using Fe(salen) immobilized in F-m-MCF-60 as catalyst, after 1 hour of reaction the liquid and solid phase were separated. The liquid phase was kept at the same reaction condition showing that the filtrate was only able to provide a slight additional conversion of around 5% (Figure 5). This gives a strong indication that the vast majority of the reaction is catalyzed by iron (salen) inside the m-MCF structure.

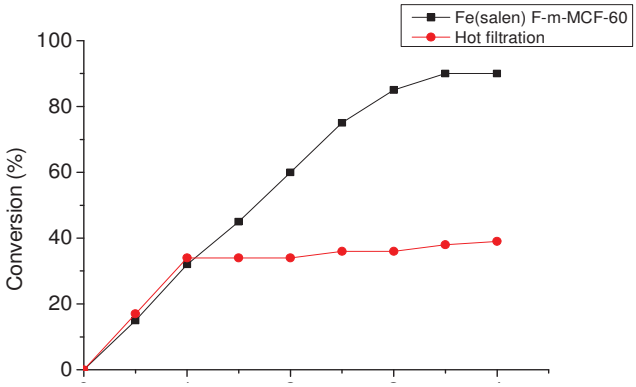

Figure 5 Time-conversion plot and leaching test as evidence for the nature of the catalyst for sulfoxidation of thioanisole

The recyclability of Fe(salen)F-m-MCF-70 was investigated in the asymmetric oxidation of benzyl phenyl sulfide using PhIO as oxidant and methanol as solvent (Table 6). This reaction was selected due to the higher enantioselectivity obtained when compared to the values obtained for thioanisole. The catalyst was recovered by filtration, and washed thoroughly with ethanol. The catalyst could be recycled two times without loss in the activity and chemical selectivity, but a slight decrease of enantioselectivity was apparent. However, a slight loss of catalytic activity was observed during third cycle. The content of iron was determined to investigate a possible explanation for this deactivation, however, the leaching of iron was insignificant.

Table 6 Recyclability of Fe(salen)immobilized in F.m-MCF-70 for the oxidation of benzyl phenyl sulfide

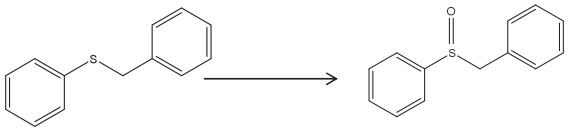

Run	Conversion (%)[a]	Selectivity (%)[b]	ee%[c]
1	80	95	63
2	79	97	55
3	61	98	0
4	60	98	0
5	52	98	0

[a] Determined with GC-FID [b] Selectivity to corresponding sulfoxide [c] Determined by chiral HPLC analysis Reaction conditions: 4 mL of MeOH, 0.4 mmol of benzyl phenyl sulfide, PhIO (0.65 mmol), catalyst (2 mol%), 20ºC, 4 hours.

UV-vis spectroscopy was used to study any possible change of the Fe(salen) complex structure inside F m-MCF-70. Figure 6 shows that the spent catalyst still presents two bands at 200-300 nm which correspond to π-π* of the phenyl ring, however the band at 350 nm which is attributed to C=N cannot be seen anymore, giving a strong indication that Fe(salen) complex suffered some changes in its configuration. Moreover, the band which corresponds to the d-d transition at 522-565 nm of Fe(salen) is not so well-defined anymore, the formation of iron oxide particles, since the presence of these particles was suggested by XRD analysis as a broad peak was observed around 50º two-theta (Appendices, Figure A21).

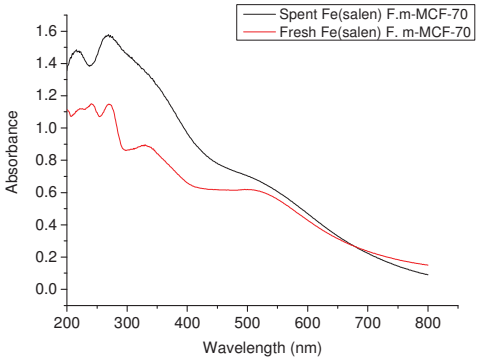

Figure 6 UV-vis spectra of fresh and spent Fe(salen) complex encapsulated in F.m-MCF-70

Experimental

Chemicals

Triblock copolymer poly(ethylene oxide)-poly(propylene oxide)-poly(ethylene oxide) (P123), Pluronic F-127, tetraethyl orthosilicate (TEOS, 98%), mesitylene (TMB, 99 %), 1-[3(trimethoxysilyl)propyl]urea (97 %), styrene (99.5 %), ethylene glycol (99 %), methyl phenyl sulfoxide (97 %) and iron(III) chloride hexahydrate ($FeCl_3$*$6H_2O$, 97 %) were purchased from Sigma Aldrich. Hydrogen peroxide (H_2O_2, 35 wt% in H_2O), acetonitrile (CH_3CN, HPLC), thioanisole (PhSMe, 99 %), and methyl sulfoxide (DMSO, 99.7 %) were purchased from Acros Organics. Benzyl phenyl sulfide ($PhSCH_2Ph$, 98 %), 3,5-di-tert-butyl-

2-hydroxybenzaldehyde (99 %) and 1-butylamine (99 %) were purchased from Alpha Aesar. (1R, 2R)- diaminocyclohexane (99 %) was purchased from ABCR. Hydrochloric acid (HCl, 37 %) was purchased from Emsure. Methanol (MeOH, 100 %), ethanol (EtOH, 100 %), dichloromethane (DCM, 99.5 %), chloroform ($CHCl_3$, 99.5 %) and toluene (100 %) were purchased from Interchema.

m-MCF synthesis

For m-MCF synthesis, 4 g of copolymer Pluronic P123 was dissolved in an aqueous acidic solution (150 ml, 1.6 M HCl) in a 500 mL polypropylene bottle at room temperature overnight. Then, 3 grams of TMB (mesitylene) was added to the reaction mixture at 35 °C dropwise and stirred vigorously during 2 h. After this period, 17 grams of TEOS was slowly added to the mixture (1.5mL.min^{-1}) and stirred vigorously during 5 minutes. After this period, the mixture was kept under static condition in the closed bottle at 35ºC for 20 hours followed by 24 hours at different temperatures 50º, 60º, 70º,80ºC. The solid product was collected by filtration, washed with distilled water, dried at 60ºC during 24h and calcined at 550ºC in static air during 6 hours. The synthesized and calcined material will be referred to as 'pristine material' in this paper.

SBA-16 synthesis

The synthesis of SBA-16 was done, following the procedure described by Kim et al..[65] The structural properties of SBA-16 were tuned by changing the composition of the mixture between F127 and P123, hydrothermal temperature and its time. Briefly, an aqueous solution of polymers was prepared in hydrochloric acid in distilled water overnight. Then, TEOS was added to the mixture at 35ºC under vigorous stirring during 15 minutes until it was completely dissolved. After this, the mixture was placed in an oven for 24h under static condition at 35ºC and the mixture was further maintained at 80ºC or 100ºC for hydrothermal treatment during different periods. Subsequently, the samples were calcined at 823K during 6 hours. The samples were designated SBA-16-X-T-t, were X (A, B, C) relates to the

composition of the mixture of polymers, T is the hydrothermal temperature and t is hydrothermal treatment time. The synthesized and calcined material will be referred to as 'pristine material' in this paper.

The starting molar composition was 0.0040 F127:1.0 TEOS: 4.0 HCl: 130 H2O for SBA-16 A; 0.00084 P1230.0038 F127: 1.0 TEOS 4.2HCl: 137 H2O for SBA-16 B, 0.0016 P123: 0.0037:1.0 TEOS:4.4 HCl:144H2O for SBA-16 C.

Functionalization of the silica surface with n-propyl

Functionalization was conducted following a procedure described by Shakeri et al..[66] 700 mg of m-MFC or SBA-16 was dried during 5 h at 140 °C to remove physisorbed water. Then, the solid was dispersed in 25 mL of dried toluene and 2.5 mL of n-propyl triethoxysilane was added to the mixture dropwise over 5 minutes under vigorous stirring, followed by the addition of 1 mL of n-butylamine. The mixture was heated to 110 °C and stirred for 48 hours under nitrogen. The obtained materials were filtered off and washed with toluene, toluene:ethanol (1:1) and ethanol and dried at 60ºC during 24 hours.

Functionalization of the silica surface with different organosilanes (entrance size determination)

In this procedure, 100 mg of m-MCF and SBA-16 was dried at 140ºC during 5h to remove physisorbed water. Then, the solid was dispersed in 3.5mL of dried toluene and 1.72 mmol of organosilane with different carbon length was added, followed by the addition of 0.15mL of n-butylamine. The mixture was heated to 110°C and kept stirring for 48 hours under nitrogen. The obtained materials were filtered off and washed with toluene, toluene:ethanol (1:1) and ethanol and dried at 60ºC during 24 hours.

Ship in a bottle synthesis

This procedure was conducted via a method described by our group recently.[61] The n-propyl functionalized m-MCF or SBA-16 (700 mg) was dried at 120°C for 6 hours under vacuum (-1.0 bar). Then, 150 mg of 3,5-di-tert-butyl-2-hydroxybenzaldehyde was dissolved in 2 mL of CH_2Cl_2 and added to the solid. The mixture was kept stirring for 2 days under

reflux at 40°C under N_2 atmosphere. Then, 37 mg of (1R, 2R)-diaminocyclohexane was added to the mixture. The mixture was stirred again for 2 days at 40°C under N_2 atmosphere. After this period, the solvent was removed by static vacuum. Then, 175.21 mg (2 equiv.) of $FeCl_3*6H_2O$ was dissolved in 3 mL of methanol and added to the solid. The system was stirred at RT for 24h. The mixture was centrifuged (4000 rpm, 5 min) and the solvent was removed by decantation. The remaining solid was washed with toluene (40mL), methanol (40mL) and CH_2Cl_2 (40mL) to remove the unconfined Fe-salen complex. The solids thus obtained were dried under vacuum at 40ºC.

Fe(salen) complex synthesis

This synthesis of the salen ligand was done following the procedure described by Jacobsen et al..[67] Briefly, a 100 mL three-necked flask was equiped with a cooler and 78.30 mg (0.686 mmol) of (1R, 2R)-diaminocyclohexane, 189.55 mg (1.37 mmol) of K_2CO_3 and 2.5 mL of distilled H_2O were added. The mixture was stirred until the dissolution of the chemicals, then, 9.5 mL of EtOH was added to the flask. The mixture was heated under stirring to 77 °C, then, 321.39 mg (1.37 mmol) of 3,5-di-tert-butyl-2-hydroxybenzaldehyde was dissolved in 5 mL of EtOH and added dropwise to the mixture and stirred for 2 h. After that, 2 mL of water was added and the reaction mixture was cooled to a temperature around 5°C over 2 hours and kept at that temperature for 1 additional hour. Crude solids were obtained by vacuum filtration and washed twice with 2 mL of EtOH. The solids were collected and dissolved in 8 mL of DCM, and washed twice with 5 mL of H_2O and once with 2 mL of brine. The organic layer was dried over Na_2SO_4; the final product was obtained after removal of the solvent using a rotavap. Yield: 72.2% (270.97 mg). IR (KBr pellet): 2960 cm^{-1} ($(CH_3)_3C$-), 2864 cm^{-1} (C-H), 1631 cm^{-1} (C=N), 1595 cm^{-1} (C=C Aromatic). ESI-MS found m/z: 546.42.

Complexation of the salen with iron was done following a procedure reported previously.[68] 104.61 mg (0.387 mmol) of $FeCl_3*6H_2O$ dissolved in 4ml of MeOH were added to 211.79 mg (0.387 mmol) of ligand dispersed in in 2 mL of MeOH. The mixture was stirred for 24 h at room temperature. After this period, the purple solid was collected and washed

with MeOH and dissolved in dicloromethane (DCM) and dried over Na_2SO_4. The solution of the power was left to stand at room temperature and crystals were obtained. IR (KBr pallet): 2960 cm^{-1} $(CH_3)_3C$), 2866 cm^{-1} (C-H), 1602 cm^{-1} (C=N). UV-Vis: λ (nm) = 229, 274 (Ar, π-π*), 351 (C=N, π- π*), 514 (Fe, d-d). ESI-MS found m/z: 600.34.

Synthesis of iodosylbenzene (PhIO)

The synthesis was based on Saltzman et al..[69] Briefly, 4.025 g (12.5 mmol) of (diacetoxyiodo)benzene was added to aqueous NaOH (3M, 18.75 mL) over a period of 5 min. The lumps of solids formed were triturated over a period of 15 min and the reaction mixture was stirred for another 45 min. Then, 12.5 mL of H_2O was added to the solution and the mixture was left stirring for 30-45 min. Büchner filtration was applied to obtain greenish solids. The solids were returned to the beaker and triturated in 50 mL of H_2O, followed by another Büchner filtration. A final purification was done by trituration of the solids in 18.25 mL of chloroform. The green solids were obtained by Büchner filtration; the solids were dried under nitrogen.

Sulfoxidation

The Fe(salen) based catalyst (1 or 2 mol % related to thioether) was charged in a glass vial together with 4 mL of solvent and 0.4 mmol thioether, followed by the addition of an oxidant (0.64 mmol). The mixture was stirred for the desired time and temperature. After this period, the solids were recovered by centrifugation (5 min, 4000 rpm), and the liquid layer was tapped off and analyzed by GC to determine conversion; the ee values were obtained by HPLC analysis. For recycle experiments, solid catalysts were recovered by filtration and washed with ethanol (35 mL) and dried under vacuum, then, a new solution mixture described above was added to the solid.

GC analysis

A small fraction of the liquid samples were taken and diluted with toluene and analyzed by GC-FID. CG analysis was performed using a PerkinElmer Clarus 500, equipped with a 30m capillary column with 5% phenyl/ 95% methylpolysiloxane as stationary

phase(AT5), using the following parameters: initial temperature 50ºC, temperature ramp 10ºC min^{-1}, final temperature 250ºC, injection volume 0.5µL.

HPLC analysis

All of the chiral HPLC experiments were carried using a Perkin Elmer Series 200 pump/-diode array detector. A chiralcel OD column of 250 x 4.6 mm was used, with a bulk stationary phase consisting of 10 µm particles of silica support physically coated with the polymeric chiral selector cellulose tris(3,5-dimethylphenylcarbamate). A flow of 1 mL/min of 80 % hexane and 20 % isopropanol was used for all experiments.

Characterization

Electron Microscopy

The morphology and sizes of the silica particles were determined with a Tecnai FEI XL 30SFEG Scanning Electron Microscope (SEM). Transmission electron microscopy was performed using a FEI Tecnai20F, operated at 200 kV equipped with CCD camera.

The samples were embedded in epoxy resin (Epofix, EMS) and cured at 60ºC overnight. Then, they were cut into thin sections with a nominal thickness of 60 nm using a Diatome Ultra knife, 4 mm wide and 35° clearance angle, mounted on a Reichert–Jung Ultracut E microtome. The sections float on water after cutting, were picked up and deposited onto a carbon coated polymer grid and left to dry.

Gas physisorption

N_2 and Ar physisorption measurements were performed at 77 K using a Micromeritics Tristar 3000. The samples were dried before the measurement under an N_2 flow at 250 °C for at least 12 h. The functionalized samples were dried at 130ºC during at least 12 h. The micropore and mesopore volume (V_p) was determined using the t-plot method. The pore size distribution of the mesoporous silica supports was calculated from the adsorption branch of

the isotherm by BJH analysis. The maximum of the pore size distribution was taken as the average pore diameter.

Elemental Analysis

Fe contents of the silica was determined by Inductively Coupled Plasma-Atomic Emission Spectroscopy (ICP-AES) using a Metrohm IC Plus 883.

UV-Vis and IR spectroscopy

UV-Vis experiments were carried out on a Varian Cary 500 Scan UV-Vis-NIR spectrophotometer with the configuration in the range of 200-800 nm with a data interval of 1 nm and at a rate of 600 $nm.min^{-1}$.

KBr pellets were prepared by mixing 15 mg of sample with 250 mg of KBr; this mixture was grinded into a fine powder, after which it was introduced to a pellet press. The solid was pressured by a 15.011 SPECAC hydraulic press to obtain the KBr pellets. The IR spectroscopic experiments were carried out on a Perkin Elmer Spectrum One FT-IR infrared spectrometer.

TGA analysis

Thermogravimetric analysis (TGA) was carried out using a Perkin-Elmer Pyris 1, a typical sample quantity of 5 mg with an air flow of 10 $ml\,min^{-1}$. A heating rate of 5 °C min^{-1} from 50ºC until 700 °C was used.

Conclusion

A chiral Fe(salen) complex was encapsulated in the nanocages of n-propyl modified SBA-16 and m-MCF. The silica structure (entrance and cage sizes) was important to determine the final loadings of Fe(salen) inside these materials. In general, the structure of m-MCF materials provides a higher loading of Fe(salen) complexes compared to SBA-16, probably due to their larger cage sizes. The catalytic activity of the materials could be tuned by changing the entrance and cage dimension of the silica structure, and adjusting them to the

specific substrate used. For the catalytic performance, the enantioselectivity of sulfoxidation reactions was just observed when PhIO was used as an oxidant as previously reported for the homogenous complex.[38] Moreover, Fe(salen) trapped in the mesoporous materials showed almost the same activity and enantioselectivity of the homogeneous counterpart. During recyclability tests, the immobilized complex showed a deactivation after the second cycle, related to decomposition of the encapsulated Fe(salen) complex and the formation of iron oxide particles.

References

1. I. Fernández, N. Khiar, *Chem. Rev.* 2003, **103**, 3651.
2. E. Wojaczyńska, J. Wojaczyński, *Chem. Rev.* 2010, **110**, 4303.
3. M. C. Carreno, *Chem. Rev.* 1995, **95,** 1717.
4. R. Bentley, *Chem. Soc. Rev.* 2005, **34**, 609.
5. J. Legros, J. Dehli, C. Bolm, *Adv. Synth. Catal.* 2005, **347**, 19.
6. S. Morita, J. Matsubara, K. Otsubo, K. Kitano, T. Ohtani, Y. Kawano, M. Uchida, *Tetrahedron: Asymmetry* 1997, **8,** 3707.
7. S. Padmanabhan, R. C. Lavin, G. J. Durant, *Tetrahedron: Asymmetry* 2000, **11**, 3455.
8. H. Pellissier, *Tetrahedron* 2006, **62**, 5559.
9. X. Gu, X. Li, Y. Chai, Q. Yang, P. Li, Y. Yao, *Green Chem.* 2013, **15,** 357.
10. F. Voss, E. Herdtweck, T. Bach, *Chem. Commun. (Camb).* 2011, **47**, 2137.
11. G. E. O'Mahony, A. Ford, A. R. Maguire, *J. Sulfur Chem.* 2013, **34**, 301.
12. J. Dad'ová, E. Svobodová, M. Sikorski, B. König, R. Cibulka, *ChemCatChem* 2012, **4**, 620.
13. K. Matsumoto, T. Yamaguchi, J. Fujisaki, B. Saito, T. Katsuki, *Chem. Asian J.* 2008, **3**, 351.
14. A. Lazar, P. Sharma, a. P. Singh, *Microporous Mesoporous Mater.* 2013, **170,** 331.
15. M. R. Maurya, A. K. Chandrakar, S. Chand, *J. Mol. Catal. A Chem.* 2007, **263**, 227.

16. W. Adam, F. Heckel, C. R. Saha-Möller, M. Taupp, P. Schreier, *Tetrahedron: Asymmetry* 2004, **15**, 983.

17. V. V Thakur, A. Sudalai, *Tetrahedron: Asymmetry* 2003, **14**, 407.

18. T. Katsuki, *Synlett* 2003, **7**, 1046.

19. C. Bolm, O. A. G. Dabard, *Synlett* 1999, **5**, 360.

20. C. Bolm, F. Bienewald, *Synlett* 1998, **4**, 1327.

21. S. Barroso, F. Madeira, M. J. Calhorda, M. J. Ferreira, M. T. Duarte, A. M. Martins, *Inorg. Chem.* 2013, **52**, 9427.

22. S. Barroso, P. Adão, F. Madeira, M. T. Duarte, J. C. Pessoa, A. M. Martins, *Inorg. Chem.* 2010, **49**, 7452.

23. J. Brinksma, B. L. Feringa, R. Hage, J. Kerschner, *Chem. Commun.* 2000, **2**, 537.

24. A. R. Silva, V. Budarin, J. H. Clark, *ChemCatChem* 2013, **5**, 895.

25. M. Matsugi, N. Fukuda, Y. Muguruma, T. Yamaguchi, J. Minamikawa, *Tetrahedron* 2001, **57**, 2739.

26. T. Kataukp, *Tetrahedron Lett.* 1994, **35**, 1887.

27. Q. Zeng, Y. Gao, J. Dong, W. Weng, Y. Zhao, *Tetrahedron: Asymmetry* 2011, **22**, 717.

28. C. Kokubo, T. Katsuki, *Tetrahedron* 1996, **52**, 13895.

29. S. Schoumacker, O. Hamelin, J. Pécaut, M. Fontecave, *Inorg. Chem.* 2003, **42**, 8110.

30. K. P. Bryliakov, E. P. Talsi, *Chemistry* 2007, **13**, 8045.

31. J. Legros, C. Bolm, *Angew. Chem. Int. Ed. Engl.* 2004, **43**, 4225.

32. J. Legros, C. Bolm, *Angew. Chem. Int. Ed. Engl.* 2003, **42**, 5487.

33. J. Legros, C. Bolm, *Chemistry* 2005, **11**, 1086.

34. L. Villalobos, T. Ren, *Inorg. Chem. Commun.* 2013, 52.

35. B. Li, A.-H. Liu, L.-N. He, Z.-Z. Yang, J. Gao, K.-H. Chen, *Green Chem.* 2012, **14**, 130.

36. J. Park, Y. Morimoto, Y.-M. Lee, W. Nam, S. Fukuzumi, *Inorg. Chem.* 2014, **53**, 3618.

37. S. Liao, B. List, *Adv. Synth. Catal.* 2012, **354**, 2363.

38. K. P. Bryliakov, E. P. Talsi, *Angew. Chem. Int. Ed. Engl.* 2004, **43**, 5228.

39. H. Egami, T. Katsuki, *J. Am. Chem. Soc.* 2007, **129**, 8940.

40. R. L. Oliveira, P. K. Kiyohara, L. M. Rossi, *Green Chem.* 2009, **11**, 1366.

41. R. L. Oliveira, D. Zanchet, P. K. Kiyohara, L. M. Rossi, *Chemistry* 2011, **17**, 4626.

42. R. L. Oliveira, P. K. Kiyohara, L. M. Rossi, *Green Chem.* 2010, **12**, 144.

43. N. Madhavan, M. Weck, *Adv. Synth. Catal.* 2008, **350**, 419.

44. B. Li, S. Bai, P. Wang, H. Yang, Q. Yang, C. Li, *Phys. Chem. Chem. Phys.* 2011, **13**, 2504.

45. L. Canali, E. Cowan, C. L. Gibson, D. C. Sherrington, H. Deleuze, *Chem. Commun.* 1998, 2561.

46. S. Bai, B. Li, J. Peng, X. Zhang, Q. Yang, C. Li, *Chem. Sci.* 2012, **3**, 2864.

47. R. Kureshy, I. Ahmad, N. Khan, S. Abdi, K. Pathak, R. Jasra, *J. Catal.* 2006, **238**, 134.

48. Z. Li, S. Wu, H. Ding, H. Lu, J. Liu, Q. Huo, J. Guan, Q. Kan, *New J. Chem.* 2013, **37**, 4220.

49. C. Baleizao, H. Garcia, *Chem. Rev.* 2006, **106**, 3987.

50. C. S. Gill, K. Venkatasubbaiah, C. W. Jones, *Adv. Synth. Catal.* 2009, **351**, 1344.

51. C. W. Jones, *Top. Catal.* 2010, **53**, 942.

52. V. Salinier, G. P. Niccolai, V. Dufaud, J.-M. Basset, *Adv. Synth. Catal.* 2009, **351**, 2168.

53. C. Li, H. Zhang, D. Jiang, Q. Yang, *Chem. Commun. (Camb).* 2007, 547.

54. A. B. Sorokin, in *Liq. Phase Oxid. via Heterog. Catal. Org. Synth. Ind. Appl.*, 2013, 321.

55. E. Möllmann, P. Tomlinson, W. . Hölderich, *J. Mol. Catal. A Chem.* 2003, **206,** 253.

56. S. Koner, *Chem. Commun.* 1998, **176,** 593.

57. S. B. Ogunwumi, T. Bein, *Chem. Commun.* 1997, 901.

58. F. Bedioui, *Coord. Chem. Rev.* 1995, **144**, 39.

59. J. Sabater, A. Corma, A. Domenech, V. Forn, *Chem. Commun.* 1997, 1285.

60. H. Yang, L. Zhang, W. Su, Q. Yang, C. Li, *J. Catal.* 2007, **248**, 204.

61. M. Shakeri, R. J. M. Klein Gebbink, P. E. de Jongh, K. P. de Jong, *Angew. Chem. Int. Ed. Engl.* 2013, **52**, 10854.

62. B. Li, S. Bai, X. Wang, M. Zhong, Q. Yang, C. Li, *Angew. Chem. Int. Ed. Engl.* 2012, **51**, 11517.

63. H. Yang, L. Zhang, L. Zhong, Q. Yang, C. Li, *Angew. Chem. Int. Ed. Engl.* 2007, **46**, 6861.

64. M. Shakeri, L. Roiban, V. Yazerski, G. Prieto, J. M. K. Gebbink, P. E. De Jongh, K. P. De Jong, *ACS Catal.* 2014, **4**, 3791.

65. T. Kim, R. Ryoo, M. Kruk, K. P. Gierszal, M. Jaroniec, *J. Phys. Chem. B* 2004, **108**, 11480.

66. M. Shakeri, R. J. M. Klein Gebbink, P. E. de Jongh, K. P. de Jong, *Microporous Mesoporous Mater.* 2013, **170**, 340.

67. J. F. Larrow, E. N. Jacobsen, Y. Gao, Y. Hong, X. Nie, C. M. Zepp, *J. Org. Chem.* 1994, **4**, 1939.

68. L. Tao, L. Qin-Xuan, R. Wen-Juan, Z. Zhi-Ang, C. Yun-Ti, *Chin. J. Chem*., 2001, **19**, 352.

69. H. Saltzman, J. G. Sharefkin, *Org. Synth. Coll.* 1973, **5**, 658.

70. M. Kruk, V. Antochshuk, J. R. Matos, L. P. Mercuri, M. Jaroniec, K. State, V. Uni, *J. Am. Chem. Soc.* 2002, **124**, 768.

71. Y. Yang, J. Guan, P. Qiu, Q. Kan, *Transit. Met. Chem.* 2009, **35**, 263.

72. T. Soundiressane, S. Selvakumar, S. Ménage, O. Hamelin, M. Fontecave, A. P. Singh, *J. Mol. Catal. A Chem.* 2007, **270**, 132.

73. A. Kilic, E. Tas, B. Deveci, I. Yilmaz, *Polyhedron* 2007, **26**, 4009.

74. B. Gigante, A. Corma, H. Garcia, *Catal. Lett.* 2000, **68**, 113.

75. W. Kahlen, H. H. Wagner, *Catal. Lett.* 1998, **54**, 85.

Chapter 6

Summary and concluding remarks

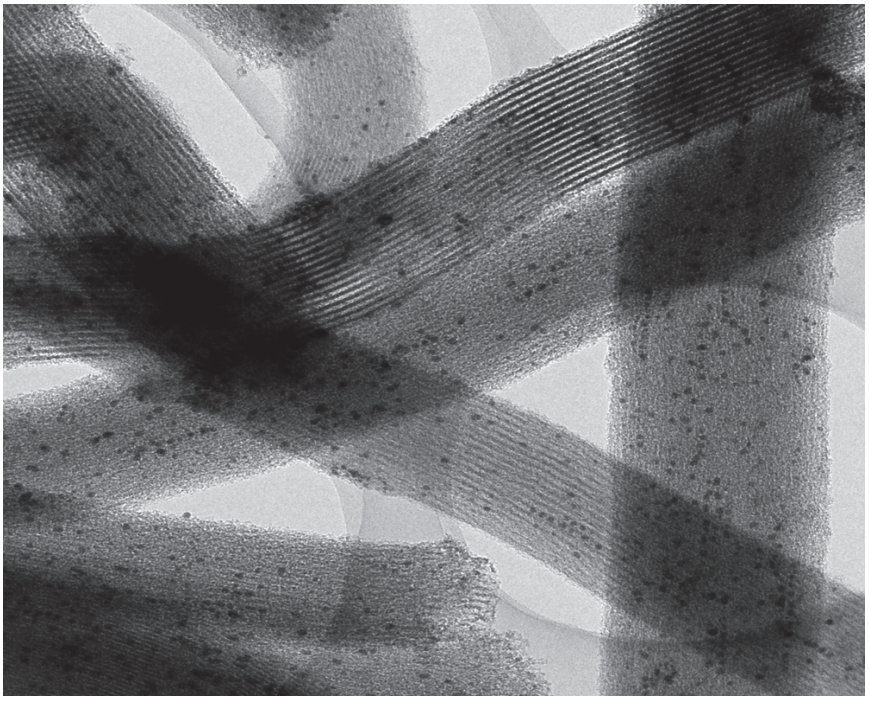

Nanomaterials have been extensively studied due to their potential in many fields of science and technology, such as energy, cosmetics, sensors, medicine, agriculture and catalysis. Thus, rational development of these materials and understanding of the process of synthesis and their structural properties are important. Especially in catalysis, the development of new synthesis methodologies has been responsible for enhanced performance in some catalytic processes. However, the degradation of these materials and their deactivation by particle growth are challenges.

The aim of the work described in this thesis was the synthesis and characterization of materials based on the confinement of metal species such as silver, palladium and an iron salen complex. Some of these materials were used as catalysts for C-C cross coupling and sulfoxidation reaction.

Chapter 2 describes the synthesis of plugged SBA-15 materials which were prepared with a variation in the degree of constriction of the pores. This variation was obtained by changing synthesis parameters such the hydrothermal treatment temperature and the silica precursor addition step. We showed the presence of nanocavities in plugged SBA-15, also giving quantitative information about the nanocavities dimensions and the plugs distribution of using gas physisorption (argon and nitrogen) and imaging silver nanostructures inside SBA-15 and plugged SBA-15. The length of the nanocavities was determined, and varied from 5 to 100 nm, depending on the synthesis procedure. For example, a plugged SBA-15 synthesized at 80ºC (hydrothermal treatment temperature) showed nanocavites around 28 nm in length on average, while a plugged SBA-15 synthesized by a different condition presented a bimodal distribution of its cavities with lengths varying from 20 to 100nm. These results demonstrate the suitability of visualization of pore-confined metal nanostructures to characterize the nature of complex porosities such as nanocavities.

In **chapter 3**, we prepared catalysts of palladium deposited on pristine and on functionalized SBA-15 structures and these materials were used as catalysts for the Heck reaction. The nature of the solvents had a large effect on metal leaching and on the reaction rates of the Heck reaction. In general, a high degree of metal leaching was related to fast

substrate conversion. The hot filtration test, poly(4-vinylpyridine) poisoning, and Pd analysis gave a strong indication that soluble species were mainly responsible for the final conversion of iodobenzene.

Moreover, the Pd particle size had little effect on the activity and recyclability of the Heck reaction especially if DMF was used as the solvent. A mixed solvent of toluene and DMF was important to decrease metal leaching. The combination of a mixed solvent and thiol groups grafted on SBA-15 was very efficient to limit Pd leaching and particle growth, which permitted this catalyst to be recycled ten times with only a slight loss of its activity. Clearly, the functionalized catalysts were more stable than the nonfunctionalized catalysts that lost their activity gradually because of metal leaching and Pd particle growth. Furthermore, the Pd on S-functionalized SBA-15 catalyst was able to catalyze the Heck reaction with different substrates to achieve good activity and selectivity in most cases.

Chapter 4 describes the synthesis and characterization of palladium nanoparticles of similar size of ~2 nm that were synthesized on different silica-based materials all functionalized with thiol groups i.e., Aerosil-380, SBA-15, Plugged SBA-15 and m-MCF. The resulting materials were used to study the influence of confinement of Pd nanoparticles in functionalized silica support on the Heck and the Suzuki reaction.

The structural stability of Pd species was influenced by the thiol-functionalized silica structure. We reported for the first time that for the Heck reaction, the combined effects of functionalization and confinement of Pd nanoparticles in the cavities of ordered mesoporous silica. Plugged SBA-15 or m-MCF were efficient to limit the Ostwald ripening, avoiding the formation of large Pd particles that were observed with non-porous silica. Despite having the same Pd particle size distributions, the materials based on OMS showed a better recyclability when compared to non-porous silica due to the retarded formation of large Pd particles. The hot filtration and PVP tests showed that homogeneous species contributed considerably to the final conversion. Stabilization of heterogeneous Heck Pd catalyst, therefore, cannot be realized by suppression of leaching. Rather, re-adsorption by functionalization in

combination with restriction of Pd particle growth by confinement is effective to extend catalyst life time.

In the case of the Suzuki reaction, the use of stronger alkaline conditions promoted a considerable damage to the silica supports. This fact resulted in a limited recyclability of all synthesized materials. However, SBA-15 showed to be the most fragile structure, which collapsed during the first cycle, resulting in a poor recyclability when compared to plugged SBA-15. The plugs and the more robust structure of plugged SBA-15 permitted the material to display a higher stability for the Suzuki reaction, providing an improvement of the recyclability results.

In the last chapter, **chapter 5**, solid catalysts which are heterogeneous at macroscopic scale but homogeneous at microscopic level were prepared by the encapsulation of Fe(salen) by a "ship in a bottle" approach. This approach permits to synthesize inside the nanocages of SBA-16 and m-MCF a "free" Fe(salen) complex, having conformational freedom and behaving as a complex in solution. These materials were used as catalysts for asymmetric oxidation of sulfides which are important chemicals for pharmaceutical companies due to their biological properties.

A chiral Fe(salen) complex was encapsulated in the nanocages of n-propyl modified SBA-16 and m-MCF. The silica structure (entrance and cage sizes) was important to determine the final loading of Fe(salen) inside these materials. In general, the structure of m-MCF materials provided a higher loading of Fe(salen) complex when compared to SBA-16, probably due to their larger cage sizes. The catalytic activity of the materials was tuned by changing the entrance and cage dimension of the silica structure, and adjusting them to the specific substrate used. For the catalytic performance, enantioselectivity of sulfoxidation reactions was only observed when PhIO was used as an oxidant as previously reported for the homogeneous complex. Moreover, Fe(salen) trapped in the mesoporous materials showed almost the same activity and enantioselectivity as the homogeneous counterpart. During recyclability tests, the immobilized complex showed a deactivation after the second cycle,

related to decomposition of the encapsulated Fe(salen) complex and the formation of iron oxide particles.

Chapter 7

Nederlandse Samenvatting

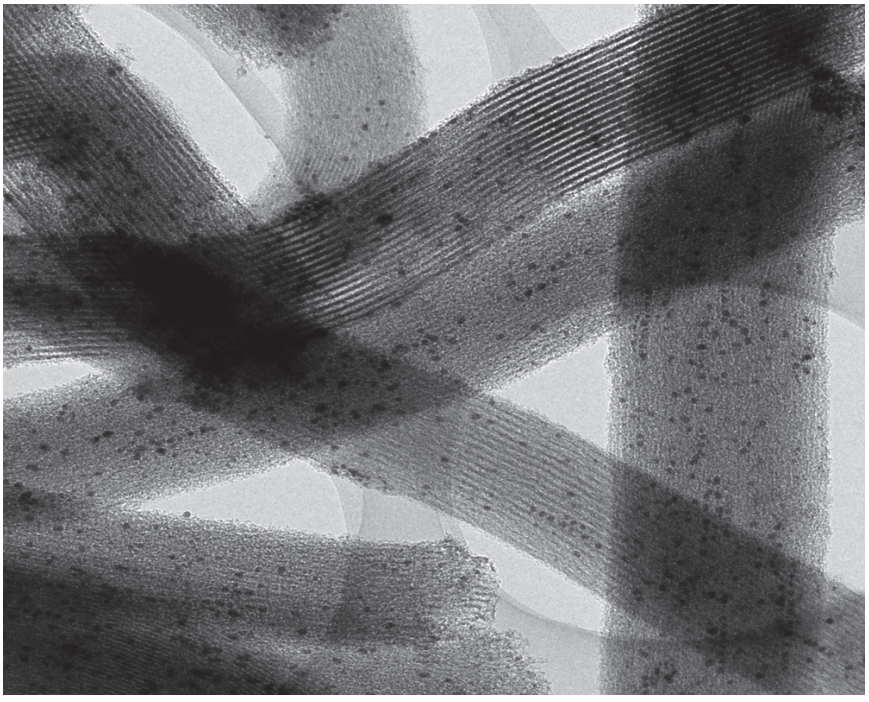

Nanomaterialen worden uitgebreid bestudeerd vanwege hun potentie in vele gebieden van de wetenschap en technologie, zoals energie, cosmetica, sensoren, medicijnen, landbouw en katalyse. De rationele ontwikkeling van deze materialen en begrip van het syntheseproces en de structurele eigenschappen zijn daarom belangrijk. Vooral in de katalyse heeft de ontwikkeling van nieuwe synthesemethodes geleid tot verbeterde prestaties in een aantal processen. De verzwakking van deze materialen en hun deactivatie door deeltjesgroei blijven echter uitdagingen.

Het doel van het werk beschreven in dit proefschrift was de synthese en karakterisatie van materialen gebaseerd op het opsluiten van metalen en metaalverbindingen zoals zilver, palladium en ijzersaleen. Sommige van deze materialen zijn gebruikt als katalysatoren voor de C-C kruiskoppeling en sulfoxidatie reacties.

Hoofdstuk 2 beschrijft de synthese van geplugde SBA-15 materialen die gemaakt zijn met een verschillende mate van porie-constrictie. Deze variatie werd verkregen door syntheseparameters zoals de temperatuur tijdens de hydrothermale behandeling en de silicaprecursor toevoegingsstap te variëren. We toonden de aanwezigheid aan van nanoholtes in geplugd SBA-15, waarbij ook kwantitatieve informatie werd verkregen over de afmetingen van de nanoholtes en de plugverdeling van deze materialen door gebruik te maken van gasfysisorptie (argon en stikstof) en door zilver nanostructuren in SBA-15 en geplugd SBA-15 af te beelden. De lengte van de nanoholtes werd bepaald en varieërde van 5 tot 100 nm, afhankelijk van de syntheseprocedure. Geplugd SBA-15 gesynthetiseerd bij 80°C (temperatuur tijdens de hydrothermale behandeling) liet bijvoorbeeld nanoholtes van gemiddeld 28 nm in lengte zien, terwijl een geplugd SBA-15 gesynthesiseerd onder een andere conditie een bimodale verdeling met lengtes van de holtes variërend van 20 tot 100 nm liet zien. Deze resultaten laten zien dat de toepasbaarheid van visualisatie van metalen nanostructuren ingesloten in de poriën gebruikt kan worden om de aard van complexe porositeit zoals nanoholtes te karakteriseren.

In **hoofstuk 3** beschrijven we de bereiding van katalysatoren door palladium af te zetten op onbehandelde en gefunctionaliseerde SBA-15 structuren, en deze materialen

werden gebruikt als katalysatoren voor de Heck reactie. De aard van de oplosmiddelen had een groot effect op het uitlogen van het metaal en op de reactiesnelheid van de Heck reactie. Over het algemeen ging een grote mate van metaaluitlogen gepaard met een snelle substraatomzetting. De hetefiltratietest, poly(4-vinylpyridine)vergiftiging en Pd analyse gaven een sterke indicatie dat voornamelijk oplosbare species verantwoordelijk waren voor de uiteindelijke conversie van joodbenzeen.

De palladium deeltjesgrootte had weinig effect op de activiteit en herbruikbaarheid van de Heck reactie wanneer DMF als oplosmiddel werd gebruikt. Een gemengde oplossing van tolueen en DMF zorgde echter voor verminderd metaal uitlogen. De combinatie van een gemengde oplosmiddelen en thiol-groepen aangebracht op SBA-15 was zeer effectief in het verminderen van Pd uitlogen en deeltjesgroei, waardoor deze katalysator tien keer herbruikt kon worden met slechts een klein verlies aan activiteit. De gefunctionaliseerde katalysatoren waren duidelijk stabieler dan de niet-gefunctionaliseerde katalysatoren en verloren hun activeit slechts geleidelijk door metaaluitlogen en deeltjesgroei. Daarnaast was de Pd op het S-gefunctionaliseerde SBA-15 in staat om de Heck reactie te katalyseren met verschillende substraten, in de meeste gevallen met goede activiteit en selectiviteit.

Hoofdstuk 4 beschrijft de synthese en karakterisatie van palladium nanodeeltjes van ~2 nm op verschillende silica-gebaseerde materialen die allemaal gefunctionaliseerd waren met thiol-groepen i.e., Aerosil-380, SBA-15, geplugd SBA-15 en m-MCF. De materialen werden gebruikt om de invloed van opsluiting van Pd nanodeeltjes in gefunctionaliseerde silicadragers op de Heck en de Suzuki reactie te bestuderen.

De structurele stabiliteit van Pd species werd beïnvloed door de thiol-gefunctionaliseerde silicastructuur. We rapporteerden voor de eerste keer voor de Heck reactie het gezamenlijke effect van functionalisatie en opsluiting van Pd nanodeeltjes in de holtes van geordende mesoporeuze silica. Geplugd SBA-15 en m-MCF limiteerden Ostwald rijping, waardoor de vorming van grote Pd deeltjes werd voorkomen die wel waargenomen werden bij niet-poreuze silica. Ondanks vergelijkbare Pd deeltjesgrootteverdeling, laten de materialen gebaseerd op OMS een betere herbruikbaarheid zien dan voor niet-poreuze silica,

veroorzaakt door de vertraagde vorming van grote Pd deeltjes. The warmefiltratie- en PVP-testen laten zien dat opgeloste species aanzienlijk bijdroegen aan de uiteindelijke conversie. Stabilisatie van een heterogene Heck Pd katalysator kan daarom niet gerealiseerd worden door uitlogen te onderdrukken. Heradsorptie door functionalisatie in combinatie met restrictie van Pd deeltjesgroei door insluiting is daarentegen wel effectief in het verlengen van de levensduur van de katalysator.

In het geval van de Suzuki reactie veroorzaakte het gebruik van sterkere alkalische condities aanzienlijke schade aan de silicadragers. Dit feit resulteerde in een beperkte herbruikbaarheid van alle gesynthetiseerde materialen. SBA-15 liet echter de meest fragiele structuur zien die instortte gedurende de eerste cyclus, resulterend in een slechte herbruikbaarheid vergeleken met geplugd SBA-15. De pluggen en de robuustere structuur van geplugd SBA-15 leidden tot een hogere stabiliteit in de Suzuki reactie en een verbetering van de herbruikbaarheid.

In het laatste hoofdstuk, **Hoofdstuk 5**, zijn vaste katalysatoren die heterogeen zijn op de macroscopische schaal, maar homogeen op de microscopische schaal, gemaakt door Fe(salen) in te kapselen via een “ship-in--bottle” aanpak. Deze aanpak maakt het mogelijk om binnenin de nanokooien van SBA-16 en m-MCF een “vrij” Fe(salen) complex te synthetiseren, dat conformationele vrijheid heeft en zich als een complex in oplossing gedraagt. Deze materialen zijn als katalysator gebruikt voor de asymmetrische oxidatie van sulfides, belangrijke chemicaliën voor farmaceutische bedrijven vanwege hun biologische eigenschappen.

Een chiraal Fe(salen) complex werd ingekapseld in de nanokooien van n-propyl gemodificeerde SBA-16 en m-MCF. De silicastructuur (ingang- en kooigroottes) was belangrijk voor het bepalen van de uiteindelijke Fe(salen) belading in de materialen. Over het algemeen zorgde de structuur van m-MCF materialen voor een grotere belading met het Fe(salen) complex dan voor SBA-16, waarschijnlijk door de grotere kooien. De katalytische activiteit van de materialen werd veranderd door de ingang- en kooiafmetingen van de sillica

structuur te variëren en aan te passen aan het specifieke substraat. Wat betreft de katalytische prestaties was de enantioselectiviteit van de sulfoxidatie reacties alleen waargenomen wanneer PhIO als een oxidant werd gebruikt, zoals al eerder gerapporteerd was voor het homogene complex. Fe(salen) gevangen in de mesoporouze materialen liet daarnaast dezelfde activiteit en enantioselectiviteit zien als zijn homogene tegenhanger. Het geïmmobiliseerde complex vertoonde tijdens de herbruikbaarheidstesten deactivatie na de tweede cyclus, veroorzaakt door de ontleding van het ingekapselde Fe(salen) complex en de formatie van ijzeroxide deeltjes.

Appendices

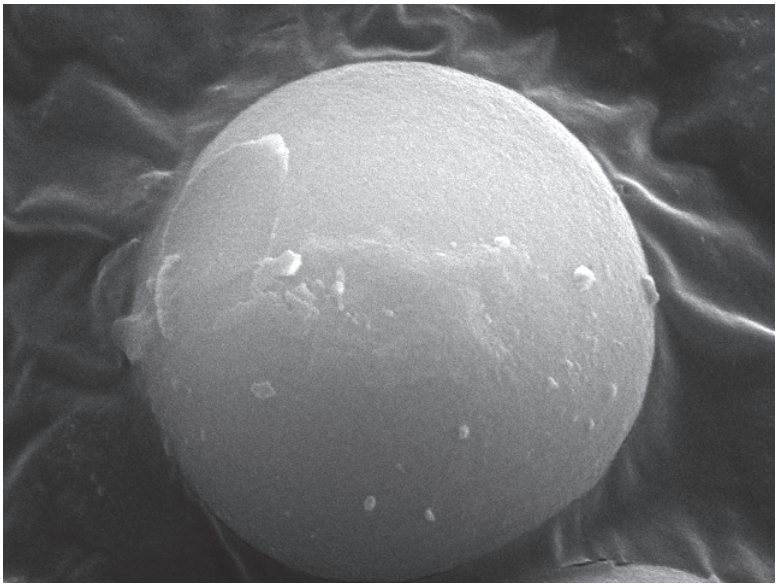

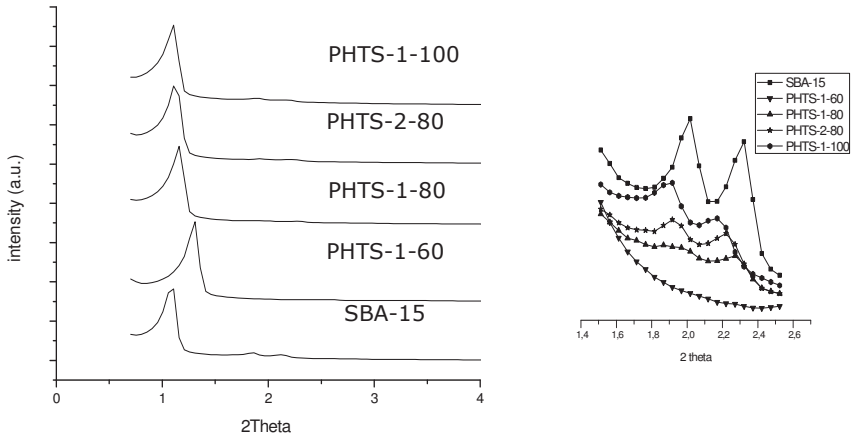

Figure A1- X-ray diffractograms of the PHTS and SBA-15

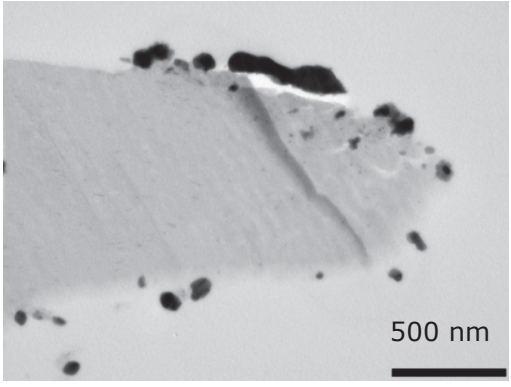

Figure A2- TEM image Ag-PHTS-1-60

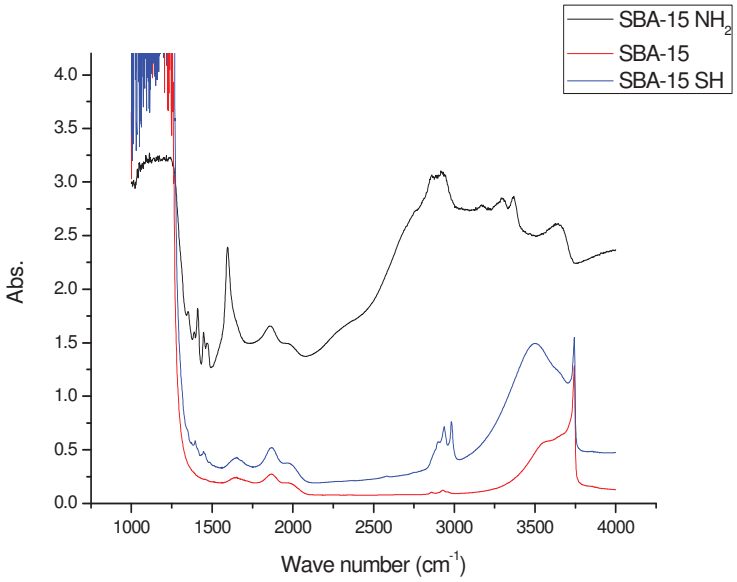

Figure A3- FT-IR analysis of SBA-15 and functionalized SBA-15

The peaks around 1307 and 1343 cm^{-1} can be attributed to CH_2 on silica surface. The adsorption around 3000cm^{-1} are also characteristic for incorporation of alkyl groups on silica surface (C-H stretch). Moreover, the two peaks around 3300 cm^{-1} are characteristic of N-H stretch on primary anime.

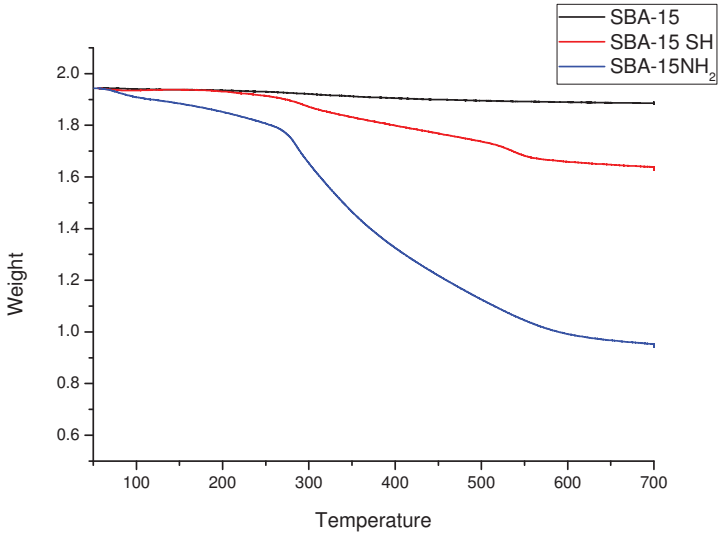

Figure A4- TGA analysis of SBA-15 and functionalized SBA-15

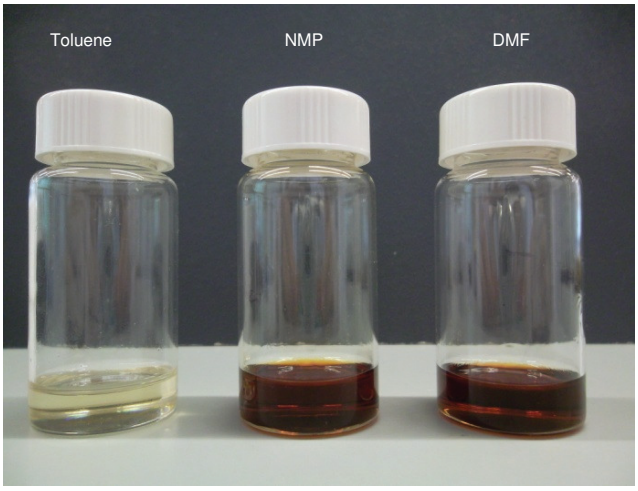

Figure A5-Solution obtained after catalysis of Pd-4.5

Table A1- Porosity of synthesized materials by N2 physisorption

Sample	S_{BET} $m^2.g^{-1}$	V_t $cm^3.g^{-1}$	D nm*
Aerosil-380	360	0.85	-
Aerosil-380 SH	290	2.7	-
Aerosil-380a SH	234	1.7	-
SBA-15	927	0.98	7.6
SBA-15 SH	704	0.79	7.2
P.SBA-15	830	0.66	6.5
P.SBA-15SH	618	0.52	6.1
m-MCF	699	0.96	22
m-MCF SH	586	0.88	21

*BJH analysis from adsorption branch

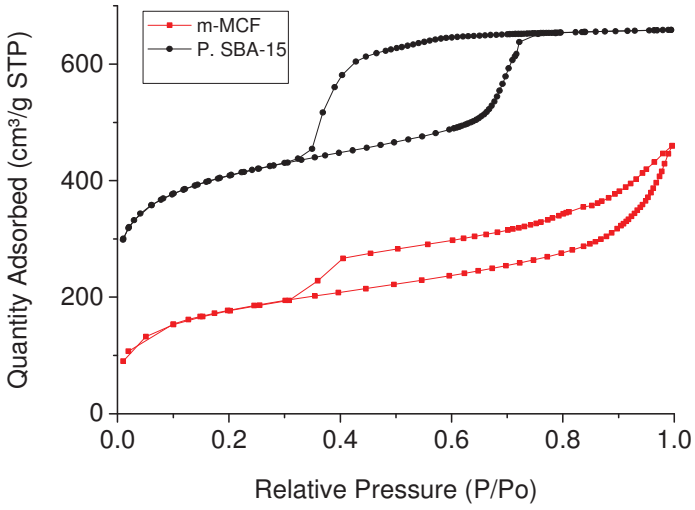

Figure A6- Ar physisorption of m-MCF and P.SBA-15

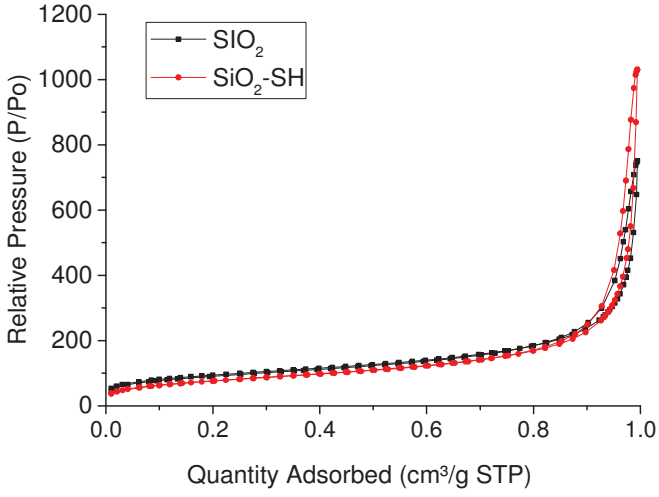

Figure A7- N_2 isotherms of Aerosil-380 and functionalized Aerosil-380

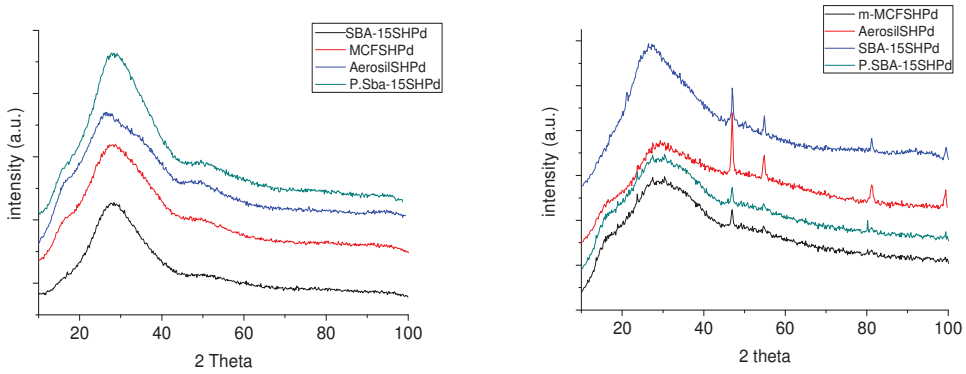

Figure A8- X-ray diffractgrams of fresh catalysts (left) spent catalysts (right)

Table A2 Conversion of the Heck reaction and the conversion after PVP poisoning test

Material	Conversion (%)	Conversion(%) after PVPy addition
SiO_2-SHPd	85	2
SBA-15SHPd	88	4
P-SBA-15SHPd	88	3
m-MCFSHPd	89	5

For the hot filtration test, the Heck reaction was allowed to run for 3 hours, the solid was filtered and the remained liquid was keep stirring under the same reaction condition. In the case of SBA-15SHPd, the conversion in the liquid phase increased from 48% to 71% after 10 hours, showing the contribution of soluble species on catalysis.

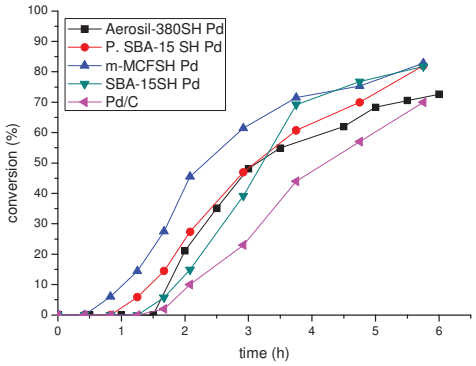

Figure A9 Plot product yield versus time for the Heck reaction between iodobenzene and butylacrylate for different materials

Reaction conditions: 22.5 mmol of iodobenzene, 34 mmol of butyl acrylate, 20 mg of supported catalyst (0.01mol% of palladium), 21.4 mmol of Et_3N, 20mL toluene+ 2mL DMF, 100ºC

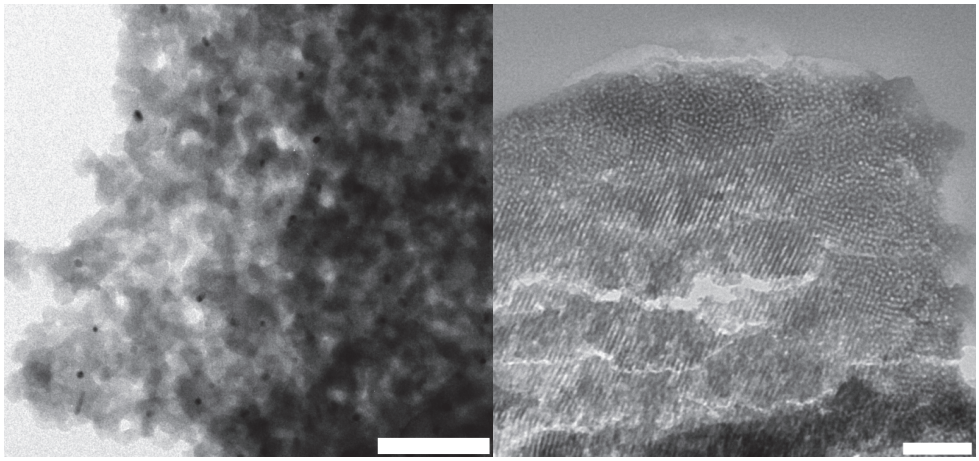

Figure A10 TEM images: Spent SBA-15SHPd (left) Spent P.SBA-15 (right) scale bars 100nm

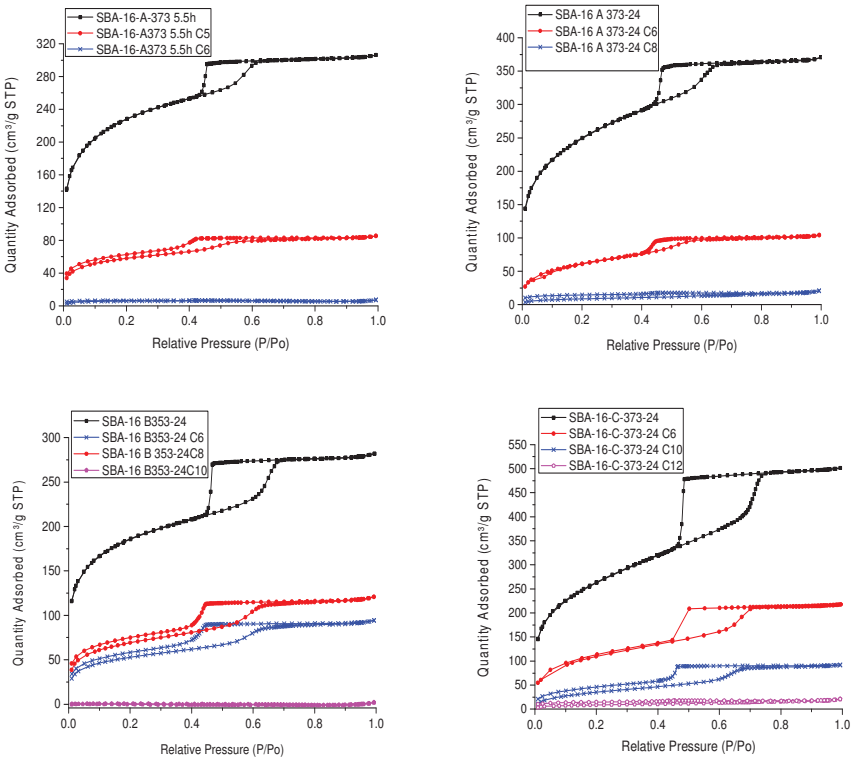

Figure A11- Nitrogen adsorption isotherms to determine the window size of SBA-16 materials after functionalization

SBA-16 materials were functionalized with organosilanes with different carbon chains. The samples were designated SBA-16 Cx, where x is the number of carbon on the carbon chain. For example, SBA-16A-373-5.5-C6 is SBA-16A-373-5.5 that was functionalized with n-hexyltriethoxysilane.

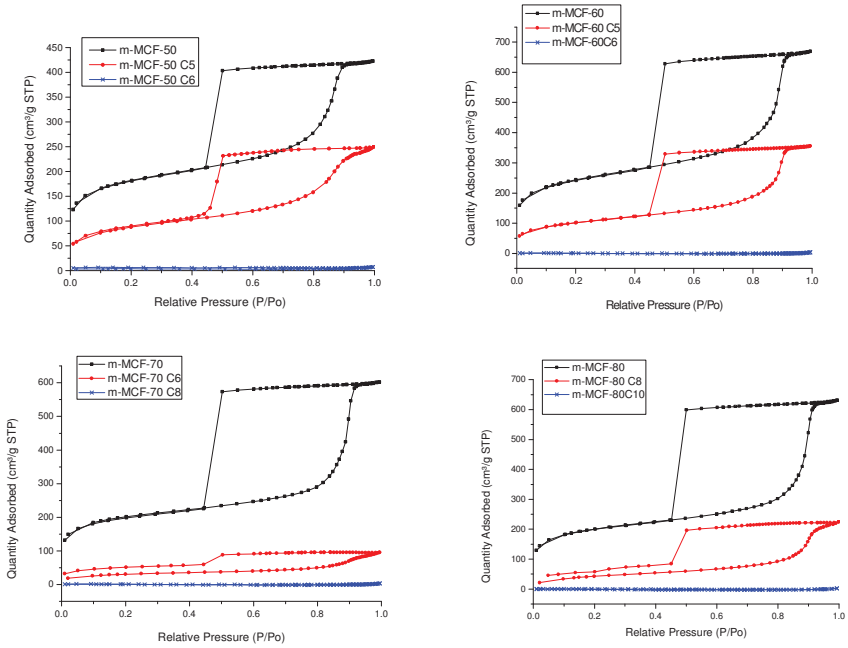

Figure A12- Nitrogen adsorption isotherms to determine the window size of m-MCF materials after functionalization

m-MCF materials were functionalized with organosilanes with different carbon chains. The samples were designated m-MCF Cx, where x is the number of carbon on the carbon chain.

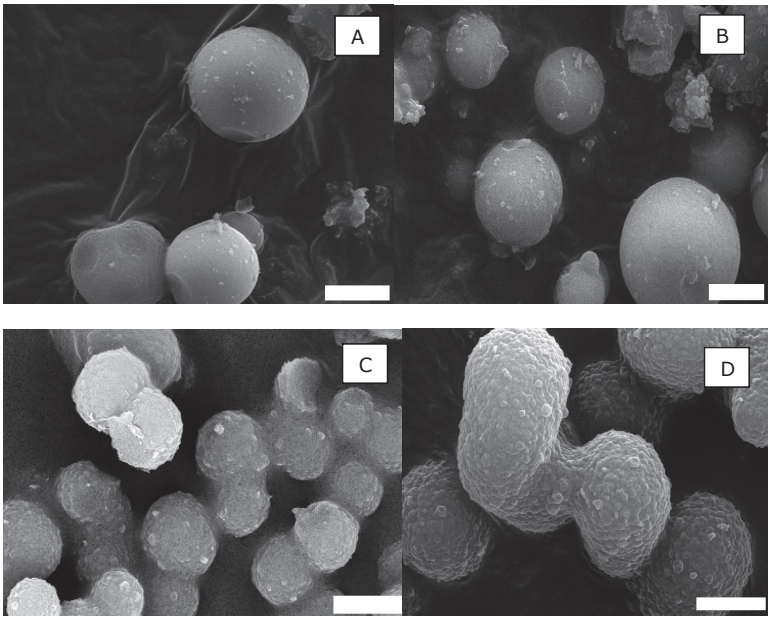

Figure A13- SEM images of pristine materials (A) m-MCF-50, (B)m-MCF-60, (C)m-MCF-70 and (D) m-MCF-80 Scale Bars: 2µm

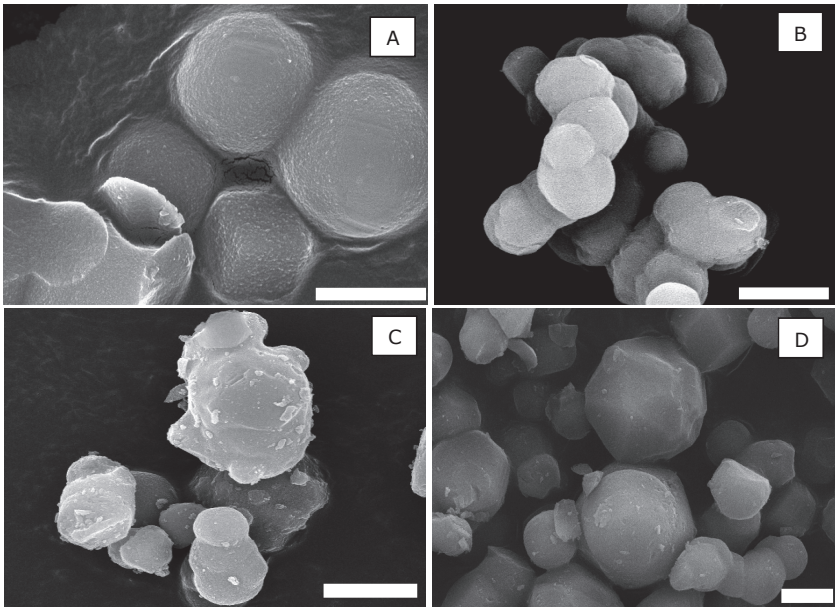

Figure A14- SEM images pristine materials (A) SBA16-A-373-5.5 (B) SBA16-A-373-24 (C) SBA16-B-353-24 (D) SBA16-C-373-24, scale bars: 2µm

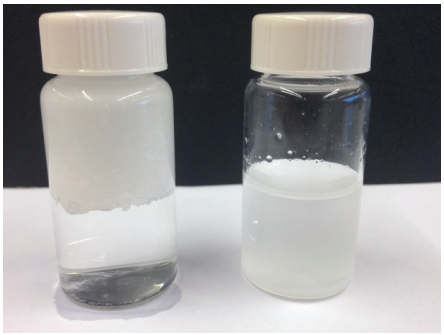

Figure A15- m-MCF-60 functionalized with n-propyl groups (left) and pristine m-MCF-60 (right) mixed with water.

Pristine m-MCF-60 is easily dispersed in water due to silanol groups on its surface. In the case of functionalized m-MCF-60, the silica does not dispersed in water due to the hydrophobic groups grafted on its surface.

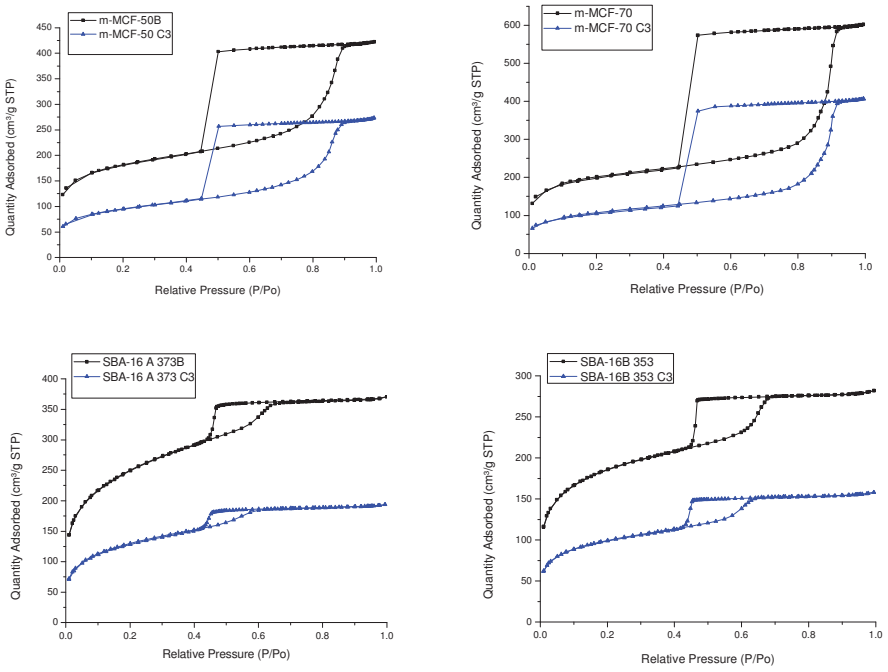

Figure A16- N_2 physisorption of pristine material and the respective material functionalized with n-propyl groups

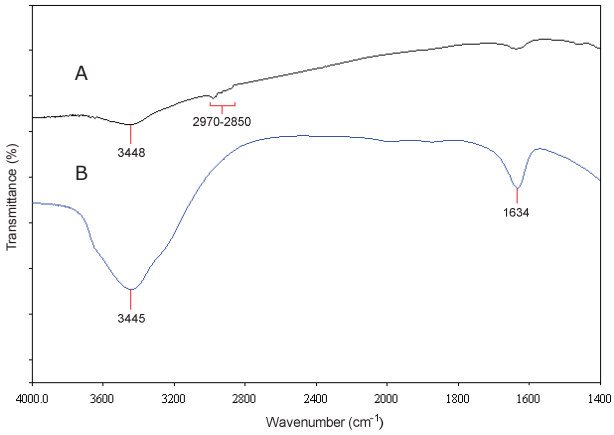

Figure A17-IR spectra (A) Functionalized MCF-60 with n-propyl groups (B) pristine m-MCF-60

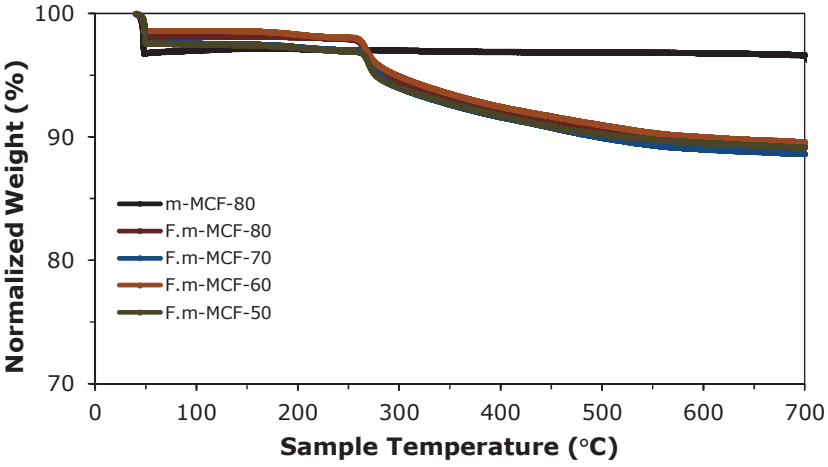

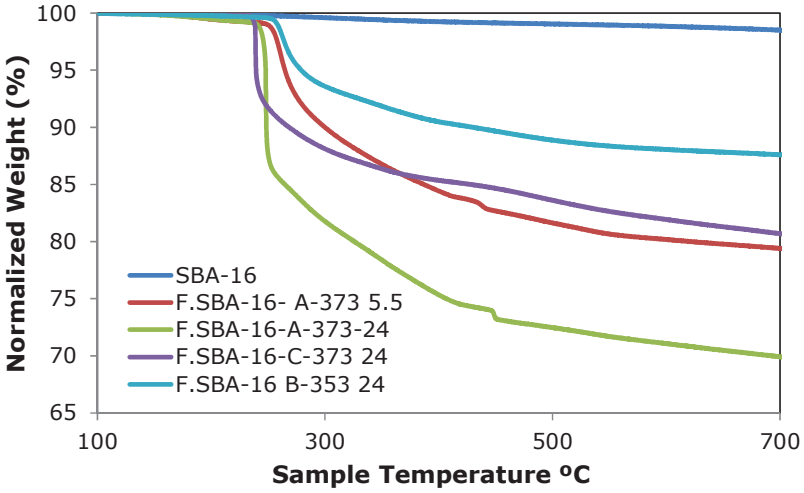

Figure A18- TGA analysis of a pristine m-MCF and functionalized m-MCFs (top frame) and a pristine SBA-16 and functionalized SBA-16 (bottom frame)

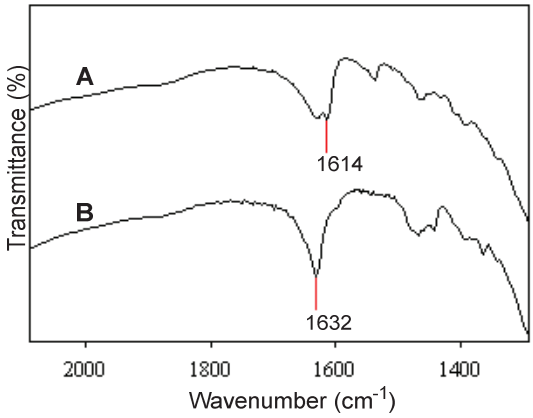

Figure A19- IR spectra of: A) Fe(salen)F.m-MCF-60, B) salen ligand F.m-MCF-60

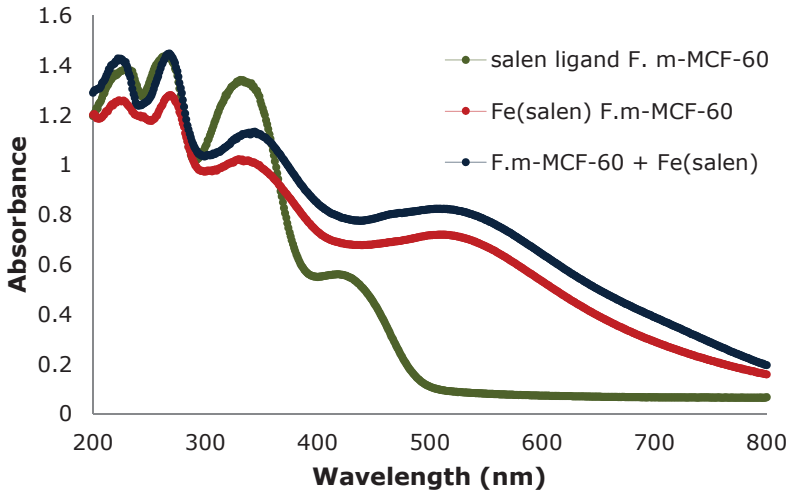

Figure A20 UV-vis spectra of salen ligand or Fe(salen) encapsulated in m-MCF-60 and physical mixture of Fe(salen) with m-MCF-60

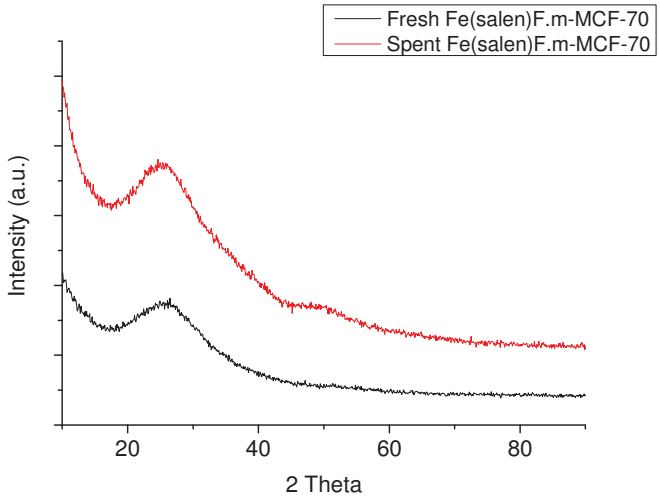

Figure A21- XRD analysis of fresh and spent Fe(salen) F.m-MCF-70

List of Abbreviations

a.u.	arbitrary units
AAS	Atomic Absorption Spectroscopy
DMF	Dimethylformamide
DSC	Differential Scanning Calorimetry
EXAFS	Extended X-Ray Absorption Fine Structure
FDU-12	Fudan University-12
FSM-16	Folded Sheet Silica-16
FT-IR	Fourier Transform Infrared Spectroscopy
GC	Gas Chromatography
HAADF	High-Angle Annular Dark Field
HPLC	High-Performance Liquid Chromatography
ICP	Inductively Coupled Plasma
IWI	Incipient Wetness Impregnation
KIT-5	Korean Institute of Technology-5
MCM-41	Mobil Composition of Matter-41
m-MCF	Modified Mesocellular Foam
MCF	Mesocellular Foam
MS	Mass Spectroscopy
NMP	N-Methyl-2-Pyrrolidone
NP	Nanoparticle
OMM	Ordered Mesoporous Material
OMS	Ordered Mesoporous Silica
PHTS	Plugged Hexagonal Templated Silica
PZC	Point Zero Charge
PVPy	Poly(4-vinylpyridine)
SEM	Scanning Electron Microscopy
STEM	Scanning Transmission Electron Microscopy
SBA-15	Santa Barbara-15

SBA-16	Santa Barbara-16
TEM	Transmission Electron Microscopy
TEOS	Tetraethyl Orthosilicate
TGA	Thermal Gravimetric Analysis
UV-vis	Ultra-Violet and Visible Light Spectroscopy
XRD	X-Ray Diffraction
ZSM-5	Zeolite Socony Mobil-5

List of publications and presentations

This thesis is based on the following publications:

Rafael L. Oliveira , Mozaffar Shakeri , Johannes D. Meeldijk, Krijn P. de Jong and Petra E. de Jongh. Mapping nanocavities in plugged SBA-15 with confined silver nanostructures, Micro. Meso. Mater., 2015, 201, 234-239.

Rafael L. Oliveira, Jasper B. F. Hooijmans, Petra E. de Jongh, Robertus J. M. Klein Gebbink, Krijn P. de Jong. Stabilization of palladium catalysts for the Heck reaction by support functionalization and solvent selection, ChemCatChem, 2014, 6, 1-9.

Rafael L. Oliveira, Wuliyasu He, Robertus J. M. Klein Gebbinkb, Krijn P. de Jong. Palladium nanoparticles confined in thiol-functionalized ordered mesoporous silica for more stable Heck and Suzuki catalysts, Catal. Sci. Tech., 2015, 5, 1919-1928.

Rafael L. Oliveira, Tom Nijholt, Mozaffar Shakeri, Petra E. de Jongh, Robertus J. M. Klein Gebbink and Krijn P. de Jong. Encapsulation of chiral Fe(salen) in mesoporous silica structures for use as catalysts to produce optically active sulfoxides. ChemCatChem submitted.

Rafael L. Oliveira, Jeroen van den Reijen, Petra E. de Jongh, Krijn P. de Jong. The preparation of supported Ag nanoparticles in SBA-15 by the controlled thermal decomposition of nitrate, in preparation.

Other publication by the author:

Rafael L. Oliveira, Pedro K. Kiyohara, Liane M. Rossi. Clean preparation of methyl esters in one-step oxidative esterification of primary alcohols catalyzed by supported gold nanoparticles. Green Chemistry, 2009, 11, 1366-1370.

Rafael L. Oliveira, Pedro K. Kiyohara, Liane M. Rossi. High performance magnetic separation of gold nanoparticles for catalytic oxidation of alcohols. Green Chemistry, 2010, 12, 144-149.

Rafael L. Oliveira, Daniela Zanchet, Pedro K. Kiyohara, Liane M. Rossi. On the stabilization of gold nanoparticles over silica-based magnetic supports modified with organosilanes. Chem. Eur. J., 2011, 17, 4626-4631.

Oral presentations by the author:

Rafael L. Oliveira, R. J. M. Klein Gebbink, K. P. de Jong. The influence of thiol groups grafted on SBA-15 in the activity and recyclability of the Heck reaction, FineCat, 2014, Palermo, Italy.

Rafael L. Oliveira, R. J. M. Klein Gebbink, K. P. de Jong. Comparison of SBA-15 and thiol-grafted SBA-15 as support of Pd catalysts for the Heck reaction, Workshop NRSC-Catalysis, 2014, Utrecht, The Netherlands.

Rafael L. Oliveira, Mozaffar Shakeri, Petra E. de Jongh, K. P. de Jong. Mapping nanocavities in plugged SBA-15 with silver nanostructures. Workshop NRSC-Catalysis, Utrecht, 2013, The Netherlands.

Rafael L. Oliveira, Mozaffar Shakeri, Petra E. de Jongh, K. P. de Jong. Mapping nanocavities in plugged SBA-15 with silver nanostructures. 23rd North American Catalysis Society Meeting, 2013, Louisville, The United States of America.

Poster Presentation by the author

Rafael L. Oliveira, Mozaffar Shakeri, Petra E. de Jongh, Krijn P. de Jong. Imaging nanocavities in Plugged SBA-15 Netherlands Catalysis and Chemistry Conference, 2014, Noordwijkerhout, The Netherlands.

Rafael L. Oliveira, Mozaffar Shakeri, Petra E. de Jongh, Krijn P. de Jong. Mapping nanocavities in plugged SBA-15, EuropaCat, 2013, Lyon, France.

R. L. Oliveira, J. B. F. Hooijmans, P. E. de Jongh, Robertus J. M. Klein Gebbink, Krijn P. de Jong. Pd nanoparticles in functionalized SBA-15 for Heck reaction, 23rd North American Catalysis Society Meeting, 2013, Louisville, The United States of America.

R. L. Oliveira, J. B. F. Hooijmans, Petra E. de Jongh, Robertus J. M. Klein Gebbink, Krijn P. de Jong. Pd nanoparticles in functionalized SBA-15 for Heck reaction. Netherlands Catalysis and Chemistry Conference, 2013, Noordwijkerhout, The Netherlands

Rafael L. Oliveira, Mozaffar Shakeri, Petra E. de Jongh, Krijn P. de Jong. A new synthetic strategy to produce plugged SBA-15. Netherlands Catalysis and Chemistry Conference, 2012, Noordwijkerhout, The Netherlands.

Acknowledgements

After four years, working and studying in The Netherlands, I would like to express my gratitude to a lot of people. I am sure that this PhD project would not have been possible without help and support of all of you. It is not easy to express my gratitude in few written words, but I will try.

First, I would like to say some words to my family. Gostaria muito de agradecer **minha família, (Dona Fatima, Senhor Assis, Elaine, Fabiola, Wanderlan, Pedro e Arthur)** por toda dedicação depositda na minha educação e na minha realização pessoal e profissional, e lógico, pelos maravilhosos momentos vividos durante todos os meu anos de vida! Vocês não tem ideia o quanto nossas conversas por Skype me ajudaram no meu período de adaptação na "fechada e fria" sociedade holandesa.

I would like to thank my supervisors Krijn de Jong, Petra de Jongh and Robertus Klein Gebbink, it has been a pleasure working with all of you. **Krijn**, thank you very much for the opportunity that you gave in your research group. During these years, I have learnt so much under your guidance and supervision, your broad experience in synthesis of nanomaterials and in catalysis was a great inspiration for me. **Petra**, thank you for sharing your knowledge about porous materials especially mesoporous silica with me; your contribution in the beginning of this project was very important. **Bert**, officially, you are not my supervisor, however, your contribution for this PhD project was very appreciated, from my point of view, we could not develop this project without your help and comments. My meetings with you were always very interesting because you gave different perspectives about the results.

I also would like to thank a lot of people who spent their time discussing results and working directly with my samples. **Mozaffar,** many thanks for all scientific contributions to this project, bringing ideas and suggesting experiments. **Hans,** thank you very much for imaging all my samples by TEM and also for transferring knowledge. Thank you for being so patient to listen my suggestions during the analysis. Wherever I go, I would like to work with a professional like you. **Marjan**, many thanks for TGA and SEM measurements. All my dedicated students who gave a very important contribution with results and discussions, **Jasper**, **Sebastiaan**, **Wuliyasu**, **Tom** and **Shahid**, I would like to thank. **Roy** is thanked for his great help with the Dutch summary of the thesis.

I also want to thank all members of Inorganic Chemistry and Catalysis with whom I spent a great time, coffee breaks, borrels, barbeques, parties, trips and lunches. I do not want to mention names because I am afraid to forget to write some of them. Thus, all PhD students and all postdoc fellows, thank you very much for sharing with me a bit of your culture, happiness and disappointments with experiments.

Another group of people that I would like to thank is my flat mates, **Anastacia**, **Tom**, **Li**, **Claire**, **Marieke**, **Veronika, Mariela** and **Narcisa** living with different nationalities made me a new person in the sense of respecting differences and contributing to broader my vision about humans.

Gostaria também de agradecer todos os amigos brasileiros feitos nessa jornada aqui na Europa, os de longo tempo (chegaram para ficar) **Luis**, **Vinicius, Manu, Daniel e Karola, Daniel de Amsterdam**, e os que conheci depois (que também são pessoas muito especiais) **Zé**, **Eduardo**, **Raquel**, **Marcia** (o demônio), **Livia** e seu marido (**faz-nada**), **Camila** (satanás), **Leticia**, **Maria**, **Tom, Fernanda,** tenho certeza que estou esquecendo nomes. Também gostaria de citar nomes de amigos que ficaram no Brasil, gostaria de usar os seus "vulgo-names", mas não posso, então, **Rafael**, **Rafaela**, **Wescley**, **Marcelo**, **Alex**, **Thiago**, **Igor, Tupac** e **Matheus**.

About the author

Rafael de Lima Oliveira was born in Fortaleza, Brazil. After the completion of his school education, he started in 2003 a chemistry study at Federal University of Ceará, his bachelor thesis was titled "Analysis and development of methodology for mercury determination in natural gas" which was performed in a collaboration between Petrobrás and Labomar under the supervision of Dr. Marcelo Dominguez de Almeida. He graduated in chemistry in 2007. In the same year, he started a master course in chemistry at Sao Paulo University (Brazil). He obtained his MSc degree in 2009, after finishing his thesis titled "Gold nanocatalysts: Preparation, characterization and catalytic performance" under supervision of Dr. Liane Marcia Rossi. After his master, he spent 8 months as a high school teacher (2010).

In 2011, he started a PhD project at Utrecht University (The Netherlands) under supervision of Prof. Dr. Krijn de Jong and Prof. Dr. Petra de Jongh in collaboration with Prof. Dr. Robertus Klein Gebbink. The research was funded by NRSCC and part of the obtained results are described in this thesis.